ELECTRON SPIN RESONANCE OF ADULT, FETAL, AND *ANAPLASMA MARGINALE* INFECTED BOVINE RED BLOOD CELLS

By

SAM E. GIUOCO

Bachelor of Science
Pan American College
Edinburg, Texas
1968

Master of Science
Oklahoma State University
Stillwater, Oklahoma
1969

Submitted to the Faculty of the Graduate College of the Oklahoma State University in partial fulfillment of the requirements for the Degree of
DOCTOR OF EDUCATION
May, 1971

ELECTRON SPIN RESONANCE OF ADULT, FETAL, AND ANAPLASMA MARGINALE INFECTED BOVINE RED BLOOD CELLS

Thesis Approved:

William J. Lewo
Thesis Adviser

Delleen L. Rutledge

C. Fremont Harris

Robert T. Alciatore

Wynn Jones

Dean of the Graduate College

ACKNOWLEDGEMENTS

The author would like to express his sincere gradtitude to Dr. W. J. Leivo for his help, guidance, and constant encouragement during the course of this investigation. Special thanks are extended to William C. Steckelberg for his many enlightening discussions and suggestions.

The Anaplasma marginale infected red blood cells used in this study came from Fort Dodge Laboratories, Fort Dodge, Iowa. They were kindly made available by Dr. Ian Anderson and Dr. E. W. Jones of the Department of Veterinary Medicine and Surgery-Clinical Research at Oklahoma State University. The author would like to express his appreciation to Dr. Anderson, Dr. Jones, and the technicians and others of that department for their continued interest and assistance in this study.

The support of the Research Foundation is gratefully acknowledged.

Finally, the author would like to express his sincere appreciation to his wife, Barbara, for her assistance in the preparation of this thesis.

TABLE OF CONTENTS

LIST OF FIGURES

Figure Page

CHAPTER I

INTRODUCTION

Preliminary Remarks

Oxidation-reduction processes, which are involved in many biological processes, invoke free radical reactions which can be studied using electron spin resonance (ESR).[1] The importance of ESR investigations in biological and medical studies arises from the general and predominant role that free radical reactions appear to play in metabolic and biochemical processes. Michaelis and his co-workers have proposed that biochemical electron transfers occur singly rather than in pairs and that as a result molecules possessing an unpaired electron (free radicals) occur as intermediates (1). From ESR studies free radicals can be detected, identified, their concentrations measured, and properties of the sample can be determined. Characteristic differences can be detected between the spectra of certain normal and abnormal cells. Electron spin resonance can also detect paramagnetic centers in solids. Donors and acceptors in semiconductors, color centers in the alkali

[1]Electron spin resonance will be abbreviated as ESR when appropriate.

halides, and any crystal defect having an associated electron may exhibit ESR absorption. Extensive ESR studies of natural, semiconducting, and synthetic diamonds have been undertaken by the author and others in this laboratory under the supervision of Dr. W. J. Leivo, but this study represents our first ESR investigation of biological materials.

Though ESR has recently been used to study normal adult hemoglobin (Hb-A), to the best knowledge of the author, there have been no reports of studies on parasitized red blood cells. There are indications that the presence of fetal hemoglobin (Hb-F) may play an important role in the resistance of neonatal animals to red blood cell parasitemia (protozoan infection). There have been no ESR studies of Hb-F cited in the literature to date.

The purpose of the present study on red blood cells and separated red blood cell components was to obtain information on the ESR spectra of normal and abnormal red cells. The samples were also subjected to various external treatments to determine the effects of such treatment on the ESR signal. Ultraviolet and x-ray irradiation, nitric oxide paramagnetic labeling, heat exposure, and atmospheric contamination were each used as individual external treatments. The value of the spectroscopic splitting factor (g) was calculated for all ESR signals obtained. Adult, fetal, and infected adult bovine red blood cells were investigated as the primary samples in this study although the ESR spectra

of other red cells (human, rodent, swine) and other materials such as collagen were also investigated as secondary samples. The infected adult bovine red cells contained a high percentage of Anaplasma marginale protozoa (anaplasmosis), and the basic characteristics of this disease will be discussed. The study will also present a brief review of the basic theory of ESR, an examination of the components of the red blood cell, and a literature review of recent related work. A discussion of the methods and equipment used in the investigation will also be included.

Electron Spin Resonance

Electron spin resonance is a form of absorption spectroscopy. It has features in common with the more familiar forms of spectroscopies such as optical, ultraviolet, and infrared. In each form, some frequency of electromagnetic radiation is passed through a sample, and the frequency of maximum absorption of energy is measured. Electron spin resonance (ESR) spectroscopy has the special feature that absorption takes place with the sample subjected to an additional magnetic field other than just the electromagnetic portion. Many atomic nuclei possess an intrinsic magnetic moment as do many electrons. Electrons also possess an angular momentum and a magnetic moment associated with their orbital motion. All of these magnetic moments can give rise to magnetic resonance and ESR absorption spectra.

Although all electrons possess spin, most materials are diamagnetic. The electrons are paired and there is no net magnetic moment, therefore, diamagnetic materials will not give ESR absorption spectra. For a material to have an ESR absorption spectrum, there must be unpaired electrons present in it. Materials containing unpaired electrons fall into two broad classes: first, paramagnetic ions from the transition groups of the periodic table, which contain partly filled electron shells; and second, free radicals and radical ions, where the unpaired electron is a valence electron normally taking part in chemical binding (2). Biological materials can contain unpaired electrons from both of these classes and ESR is the most sensitive method for detecting these paramagnetic centers or free radicals. The approximate minimum number of free radicals detectable by ESR is related to the sensitivity of the equipment by ΔH and τ, where ΔH is the width of the free radical signal and τ is the time required to sweep through the resonance frequency position. For most free radicals $\Delta H \simeq 10$ gauss and τ average $\simeq 10$ sec. These values give a detectable free radical minimum of approximately 3×10^{11} radicals/gm of sample. These capabilities make ESR at least 100 times more sensitive than the other methods of obtaining spectra (3).

Electron spin resonance absorption can be observed only if an unpaired spin is associated with the sample being studied. The unpaired electron interacts with an applied high frequency microwave field producing transitions

between Zeeman levels which are established by an external magnetic field. This phenomena of ESR can best be discussed by first considering a simple system in which an unpaired electron is associated with an atom or ion in a single crystal. Only the interaction of the electron with the externally applied magnetic field will be considered. Relaxation, hyperfine interactions, spin-spin and spin-orbit interactions, and quadrupole interactions will not be discussed here. For a more detailed explanation of ESR theory see Appendix A.

Before the external field is applied, the energy levels of interest are degenerate. When the external field is applied each degenerate level will split into two levels, one with an energy above the original energy and one with an energy below the original. The energy splitting of the two levels is given by

$$\Delta E = \gamma \hbar H_o \qquad (1.1)$$

where γ is the gyromagnetic ratio and $\hbar$ is Planck's constant divided by 2π. A transition between the two levels can therefore be caused by an introduction of energy ΔE into the system. Since $\Delta E = \hbar\omega$, where ω is the angular frequency of the radiation energy, then the conditions for transition are met when

$$\omega_o = \gamma H_o. \qquad (1.2)$$

Classically the magnetic moment vector precesses about the applied magnetic field direction with an angular frequency

$\omega = \gamma H_o$, and the precession frequency is seen to correspond to the radiation energy frequency required to cause a transition between spin energy levels. This correspondence phenomena is known as resonance. It occurs at radiation frequencies in the x-band region of the microwave spectrum for field strengths of several kilogauss. To obtain a useful expression for this resonance condition in ESR, a new parameter (g) needs to be defined. The position of the ESR resonance signal on the recorder trace locates the field at which resonance occurred, and the g-value is calculated from this. This value is a measure of the contribution of the spin and orbital motion to total angular momentum. As the ratio of spin magnetic moment to spin angular momentum is twice as large as the ratio of orbital magnetic moment to orbital angular momentum, $g \simeq 2$ for totally free electrons, but relativistic correction makes this value approximately 2.00232 for a completely free spin. Free radicals have g-value very close to 2 also, and these may be determined by measuring the exact magnetic field strength at which the resonance occurs. The field strength is usually measured by using a nuclear magnetic resonance probe and measuring the proton resonance frequency in the same field. The g-factor is the spectroscopic splitting factor given by

$$g = \frac{\gamma \hbar}{\beta} \qquad (1.3)$$

where β is the Bohr magneton $\frac{\hbar}{2mc}$ (4). The expression for the resonance condition in ESR can now be obtained using

the frequency for the transition condition and the new parameter (g), as given respectively by equations (1.2) and (1.3), and is given by

$$h\nu = g\beta H \qquad (1.4)$$

where $\nu = \frac{\omega}{2\pi}$ represents the microwave frequency. The reader interested in a detailed theoretical picture should refer to Appendix A where a reasonably complete treatment is undertaken by the author.

Basic ESR Spectrometer

Many ESR spectrometers operate in the x-band region of the microwave spectrum which is in the 3cm wavelength range and corresponds to a frequency of about 9.5Ghz. The condition for resonance is given by

$$E = h\nu = g\beta H \qquad (1.5)$$

where g for free electrons is approximately 2.00232 (2). When this value of g is substituted into (1.5) along with the values of h, ν, and β, as previously discussed, a value of magnetic field, H, is obtained which is approximately 3,400 gauss. A magnetic field of approximately 3,400 gauss is therefore required to produce free electron resonance in the region of the microwave spectrum.

To detect ESR the sample is placed in a reflection microwave cavity or a transmission microwave cavity in the magnetic field of an electromagnet. The reflection cavity offers the most versatility and is employed most often when a bridge spectrometer is used. This discussion will be

limited to a reflection cavity spectrometer. Since it is inconvenient to vary the microwave frequency, the magnetic field is scanned so that the resonance condition (1.5) is satisfied. The field configuration of the cavity must be selected to place the microwave magnetic field perpendicular to the electromagnet field at the position of the sample in the cavity. When the resonance condition is satisfied energy will be absorbed from the microwave field and detected by additional instrumentation.

The electron spin resonance spectrometer consists of several basic components as shown in Figure 1. The components are as follows:

(1) An electromagnet and magnet power supply with a method by which the field can be swept linearly through the resonance line.

(2) A modulation system that introduces a small alternating component to the sweep of the magnetic field and provides a reference voltage for the phase-sensitive detector used in the detection system.

(3) A sample cavity in which the sample is placed.

(4) A microwave circuit that introduces microwave energy into the cavity and permits monitoring of the reflected energy.

(5) A source of microwave energy that is frequency stabilized and has a power output near 100 milliwatts.

(6) An ESR signal amplifier and a phase-sensitive detector operating at the modulation frequency.

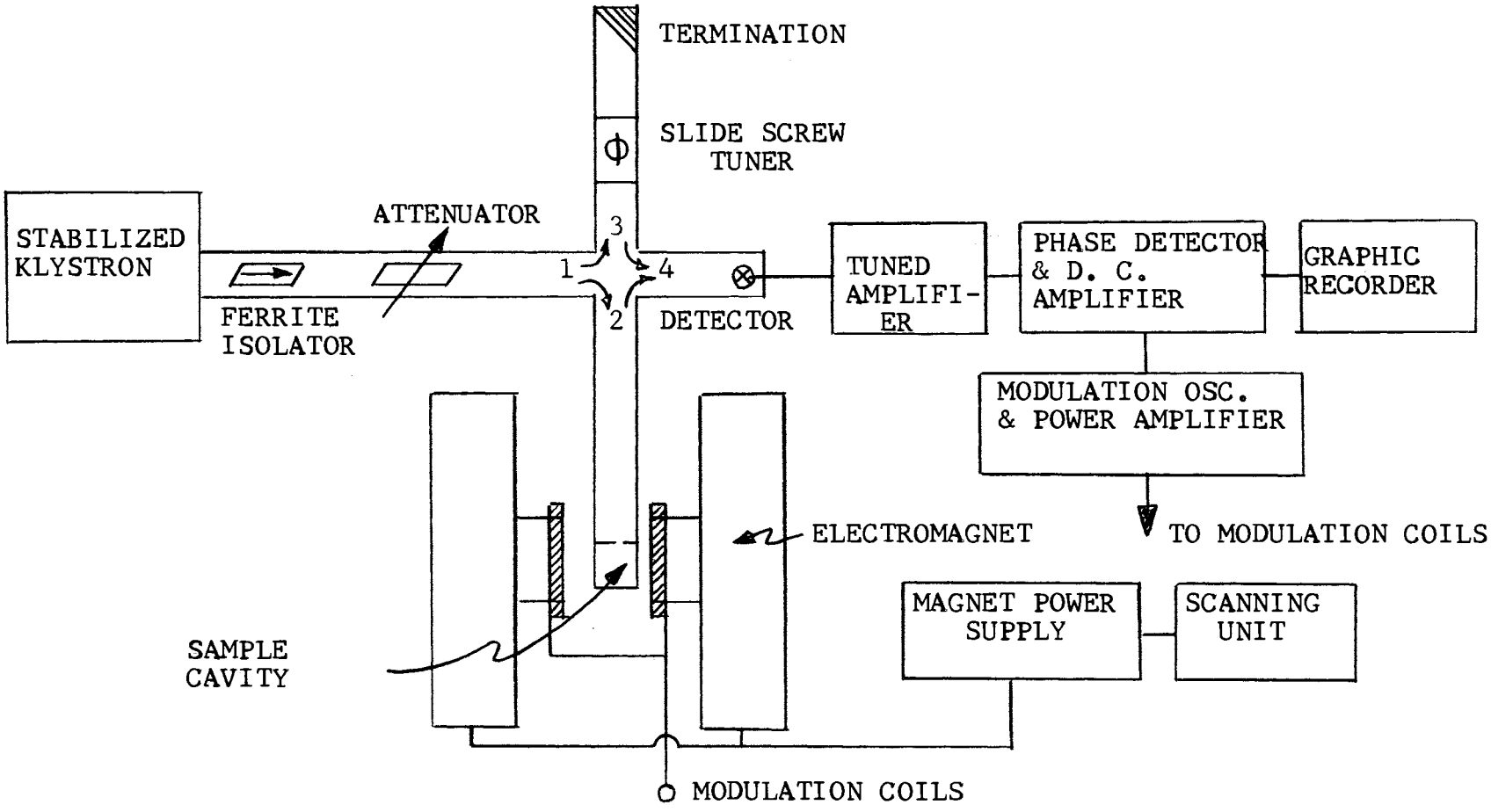

Figure 1. Basic components of an ESR bridge spectrometer. (After Bell (5).)

(7) A graphic recorder or oscilloscope which records the output of the phase-sensitive detector.

These basic components are usually used in one form or another though they may be modified. Additional components are usually included which increase stability and signal-to-noise ratio for increased sensitivity.

The spectrometer used in this research was constructed mainly by Bell of this laboratory using fundamental ESR design techniques (5). It is a microwave bridge spectrometer which utilizes a reflection cavity and consists of many of the components previously mentioned. The complete spectrometer used in this research is discussed in Appendix B, and a brief description of the functions of the different components is given.

CHAPTER II

REVIEW OF SELECTED LITERATURE

Introduction

During the last few years, tremendous advances have been made in the instrumentation of electron spin resonance. These advances have brought about a large diversification of applications of this technique in the fields of Physics, Chemistry, and Biology. High resolution ESR has recently become a powerful technique for investigating even the complex molecular and electronic structure of biological compounds. The high sensitivity and resolution of recently developed spectrometers has made possible many new applications and has yielded data not obtainable by other methods. Electron spin resonance techniques have been applied to biological free radical studies, hemoproteins, and research on tissue structure. New spin label chemicals have been developed which greatly broaden the possibilities for the application of ESR techniques (6).

The literature reviewed in this study will relate only to the biological applications of ESR. Vast amounts of material have been written recently and no attempt will be made to review all of it. Only a brief outline of a few

of the studies will be presented. Early applications and recent developments will be reviewed with major emphasis being placed on those studies which relate to sample irradiation or external treatment of some type, paramagnetic labeling, and hemoglobin molecules.

Most of the work undertaken by the method of ESR has been done on lyophilized samples. The lyophilic drying process (freeze-drying) offers a number of advantages which make it highly valuable for ESR work on biological materials, and this process retains the native properties of the specimens (7). These advantages will be discussed in greater detail in Chapter III of this study.

One of the earliest ESR studies of biological materials was conducted by Commoner, Townsend, and Pake in 1954 (8). They discovered that free radicals can be detected in a wide array of biological systems, and tissues from a number of plants, insects, and animals were lyophilized and investigated using an ESR spectrometer. In 1956 Commoner and others reported on the effects of light on the ESR absorption exhibited by suspensions of chloroplasts (9). They found that illumination of such preparations induced a large and rapid formation of paramagnetic material. These early experiments of Commoner, et. al. pointed the way to a number of ESR investigations of biological materials, but it was not until almost 1965 that a real interest began to develop. Extensive study in this area began in the late 1960's.

In 1965 Vithayathil, Ternberg, and Commoner extended some of the work begun by Commoner in 1954 (10). In his earlier studies, Commoner had found that the free radical content of mouse liver hepatoma was only two-thirds that of normal mouse liver and that certain ESR signals, normally found in animal tissue, were absent in these surviving tumor tissues (8,11). This later paper reported that soon after carcinogenic chemicals were administered to the diet of Holzman rats a transitory free radical appeared in the ESR spectra of their tissues. This new ESR signal was the earliest known specific response to a carcinogenic stimulus.

Most of the signals obtained in these early studies were hard to resolve and exhibited an undesirably low signal-to-noise ratio. Many papers appeared in the literature which seemed to display inconsistant results for similar samples, and the necessity for more standardized methods soon became apparent. More details were required regarding the exact temperature, power level, gain settings, and sample size used in each ESR experiment. The use of a multichannel analyser as a computer to calculate average transients was incorporated by some to improve the signal-to-noise ratio of their ESR spectra (12). The effect of microwave power variations on ESR characteristics was outlined in some detail by Swartz and Molenda, and several papers were written which indicated differing opinions on the effects of air, storage, and freeze-drying (13-18, 3).

The work of Swartz and Molenda led to the use of mic-

rowave power variations as a means of extracting certain valuable information from observed ESR spectra in various biological materials. Vanin and Ruuge undertook a quantitative evaluation of the relaxation parameters of certain paramagnetic centers in 1967 (19). They employed the method of continuous saturation of the absorption signals and rapid passage effects to differentiate various ESR signals and obtain data on the nature of the centers responsible for these signals.

Important work was done in many other areas, and ESR studies continued to increase in numbers. A great deal of interest developed in experiments which might utilize ESR for medically related investigations. In addition to the cancer related work already mentioned, a study in 1965 indicated a variation in ESR absorption amplitude between normal human blood and that from humans with leukaemia. Pavlova and Livenson discovered that the normal ESR spectra from human white blood cells increased by a factor of approximately ten when the donor had one particular type of leukaemia (20).

The discussion just completed has contained a brief review of literature related to various areas of ESR investigation in biological materials and has given the reader some insight into the historical development of this area of study. The paragraphs that follow will give a brief review of ESR work in three more specifically defined areas. The emphasis will be placed on those studies which relate

to sample irradiation, paramagnetic labeling, and hemoglobin molecules. The topic covering paramagnetic labeling will include discussions of the work on the hemoglobin molecule and its derivatives. It will also introduce a new and interesting field concerned with ESR investigations on spin-labeled phospholipids.

Irradiation Studies

In most of the early ESR studies of radiation damage, polycrystalline materials were irradiated at room temperature, and the spectra were recorded. Gordy and his coworkers carried out the most extensive early survey of this kind (21-26). Materials studied included amino acids, peptides, polypeptides, proteins, nucleic acids and their constituents, fatty acids, enzymes, lipids, hormones, mitochondria, various organs, and many others. Most of this work indicated that irradiation produced radical species which were stable for long periods at room temperature and could be detected by ESR.

In 1963, Drew and Gordy reported that paramagnetic gases modify the electron spin resonance spectra of irradiated organic substances (27). In particular, they noted that molecular oxygen, with two unpaired electrons, reacted with protein radicals to cause spectral changes due to radical decay. This work was extended by Henriksen in 1967 (28). He reported that the reaction with oxygen resulted in a transient ESR signal consisting of a single line with

a g-value of 2.007, and a width of approximately 13 gauss. There have been recent attempts to establish, on a molecular level, the relationship, if any, between the effects of radiation and aging on proteins. This work has been directed mainly toward samples of human collagen because a considerable portion of all body proteins is collagen. It has a slow cell turnover rate, and the formation of additional cross-linkages in collagen has frequently been postulated as occurring in aging. Irradiation of collagen samples is reported to produce an ESR signal, and two related studies will be mentioned here.

In 1964 Patten and Gordy reported that irradiating a collagen sample with x-rays produced a doublet ESR signal (29). Two years later Forbes and Sullivan found that collagen irradiated with UV-light displayed a singlet ESR spectrum (30). They collected their samples from Achilles tendons of male and female donors whose ages ranged from 0-30 and 81-90 years. They attributed their signals to unpaired electrons located predominantly on the aromatic nuclei of the tyrosine and phenylalanine residues.

In recent years, the conviction has been growing that radiation damages the vital DNA macromolecule. The importance of DNA in the life of the cell has naturally stimulated several ESR studies of radiation damage in DNA. Many of the papers previously mentioned under the topic of irradiation study have also dealt with samples of DNA. Shields and Gordy reported that the ESR signals in DNA are stable

for several days under vaccum or in dry air, but decay rapidly in moist air (26). They also reported a single line spectrum for their samples while other workers reported more complex signals. The amount of ESR irradiation work done on DNA is very extensive and the reader interested in a more detailed review should consult Wyard's chapter on this subject (2).

In recent years, ESR studies of irradiated biological materials have tended to drift away from polycrystalline samples. Single crystals of the simpler biological molecules have been irradiated and radicals have been produced which were oriented in these crystals. In polycrystalline materials the radicals are not oriented, and the resulting average spectrum is not highly resolved. The spectra of single crystals were found to be very different. They showed many more lines and much narrower lines which allowed quantitative orientation studies to be made (2).

Paramagnetic Labeling

The spin label method involves the synthesis of a stable free radical, usually a nitroxide, which can be located in a particular region of a biological structure. The ESR spectrum of the spin label is then used to obtain information about the region of the structure (6). Spin labels have been useful in a number of ESR investigations in many biological structures. Most, however, involve the labeling of a hemoglobin molecule with a nitrosyl complex.

Nitric oxide is the label used most often, and these studies will be reviewed under the hemoglobin topic. Some other equally interesting studies have been done which label the hemoglobin molecule with some label other than a nitroxide. One such study was undertaken by Bemski, et. al. in 1969 (31). Bemski added $CuCL_2$ to hemoglobin by direct mixing and formed a copper-hemoglobin complex. He reported that the ESR spectrum of Cu(II) bound to human hemoglobin indicated that two cupric ions bind to the hemoglobin molecule. The binding sites are identical and display resolved hyperfine structure. Bemski predicts that these paramagnetic ions will become a useful additional marker for proteins.

Liquid-Crystals

Spin labels have also been useful in developing a new approach to the study of model membranes. In the Varian laboratory, techniques have been developed for producing thin films of oriented phospholipids (liquid crystals) on flat quartz plates (6). Spin-labeled lipids are then incorporated into these films. These impurities become aligned through interaction with the mesophase host molecule. Electron spin resonance may then be used to study both the host and the impurity. Basic properties of the host may be determined from the positioning and subsequent ESR of the impurity (32). In this manner liquid crystals have been shown to be a suitable anisotropic liquid matrix for ESR

studies of dissolved molecules added as impurities. In such experiments the elongated molecules of the nematic phase align along the magnetic field direction. The transitional and rotational motions are those of a liquid, but the alignment provides a directional ordering which prevents the complete averaging of the tensor properties. The resulting residual anisotropy can furnish information about the dissolved molecules, now aligned with the mesophase lattice, and the mesophase solvent (33).

In investigations along this same line, Keith and others found that a living organism could incorporate a spin-labeled lipid into phospholipid complexes within its system (34). They grew an isolated mitochondria on a medium containing the spin-labeled lipid and were able to obtain an ESR signal from the labeled mitochondria. Keith, et. al. used a nitric oxide (NO) labeler in their experiment. Waggoner and others report similar results in working with several nitroxide labels (35). They report ESR signals from the spin-labeled lipids which consist of three lines whose separation, line width, and relative amplitudes are dependent upon the temperature of the lipid during the experiment. Studies have been carried out on thin films by other workers in recent months. Egg lecithin and bovine brain lipids are two substances recently studied (6). All of the investigators mentioned above report that the amounts of cholesterol and water present in the lipid lattice were found to have marked effects on the organization of the

lipid film and, consequently, caused drastic changes in the ESR spectra observed. The reader interested in liquid crystals and their uses should refer to the work of Fergason and others (36-39).

Hemoglobin

Although hundreds of new labels have now been synthesized and are available commercially, the most common labeler is still the paramagnetic nitric oxide molecule. Nitric oxide has an unpaired electron, in a loose orbit, which readily links with complexes of transitional metals. The attachment of (NO) to the diamagnetic compounds leads to the formation of paramagnetic nitrosyl complexes. That hemoglobin reacts with nitric oxide is well known, but there has been some disagreement as to the mechanism of this reaction. Keilin and Hartree reported the most conclusive findings early in 1937 (40). They found that reduced hemoglobin combines with (NO) to form NO-Hb and that oxyhemoglobin must first be reduced to hemoglobin before it can attach (NO). The findings of Keilin and others are widely accepted today.

Since ESR was introduced for the study of molecules of biological interest, hemoglobin and myoglobin have been the most extensively studied metalloprotein. Most of these investigations have dealt with nitric oxide, adult, hemoglobin.

In 1967 Shiga and others studied the isolated Alpha

and Beta subunits from human adult hemoglobin and found that subtle changes in heme-NO linkage in subunits of different structures resulted in marked alteration of the ESR spectrum of the NO-derivatives (41). Much of the early work with nitrosyl complexes of heme-iron obtained different spectra parameters. Vanin and Chetverikov attempted to find the reasons for these discrepancies and published a report on their findings in 1967 (42). They found that, in many cases, the workers were looking at complexes formed with non-heme iron. They indicated that the nitric oxide probably attaches to the vacant coordination site of the heme complex and that these vacant sites are different in heme and non-heme iron. These studies were extended and broadened by the work of Kon in 1968 (43). He reported that the unpaired electron was not localized on the (NO) group as previously assumed but was instead loosely associated with the nitrogen in the NO. The ESR spectrum showed rhombic symmetry about the paramagnetic center.

The reader interested in a more extensive review of the related literature, up to and including 1969, should refer to the book by Wyard (2).

CHAPTER III

SAMPLES AND SAMPLE PREPARATION

Bovine Anaplasmosis

Bovine red blood cells which were highly parasitized with anaplasma protozoan bodies were one of the three primary samples used in this study, and a brief description of the disease will be given in the paragraphs which follow. The discussion will be limited to brief comments on the symptoms, transmission, and stages of the disease.

Symptoms

Cattle of all ages are susceptible to bovine anaplasmosis, but the severity of the disease and the frequency of fatalities is directly related to increased age (44). Some of the more obvious signs of anaplasma parasitemia involve the absence of skin color due to a loss of blood. This pallar is especially noticable on the nose, udder, mucous membranes of the eyes, and vulva of the female. If a vein is punctured a thin watery blood is revealed. The loss of red blood cells causes anemia which results in weakness, depression, and physiologic adjustments of the respiratory and circulatory system. These recogniz-

able signs do not occur until 40 to 50 percent of the total red blood cell mass is lost (45). Signs of respiratory and circulatory adjustments to these red blood cell losses usually include increased pulmonary ventilation and increased cardiac rate. The increased ventilation is necessitated by the subsequent decrease in normal oxygen transport (45). Loss of appetite, lowered production, and weakness are observed and, in advanced cases, muscle tremors, weight loss, and dehydration are common. Loss of adequate oxygen to the brain occurs in many animals and they become restless and excited. The feces are usually bile stained and diarrhea may occur. If the animal is placed under circumstances of stress, heart failure may occur. These stress conditions may result from restraint, exercise, treatment, or extreme obesity (45). Death results from cardiac failure which is usually immediately preceeded by weakness, tremors, rapid and irregular heart beat, a weak pulse, and, often, a subnormal temperature. Mortality rates vary from almost none in the young to 60 percent or more in adult and aged animals. Deaths seem more frequent in fat animals than in lean animals, and the disease is fatal to bulls more often than cows. Some deaths have occurred in young cattle when circumstances of extreme stress were experienced. These circumstances include castration and other such traumatic treatments (44). Temporary infertility has been observed in bulls infected with the disease, and cows infected during advan-

ced pregnancy frequently abort (45).

Signs of a decline in the parasitemia, which indicate an animal has begun convalescence, include return of appetite, heavy drinking, normal body temperature, and, frequently, a depraved appetite, exhibited by eating dirt. These symptoms should be recognized and precautionary measures employed as treatment at this time could be extremely hazardous.

Transmission

Anaplasmosis is transmitted mainly by arthropod vectors (46). The most potent source of infection to other animals is a cow with acute infection, but since anaplasma bodies survive for extended periods in certain ticks, these arthropods act as a secondary source of infection. The carrier cattle act as reservoirs from which mechanical and biological transmission can occur.

Mechanical transmission usually refers to infection from blood sampling needles or other instruments that might be used on several cattle, but it can refer to transmission from some mechanical vector. Transmission of the disease by mechanical means over distances greater than a mile is highly unlikely, and if the time interval between feedings or injections is more than five minutes, the infection will not be transmitted (46).

Biological vectors, on the other hand, retain viable anaplasma bodies for long periods. The organisms are

passed through different development stages of ticks and tick eggs. Biological transmission can occur from several days to several years after initial infection of the tick. Tick-infected pastures cannot be considered free from anaplasmosis for at least six years after the disease has occurred (46).

Vectors involved in anaplasmosis transmission include nineteen species of ticks, nine species of horseflies and deer flies, two genera of mosquitoes, and some stable flies. Isolation of infected animals can be an effective means of retarding transmission, but, in areas where ticks transmit the disease, wild-life transmission makes isolation impossible. Pastures may be, or may become, contaminated with vector ticks capable of infecting cattle or deer.

Anaplasmosis is found in 40 states to some degree, but disease incidence is highest on the Pacific coast, in the inter-mountain states, in the Mississippi Valley, on the Gulf Coast, and on the southern Atlantic Coast. Cases are more frequent in the summer and fall when the vectors are active. In warm climates cases may be observed throughout the year.

Stages

Anaplasmosis is manifested by a rapidly progressive anemia which invokes a certain characteristic syndrome. This syndrome may be divided into a prepatent period, a period of increasing anemia, maximal anemia, and convales-

cence (47). The first period extends from the time of infection until parasitemia is clearly evident. This usually takes from three to six weeks. The location of Anaplasma marginale during this period is not known, but the presence of initial bodies in the plasma has been postulated (44).

The patent period of the disease is indicated by the appearance of anaplasma bodies in the circulating red blood cells. The manner in which these cells are infected is not known, but invasion of mature red blood cells by initial bodies from the plasma has been suggested. Parasitized cells are rapidly removed from the circulation and maximal anemia occurs about two days after peak parasitemia. The removal of the infected red blood cells results from phagocytosis by the reticuloendothelial system, especially the spleen. The number of infected cells doubles daily for several days and the anemia advances in a parallel manner. Animals frequently lose as much as 75 percent of their circulating red blood cells (3 to 6 gallons of whole blood) (48).

After peaking out, the parasitemia declines as rapidly as it increased, and amounts of greater than 1 percent of the total red blood cell mass do not remain infected more then three weeks. Convalescence usually last about two months and 75 percent of the preinfected red blood cell mass is replenished in about three weeks after the time of maximal anemia.

Infected red blood cells used in this study were obtained from Fort Dodge, Iowa through the cooperation and assistance of Dr. I. Anderson and Dr. E. W. Jones of the Department of Veterinary Medicine and Surgery-Clinical Research at Oklahoma State University. All samples came from adult female Holsteins and were about 50 percent infected with Anaplasma marginale.

Red Blood Cell Components

All of the primary samples used in this investigation were red blood cells or red blood cell components, and a brief discussion of this cell and some of its major parts will be presented. The discussion will be limited to the normal red blood cell, normal adult hemoglobin (Hb-A), and fetal hemoglobin (Hb-F). The author will not present any of these topics from a theoretical approach as such a discussion is beyond the scope of this study. The physical properties, similarities, and variances of these major components will be briefly outlined.

Red Blood Cells

The red cell is a biconcave disc approximately 7.5 microns in diameter and 2.5 microns thick which is smaller than most nuclei of other cells. There are some $5x10^6$ red cells in a mm^3 of normal human blood (49). They have an average life span of 120 days in a normal system but can have much shorter life spans in cases of blood abnormalities

(42 days with sickle-cell anemia)(50). Red cells are individually straw-colored but appear red in the blood when they stack up like poker chips. They are not true cells as they contain no nucleus at maturity. The cytoplasm of the red cell is made up largely of hemoglobin and water in a semi-permeable membrane.

As previously mentioned, the mature red cell does not have a nucleus and cannot go through the division process of mitosis. It travels through the body for approximately 120 days being slowly worn away by constantly colliding with the walls of its various pathways. When the red cell membrane wears out the body disposes of the heme by breaking the porphyrin ring and taking out the iron, which stays in the body to be used in making a new heme, leaving only a red and green substance (bile pigment) in the blood. These pigments are extracted from the blood by the liver and leave the body.

Hemoglobin-A

The hemoglobin molecule is a protein and each hemoglobin molecule is about 7 millimicrons in diameter. The hemoglobin is the iron containing red pigment which colors the red cell. Its function is to carry oxygen and CO_2 in the blood stream, and each red cell contains approximately 270×10^6 hemoglobin molecules. About 95 percent of these will have oxygen attached to the heme molecule iron atoms each time the red cell leaves the lungs (49). The hemoglo-

bin molecule is made of essentially two separate parts, the heme group and the globin.

The active centers of the hemoglobin are the four heme groups. Each is a protoporphyrin ring which has at its center an iron atom in ferrous state (Figure 2a) (51). The iron is held by coordination with the four nitrogen atoms of the ring. When the whole group is connected properly to the globin chain, the iron atom is able to reversibly combine with molecular oxygen. The iron would then be oxidized to ferric iron (methemoglobin) if it were not for the presence of the enzyme (methemoglobin reductase) which constantly reduces the iron back to the ferrous state. This reductase is one of the few non-hemoglobin proteins in the mature red cell and makes up less than 2 percent of the proteins available (98 percent of all red cell protein is hemoglobin of only one type) (51). One of the ways changes in the hemoglobin state will show up is in the optical absorption spectra of the hemoglobin molecule (Figure 2b). The spectrum shown is for normal hemoglobin in the methemoglobin (oxidized) state. Any variations in the hemoglobin structure would show up as shifts and abnormal peaks in the spectrum. This typical spectrum, with low absorption in the 590mμ to 620mμ, gives the normal hemoglobin its reddish color. In oxyhemoglobin and hemoglobin (iron in the ferrous state) the small absorption rise from 620mμ to 630mμ would not be present. This absorption in the methemoglobin (ferric form) gives it a more brownish red

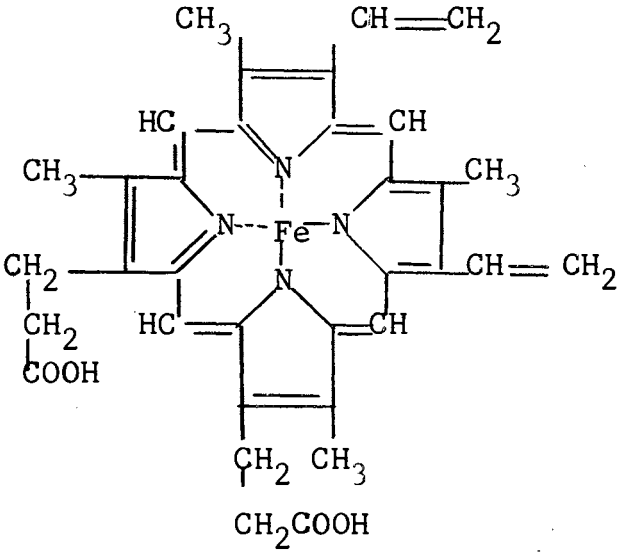

(a) The Heme Ring (Ferrous State).

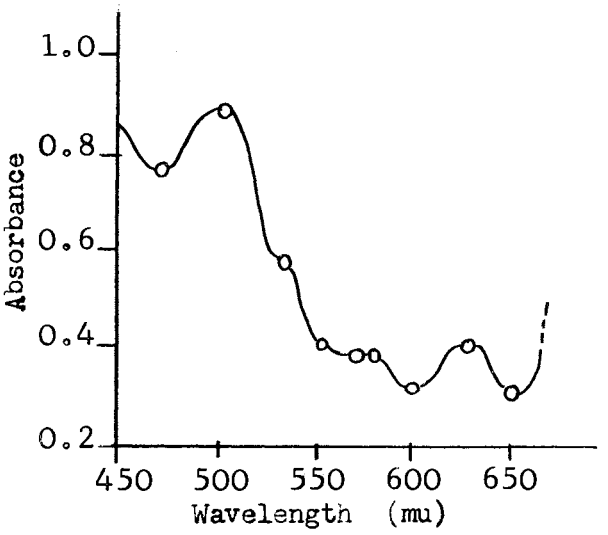

(b) Methemoglobin Spectrum.

Figure 2. The Heme Ring (a) and Methemoglobin Optical Spectrum (b). (Source: Ingram (51))

color than the ferrous forms which are brighter red.

The globin is the protein part of the hemoglobin and makes up some 95 percent of the total volume. It is composed of four polypeptide chains each of which is made up of a long linear array of amino acids. The specific arrangement of these amino acids is very important and any change will cause an abnormal blood trait. Normal adult human hemoglobin (Hb-A) has 560 amino acids. The four we are interested in are aligned as follows: theonine; proline; glutamic acid; glumatic acid. If some mutation in the DNA (deoxyribonucleic acid) molecule causes just one of these amino acids to be replaced, an abnormal condition will exist. If the chain is altered as follows: theonine; proline; valine, glumatic acid; hemoglobin-S (sickle-cell anemia) will be produced. If the glutamic acid is replaced by lysine instead of valine then hemoglobin-C will be the result and so on. The reader interested in a more detailed model of the hemoglobin molecule should consult the study by Perutz and others (52).

The spin state of the central Fe atom is closely related to the ligand bound to these macromolecules. Ferrous iron of hemoglobin in arterial blood is low spin while it is high spin in venous blood. The g-values for high spin Fe^{3+} are 6 and 2, while low spin Fe^{3+} g-values are approximately 2.7, 2.3, and 1.8(53). These values are for separated human adult hemoglobin at the temperature of liquid helium. The values are those reported by Tasaki in

1970 (53).

Hemoglobin-F

The first abnormal hemoglobin to be discovered was fetal hemoglobin, the hemoglobin of the newborn, in 1866 (51). It differs from Hb-A in its ultraviolet absorption pattern, its alkali resistance, and its amino acid composition. Fetal hemoglobin displays a well resolved tryptophane absorption band at 289.8mμ while Hb-A displays only a slight inflexion at about 291.0mμ. The visible and infrared absorption spectra of the two hemoglobins do not show significant differences(54). The alkali resistances of the hemoglobins, and other chemical differences, will not be discussed here but complete treatments of these subjects may be found in the literature (see for example Ingram, Roughton, or Perutz (51,55,52)).

The amino acid composition of human Hb-F shows the characteristic number of four amino end groups and therefore four peptide chains. Two of the chains are identical to the Alpha chains of the Hb-A atom and begin with the Valine-Leucine amino acids. The other two chains differ from the Beta chain of Hb-A as they do not begin with the Valine-Histidine-Leucine amino acids. These two chains in Hb-F begin with a Glycine in place of the Valine and are called Gamma chains (51). The heme groups of these Hb-F molecules would therefore connect differently to the globin chains and the iron would be in abnormal surroundings.

These abnormal surroundings in its protein enviornment would probably cause changes in its ESR absorption. In the present study a significant difference was noted between the ESR of Hb-A and Hb-F(see Results and Observations cited in Chapter IV). This observation on Hb-F has not been cited elsewhere in the literature to date, but other workers have reported variances in the ESR signals for one other abnormal type of hemoglobin. Hayashi, et. al. investigated the ESR spectra of Hb-M, in which the normal histidine residues of Hb-A are replaced by tyrosine residues, and found a slight variance displayed in the ESR spectra. They attribute these variances to changes in the oxidation state of two of the iron atoms (56,57).

Chernoff and others have established that Hb-F is the major hemoglobin in neonatal man and that it makes up as much as 85 percent of the total amount (58). They indicate that the content of fetal hemoglobin in the adult human decreases to less than 1 percent. There has been some indication in the literature that the presence of fetal hemoglobin during the first three or four months after birth plays a significant part in the resistance of newborn children to malaria (59). Work done by Lee, Odell, Jones, and others at Oklahoma State University has indicated that the amount of Hb-F in cattle ranged from 68.7 to 97.1 percent in newborn calves. Their data also indicated a rapid decline in Hb-F with aging and they report less than one percent in cattle 22 weeks old.

Lee, et. al. indicate that the percentage of Hb-F and the resistance to Anaplasma marginale infection decrease simultaneously in calves. The presence of fetal hemoglobin may play an important role in the resistance of neonatal calves to anaplasmosis.

Methods

The infected bovine red blood cells used in the study were obtained from Fort Dodge Laboratories, Fort Dodge, Iowa. In almost all cases the samples arrived at the Oklahoma State University Veterinary Medicine and Surgery-Clinical Research Laboratory on the same day the infected cow was bled. All normal adult and fetal bovine red cell samples came from the Oklahoma State University dairy barn.

The samples were collected using either heparin or dipotossium ethylene diaminetetraacetate (EDTA) as an anticoagulant. They were then washed by centrifuging at 1750 rpm for 20 minutes while in an isotonic saline solution (0.85gm NACL to 100ml distilled water) with a ph of 6.5-7.0. This process was repeated at least three times for each sample collected. The spinning process also separated the whole blood components into layers in the centrifuge test tubes. The red blood cells were packed in a loose layer at the bottom, the white cells were in a thin layer on top of the red cells, and the wash and other components were in a relatively liquid layer at the top. For this study, only the red cells were needed and all other com-

ponents were drawn off and discarded after each wash. After three washings most white cells and other components had been effectively separated from the red cells.

For some parts of the study, the red cell membrane was desired, in a separated state, free of other red cell constituients. To accomplish this final separation, the isolated red cells were completely hemolyzed (broken-up) by violent mixing with non-isotonic distilled water. After hemolyzing, the red cells were spun at 35,000 x g for fifteen minutes. The process was repeated several times to insure complete hemolysis. The red cell membranes were tightly packed on the bottom surface of the centrifuge test tubes, and the hemoglobin and supernate were in liquid form above. The membranes were then washed repeatedly, by the process previously discussed, until all traces of supernate and hemoglobin were eliminated.

Paramagnetic impurities in the sample, sample holder, or associated apparatus could produce unwanted ESR spectra. Extensive checks were made of all the materials mentioned above to be certain they were free of such signals.

Lyophilization

In order to observe ESR absorption in the biological samples used in this study, it was necessary to develop new techniques for sample preparation. The samples had to be lyophilized because water radically reduces the signal size due to its large dipole moment with respect to the

microwave electric field (3). The higher the microwave frequency the more this effect is noticed. It was therefore necessary to design and build a lyophilizer specifically suited to the sample size and control demands of this study. It was necessary to establish an accurate measure of sample drying time in order to standardize our sample humidity and thus prevent small variations in moisture content from producing large changes in signal size and shape. The system designed for the study is shown in Figure 3. The samples had to be sealed, after drying, without exposure to the atmosphere. In order to do this, the lyophilizer was flooded with dry argon filtered through a molecular sieve Type-5A. The argon was introduced after the drying cycle was completed, and it was kept at a continuous high flow rate to prevent the samples from being exposed to the atmosphere. The samples were sealed with a soft wax and capped with a quick drying, non-venting glue before being removed from the lyophilizer. They were then stored at $0^{o}C$. The sample tubes used in the study were fused-quartz tubes of 3mm I.D. and 4mm O.D.. They were especially suited to fit into the small space available in the microwave cavity of the ESR spectrometer and were ordered from Varian Associates, Palo Alto, California.

An average pressure of $5x10^{-4}$mm Hg was maintained during the drying process, and the samples were kept at a low temperature until they ceased to out-gas. The temperature was kept at either $77^{o}K$ (liquid nitrogen) or approximately

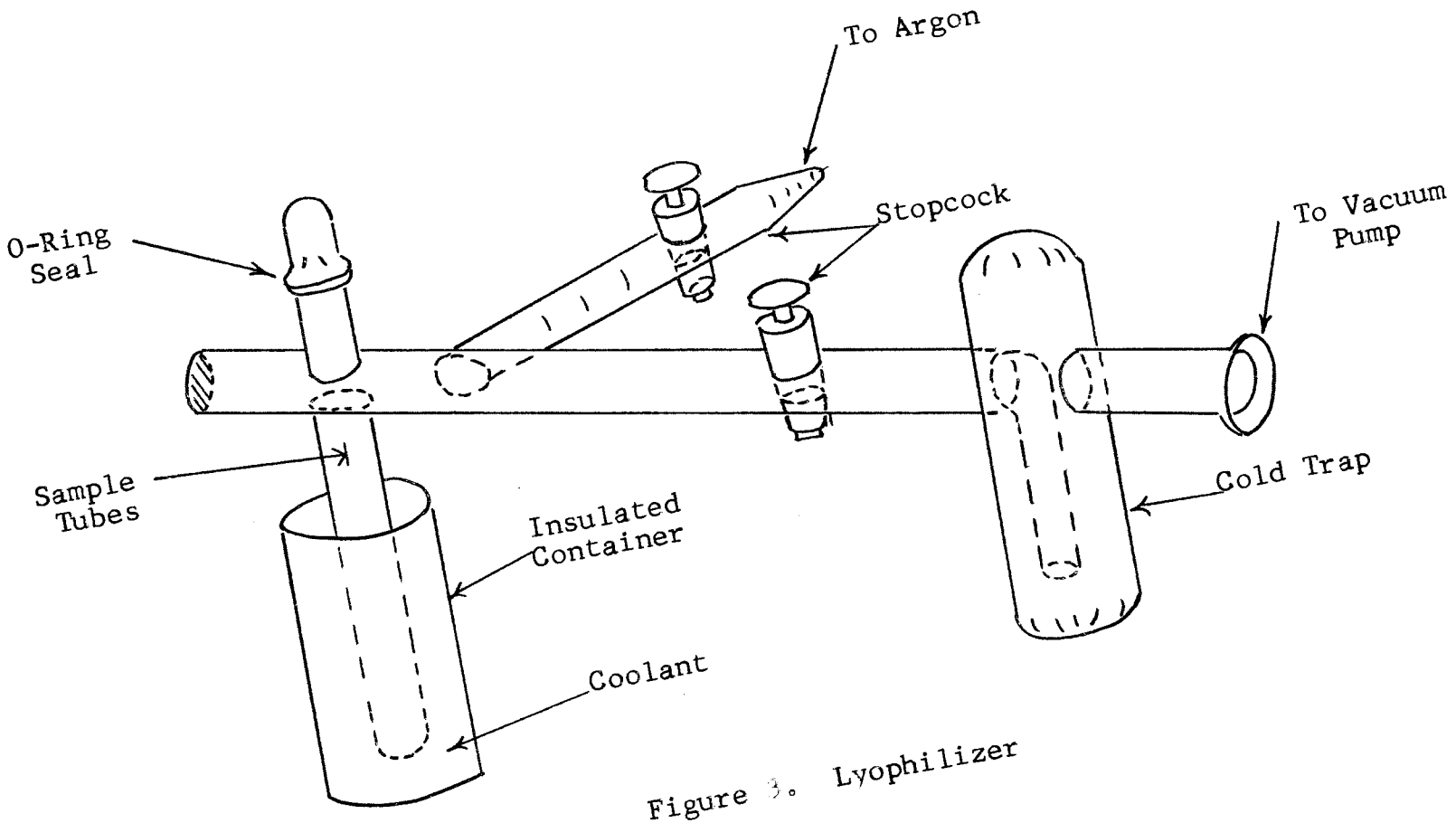

Figure 3. Lyophilizer

-60°C (dry ice and acetone). The latter method was found to give better results and reduce the drying time by more than half. Using dry ice and actone, in a container similar to the one shown in Figure 3, a temperature of -60°C was maintained for more than 12 hours without replenishing the coolant.

A sample volume of .0555cc was found to be optimum for efficient drying while still being large enough to give an ESR absorption signal of sufficient amplitude. A maximum of six quartz tubes, containing .0555cc of sample each, could be placed into the lyophilizer at one time. Insertion and removal was accomplished by removing the cap and o-ring seal shown in Figure 3. Drying time varied with temperature and amount of sample material in the system and averaged about 21 hours for a maximum load (6 samples) at -60°C.

CHAPTER IV

RESULTS AND DISCUSSION

General Remarks

Remarks on Experimental Observations

The ESR spectra of normal red cells and separated red cell components were obtained and standarized using samples from newborn and mature bovine and human donors. After sample preparation and lyophilization techniques had been developed and systemized, infected adult, normal adult, and normal fetal bovine red cells and red cell components were investigated. The infected samples were obtained from cattle highly parasitized with anaplasma protozoan bodies. A comparison was made between the ESR spectra of the various samples, and their spectroscopic splitting factors (g-values) were calculated. The samples were then subjected to various external treatments to determine the effect of such treatments on their ESR signal. Ultraviolet and x-ray irradiation, nitric oxide paramagnetic labeling, heat exposure, and atmospheric contamination were each used as individual external treatments on all samples. All of the red blood cell samples used in this study displayed ESR absorption signals near $g \simeq 6$ and $g \simeq 2$. Only the signals near $g \simeq 2$

will be discussed as they were of primary interest in this investigation. The samples were lyophilized polycrystalline (powered) materials. In polycrystalline materials the ESR signal sources are not oriented in any preferred direction, and the resulting average spectra are not highly resolved. All of the samples used in this study displayed three characteristic peaks of this nature near $g \simeq 2$. Differences were observed in the relative splitting and positioning of the peaks, and their g-values were different.

All data was taken at room temperature although some of the runs during the standardization process were made at approximately $77^{o}K$ (liquid nitrogen). Liquid nitrogen temperatures did not reduce the broadening of our signals enough to warrent further observations at this temperature (53).

A description of the samples used, the ESR spectrometer power and gain settings, and any other pertinent information will be given as each sample is discussed.

G-Value Calculations

The g-value and its relationship to ESR absorption signals were discussed in detail in chapter one of this study. A brief review of its properties will be given here, and the methods used to calculate the g-values determined in this study will be discussed.

The spectroscopic splitting factor (g) is given by

$$g = \frac{\gamma \hbar}{\beta} \qquad (4.1)$$

where (β) is the Bohr magneton ($\frac{\hbar}{2mc}$), (γ) is the gyromagnetic ratio and ($\hbar$) is Planck's constant divided by 2π . The microwave frequency required for a resonance transition is given by

$$\omega_o = \gamma H_o \qquad (4.2)$$

where (ω_o) is the angular frequency of the radiation energy, and (H_o) is the value of the externally applied magnetic field at resonance. When equations (4.1) and (4.2) are combined, the equation for (g) becomes

$$g = \frac{\nu_o h}{\beta H_o} \qquad (4.3)$$

where $\nu_o = \frac{\omega_o}{2\pi}$ represents the microwave frequency at resonance.

The position of the ESR absorption signal on the recorder trace was used to locate the value of the magnetic field at which resonance occurred, and the frequency of the stabilized, reflex klystron (VA 201B) was measured with a h/p 524D electronic counter. These values were used to calculate g, and a discussion of the related components can be found in Appendix B.

In order to use the position of the ESR signal on the recorder trace to locate the value of the magnetic field, the exact scan rate of the magnetic field during each run had to be determined. The value of the field at several points on the trace was measured using a nuclear magnetic resonance (NMR) detector. The detector probe was supported by a clamp around one of the magnetic pole pieces, and the

frequency of the NMR oscillator was measured with the h/p 524D. The frequency of the oscillator is related to the proton resonance, and the relationship between this frequency and the magnetic field is given by

$$H = \frac{2\pi}{\gamma_p} \nu_p = 2.34868 \times 10^4 \nu_p \qquad (4.4)$$

where γ_p 2.67530×10^4 radian sec^{-1} $gauss^{-1}$ is the gyromagnetic ratio of the proton (60).

A nuclear magnetic resonance absorption frequency was measured and recorded for nine locations on the recorder trace during each run. Each location was marked on the trace using a keying switch which induced a short duration signal at the recorder. The displacement of each mark was measured and recorded with the NMR frequency at that point. The scan rate was computed from the slope of the frequency vs displacement graph obtained from this data.

If the field inside the sample cavity had been of the same value as the field outside the cavity (at the NMR probe), the value of H_o could have been taken directly from the graph discussed above. The field inside the cavity was found to differ by an appreciable amount however, and it was necessary to calculate a field correction factor for each run.

If the value of H_o were exactly known for some sample with an ESR absorption near the ESR absorption of the samples used in the study, it would be possible to include this sample as a reference in each run. The known value

of this reference signals H_o could be compared with the value of H_o found from the scan rate graph, and a field correction factor would be represented by the difference $(H_{oref}-H_o)$. This correction factor could be added to, or subtracted from, each point taken from the graph. The field correction factors used in this study were calculated in the manner discussed above. Diphenylpicrylhydrazyl (DPPH) was used as a reference sample. The value of H_{oref} for each run was calculated using a known DPPH g-value of 2.0036 and the measured klystron frequency (9.1 GHZ). An example of a reference data run, showing the scan rate marks and the DPPH ESR signal, can be seen in Appendix D (Figure 31).

A standard FORTRAN IV program was written and employed to calculate all of the values mentioned above. The program was written in three parts. The first part is the main program. It contains all reading and writing functions, and invokes the two subroutine subprograms. The second part is the subroutine used to calculate the scan rate. It applies a least-squares fit routine to the frequency and displacement data for each run, and computes the slope of the resulting relationship. The third part is the subroutine used to calculate field values, field correction factors, and g-values.

The complete program and a sample of output data is presented in Appendix C.

Data Presentation

The actual recorder graphs could not be photographed directly because of the color of ink used in the recorder pen. Therefore, it was necessary to trace the actual graphic representations as accurately as possible and use these tracings to represent the data runs for this study in the body of the text. Since it was desirable to include actual copies of selected recorder graphs showing all noise and exact signal ratios, these were Xeroxed individually and appear in Appendix D of this study.

The representations presented in the body of the text, and the actual recorder graphs in Appendix A, are fully documented with conditions maintained during the run. The scan rate, microwave power, signal amplifier gain, signal modulation amplitude, detection phase, and calculated g-values are listed for each run.

Observations

The observations made during this study can be divided into six distinct phases which parallel the investigative stages of the study. The data will be presented, and the findings discussed, under the subtopic which relates to that stage of the investigation. The subtopics include standardization, initial sample investigation, and the four external treatments (irradiation, paramagnetic labeling, heat treatment, and atmospheric contamination).

Standardization

In order to observe ESR absorption in the biological materials used in this study, it was necessary to develop new techniques for sample preparation and signal detection. Samples displayed variations in signal size and shape which were dependent upon the amount of sample, dryness of the sample, temperature of the sample before and during runs, and gain and modulation settings on the ESR spectrometer. The spectra selected represent only a small portion of the two to three hundred data runs taken and are presented here only as a general indication of the types of signals obtained at the beginning of the study. As new techniques were developed and put into practice, the quality of the signals improved. This phase of the investigation was not terminated until consistently noiseless signals could be reproduced several times with identical size, shape, and g-values.

Figure 4(a) shows one of the early signals obtained from a sample of separated red blood cells from a fetal calf (3-4 days old). The blood was collected in EDTA, dried, and stored at $0^{o}C$ for 15 days before the run was made. The signal-to-noise ratio is very poor, and the shape of the signal cannot be determined. Figure 4(b) shows a signal obtained from samples of the same type. This sample was dried and sealed more effectively and shows much more detail and less noise. The instrument settings for

(a) Poor Seal

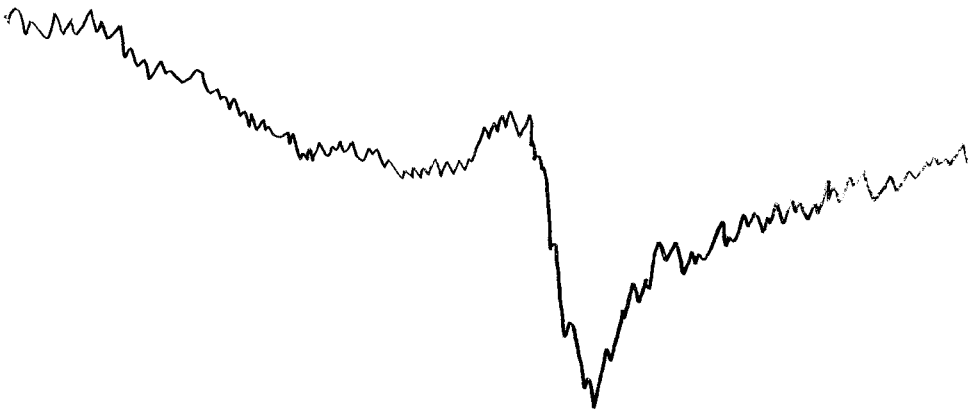

(b) Better Seal

Figure 4. Early fetal red cell ESR spectra. (a) gain was 5x100, M.A. was 4x100, -10 db, (b) gain 6.3x100, M.A. 5x100, -10 db.

runs 4(a) and 4(b) are shown on the figures. Two additional signals from samples similar to those in Figure 4 are shown in Figure 5(a) and 5(b). These samples were run after better drying techniques had been developed. Figure 5(a) shows a spectrum run at 77°K. The sample size used was the same as that used in Figure 4. Each of these runs were made with approximately 0.025cc of separated red cells in the sample tube (before drying). Figure 5(b) is the spectrum of a sample run at room temperature. The drying technique was the same as that used in 5(a) but the sample size was .055cc. This amount was found to be optimum and allows rapid and complete drying while still giving a large resonance signal. Both 5(a) and 5(b) were run using a magnetic field scan-box setting of 162-1. Therefore, they should both display the same resultant scan rates, and their signals should compare directly, just as their g-values do. Figure 5(a) shows a scan rate of approximately 17 gauss/inch while Figure 5(b) has a 23 gauss/inch scan rate. Because constantly varible scan rates were experienced on identical scan box settings, it was necessary to calculate the scan rate for each data run individually. Therefore, many signals could not be compared directly and it was necessary to first compare their respective scan rates and then scale them to an equal number of gauss/inch.

Separated red cell membranes were also investigated. They were obtained by hemolysis of the red cells as explained in Chapter III. Figure 6(a) represents one of the

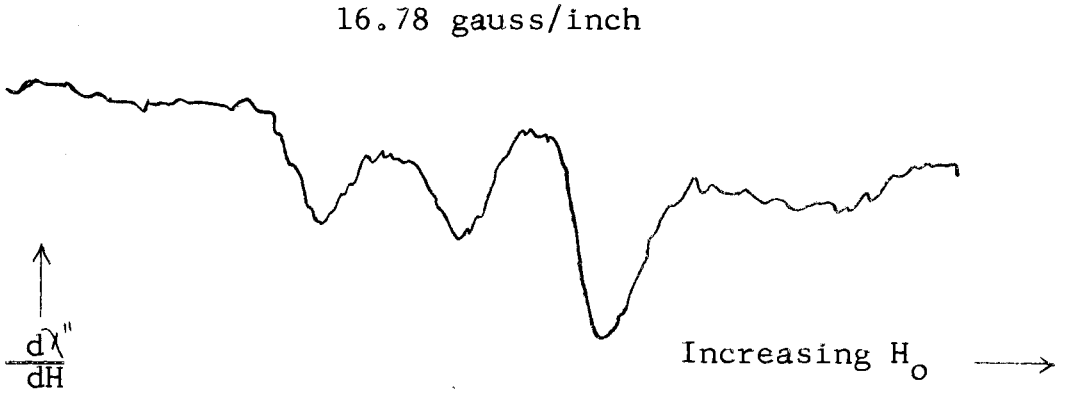

(a) 77°K, 0.025cc

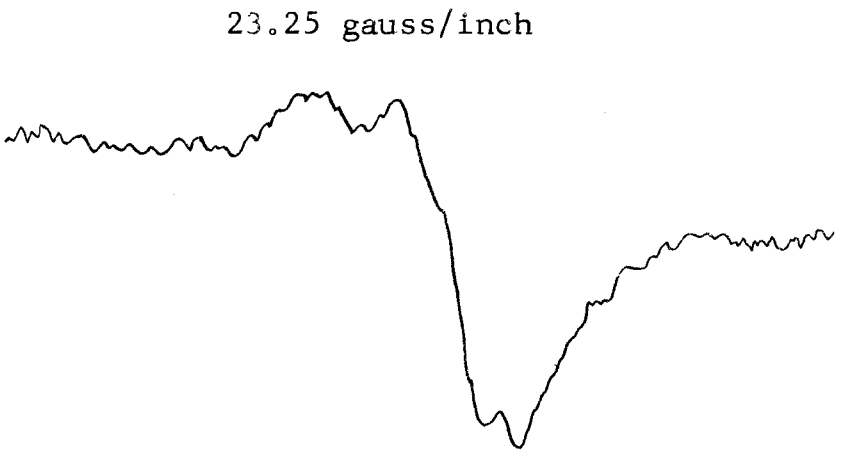

(b) 25°C, 0.055cc

Figure 5. Later fetal red cell ESR Spectra. (a) gain 5x100, M.A. 4x100, -15db, (b) gain 5x100, M.A. 4x 100, -15db.

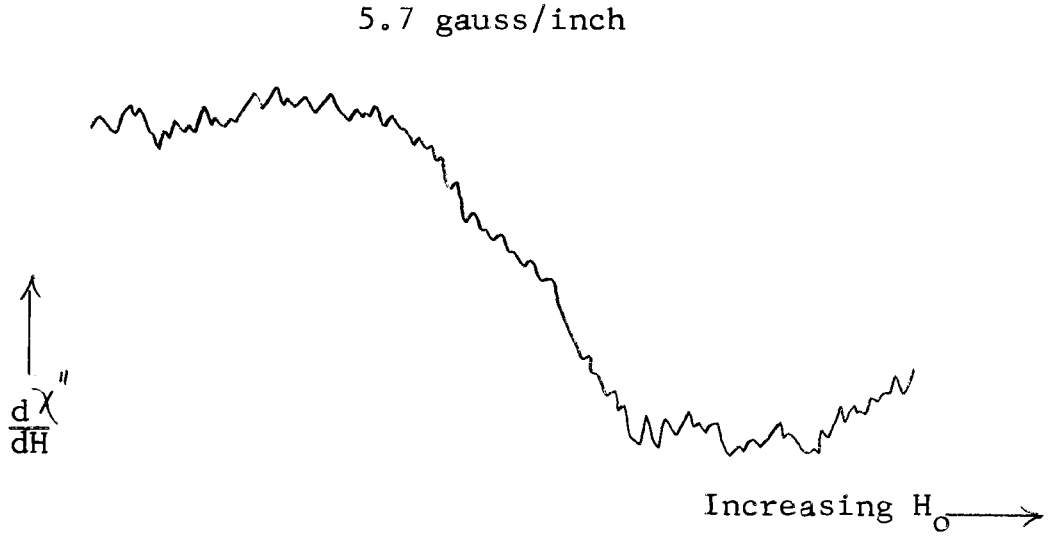

(a) Early run

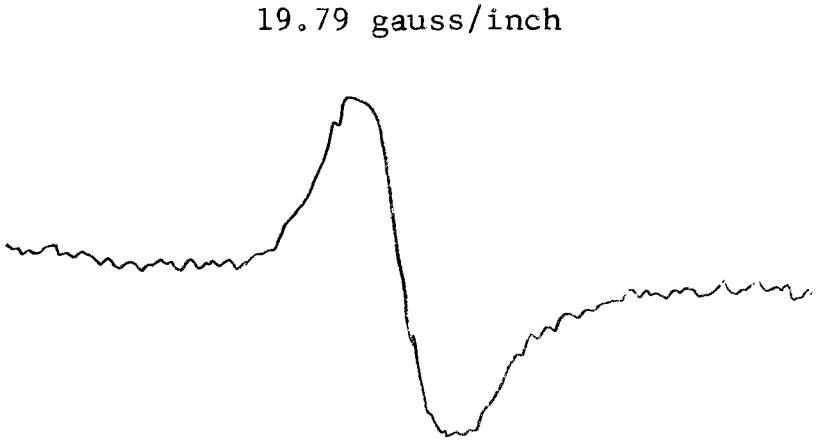

(b) Later run

Figure 6. ESR Spectra-Red Cell Membrane. (a) gain 6.3x100, M.A. 4x100, -15db, (b) gain 5x100, M.A. 4x100, -15db.

early runs on a red cell membrane sample. The membranes were separated from a large sample of red cells obtained from a normal adult female bovine. Heparin was used as an anticoagulant and the sample size was approximately 0.055cc before drying. The signal is very small, and the signal-to-noise ratio is unsatisfactory. The poor qualtiy of this signal was caused by improper drying techniques. Red cell stroma (membrane) in a separated and packed state are more difficult to dry properly as some water is trapped between the inner and outer layers of each membrane. They also appear to absorb moisture from the atmosphere more rapidly than an equal volume of whole red cells and must be sealed much more carefully. Figure 6(b) represents a later signal of the same sample size. The scan box settings were the same for both runs.

This investigation concentrated primarily on bovine red blood cells and bovine red blood cell components, but, during the standarization phase, many other samples were run for comparison purposes. Figure 7 represents the spectra of two of these secondary signal sources. Figure 7(a) is the ESR spectrum of unirradiated collagen. The sample was obtained from the tail of an adult female white rat. It was washed in a cold saline solution and then cooled to 77^{o}K. Liquid nitrogen temperature was maintained until lyophilization was completed. The ESR absorption of human red blood cells from a 29 year old male donor is shown in Figure 7(b). Heparin was used as an anticoagulant and the

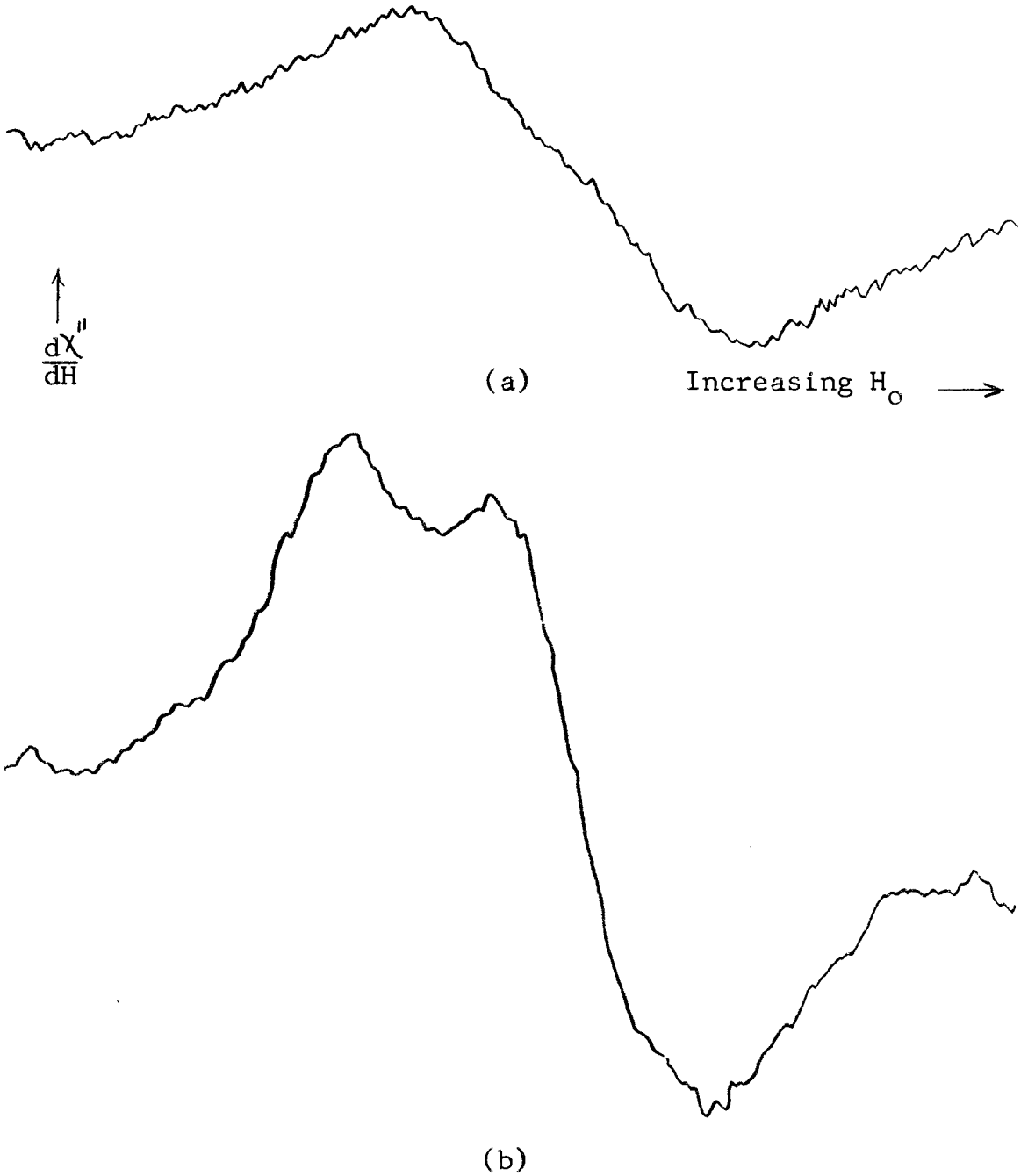

Figure 7. Secondary Signal Sources. (a) rat tail collagen, gain 4x100, (b) human red cell, gain 5x100, M.A. 4x100, -15db on both runs.

sample size was 0.055cc before drying. These runs were made near the end of the standardization phase, and the signal-to-noise ratio is good, showing only a small noise level.

Initial Sample Investigation

The ESR absorption spectra of normal and infected adult and normal fetal bovine red blood cells were investigated extensively before external treatments were applied. Figure 8 shows the results of runs on normal and infected adult bovine red blood cells. The dashed line (Figure 8a) represents the ESR absorption of Anaplasma marginale infected red blood cells. Parasitemia was evident in 54 percent of the donors red cells. The sample was obtained from a 4½ year old female Holstein and was furnished by Fort Dodge Laboratories through Dr. Ian Anderson and Dr. E. W. Jones of the Department of Veterinary Medicine and Surgery-Clinical Research at Oklahoma State University. Figure 8 (b) (solid figure) is the spectrum of red blood cells from a normal adult female Holstein. Heparin was used as an anticoagulant in both samples and sample size was 0.055cc before drying. The scan rates of these two runs were approximately equal (6.41 gauss/inch) and the signals could be compared directly. The similarity shown in Figure 8 was found to exist in all runs of normal and infected adult bovine red blood cells. The splitting between the two peaks on the low field side is 3.9 gauss.

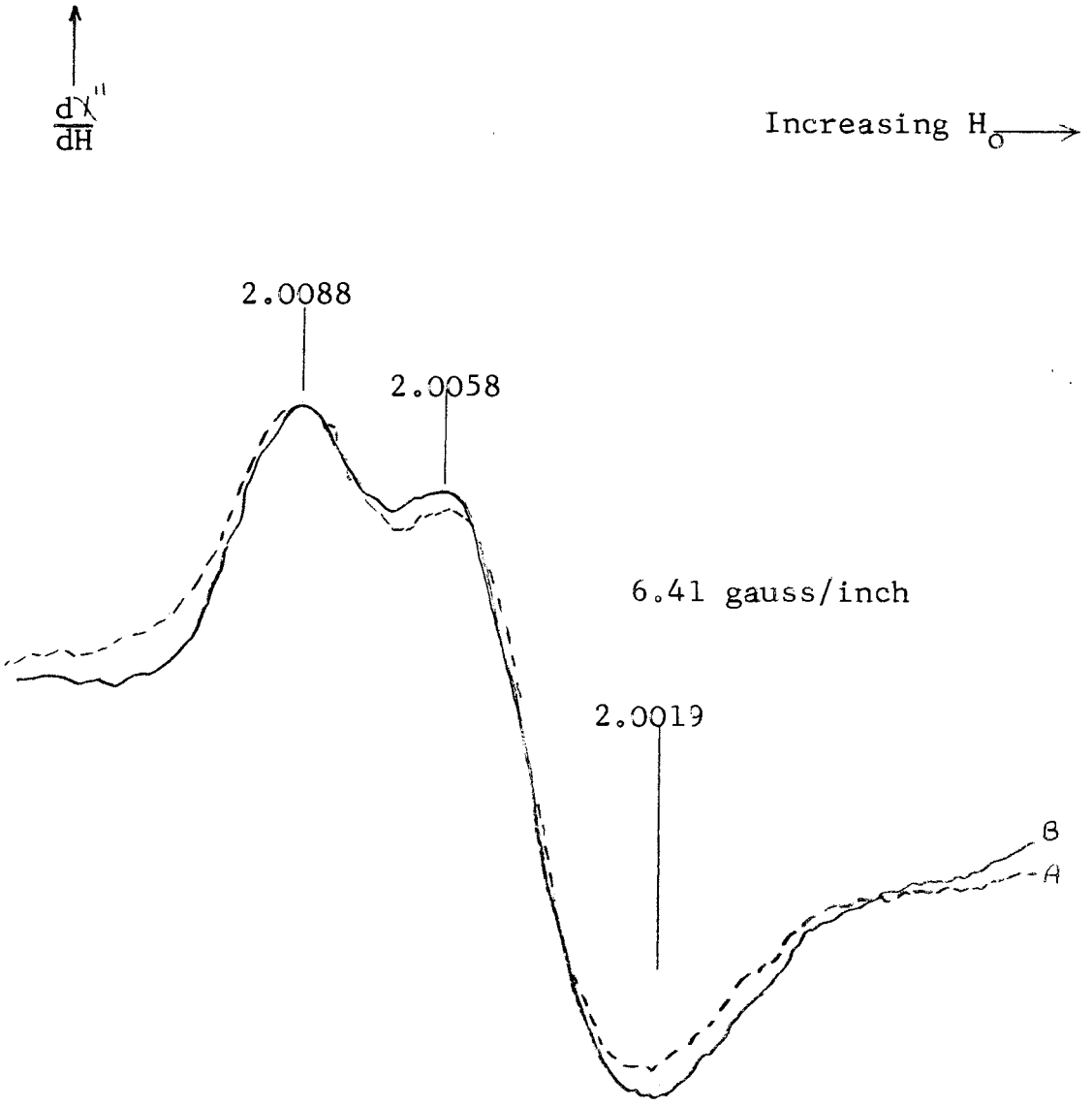

Figure 8. Adult Red Cell ESR Spectra. (a) infected sample, (b) normal sample. Gain and M.A. 4x100, -20db temperature 77°K.

The characteristic anemia of anaplasmosis is believed to result from erythrophagocytosis (45). The mechanism for this red blood cell phagocytosis is believed to be mainly in the reticuloendothelial system and specifically the spleen, but the changes which occur in the red cell to cause phagocytosis are not clearly understood in anaplasmosis. The anaplasma body apparently does not physically destroy the red cell for there is little evidence of intravascular hemolysis (44). The ESR spectrum of anaplasma infected red blood cells does not indicate any changes in the heme to globin arrangements, nor is there any indication that the spin state or oxidation state of the iron is altered. If chemical changes occurred in the amino acid groups or if foreign chemical substances were introduced, there would almost definitely be an indication in the ESR absorption spectrum produced.

The spectra of the adult red cells showed signals at g=2.0088 $\pm$ .0004, 2.0058 $\pm$ .0005, and 2.0019 $\pm$ .0001 as shown on the figures.

Figure 9 represents the spectra of normal adult bovine red blood cells (9a) and normal fetal red blood cells (9b). The signal at g=2.0088 is common to both spectra. Fetal red blood cells show an additional signal at g=2.0158 and the signal at g=2.0058 is missing. The normal adult sample displays a signal which is more narrow, having a third peak at g=2.0019. The third peak of the fetal spectrum lies at g=2.0002.

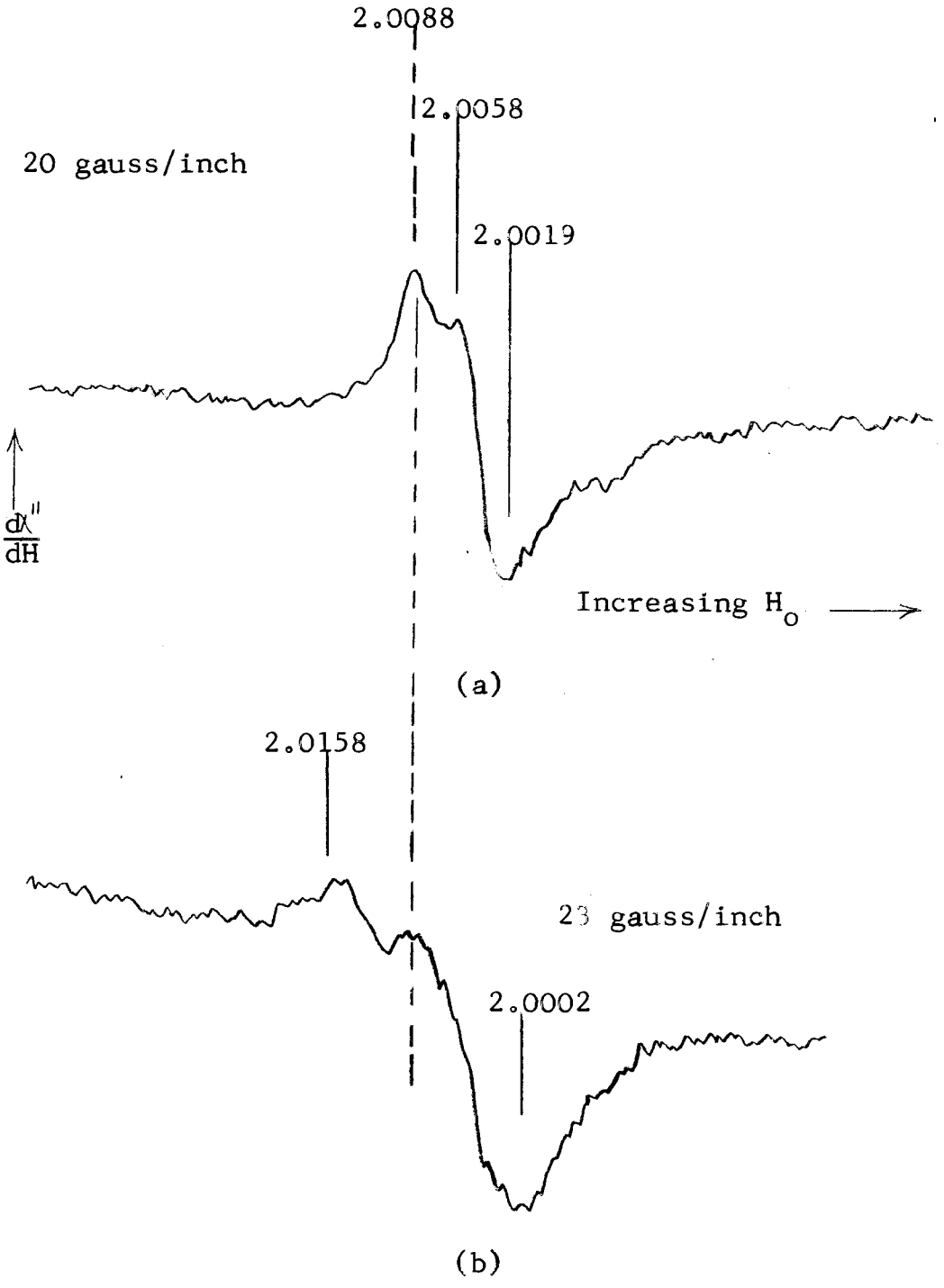

Figure 9. Adult and fetal red cell ESR spectra. (a) adult sample, -15db, (b) fetal sample, -10db. Gain 5x100, M.A. 4x100 on both runs.

The differences in these spectra are probably caused by the abnormal amino acid chain in fetal hemoglobin. The replacement of the normal Beta chain by the Gamma chain, as discussed in Chapter III, probably causes a change in the coordination sites of the heme to globin arrangement. This change in the electronic configuration of the heme-iron's surroundings would be expected to create an ESR absorption signal with a different g-value from that normally displayed. The common Alpha chain in the hemoglobin molecules of adult and fetal bovine red blood cells probably results in the common signal at g=2.0088.

The sample used in Figure 9(b) was obtained from a 3-day old holstein calf. An analysis by the Oklahoma State Department of Veterinary Medicine and Surgery-Clinical Research found the sample to contain approximately 75.5 percent Hb-F and 24.5 percent Hb-A. As briefly discussed in Chapter III, the amount of Hb-F declines rapidly with age reaching a level of less than 1 percent in about 20 weeks. Figure 10 shows the ESR of red blood cells taken from a six week old weaned calf. The anticoagulant is EDTA and the amount of sample is approximately 0.055cc before drying. According to work done by Lee, Odell, E. W. Jones, and others at Oklahoma State, the amount of Hb-F present at this time would be no more than approximately 45 percent and could be as low as 20 percent or less (58, 59). The spectrum shown in Figure 10 displays a prominent signal at g=2.0058, and only a trace of the g=2.0158 signal

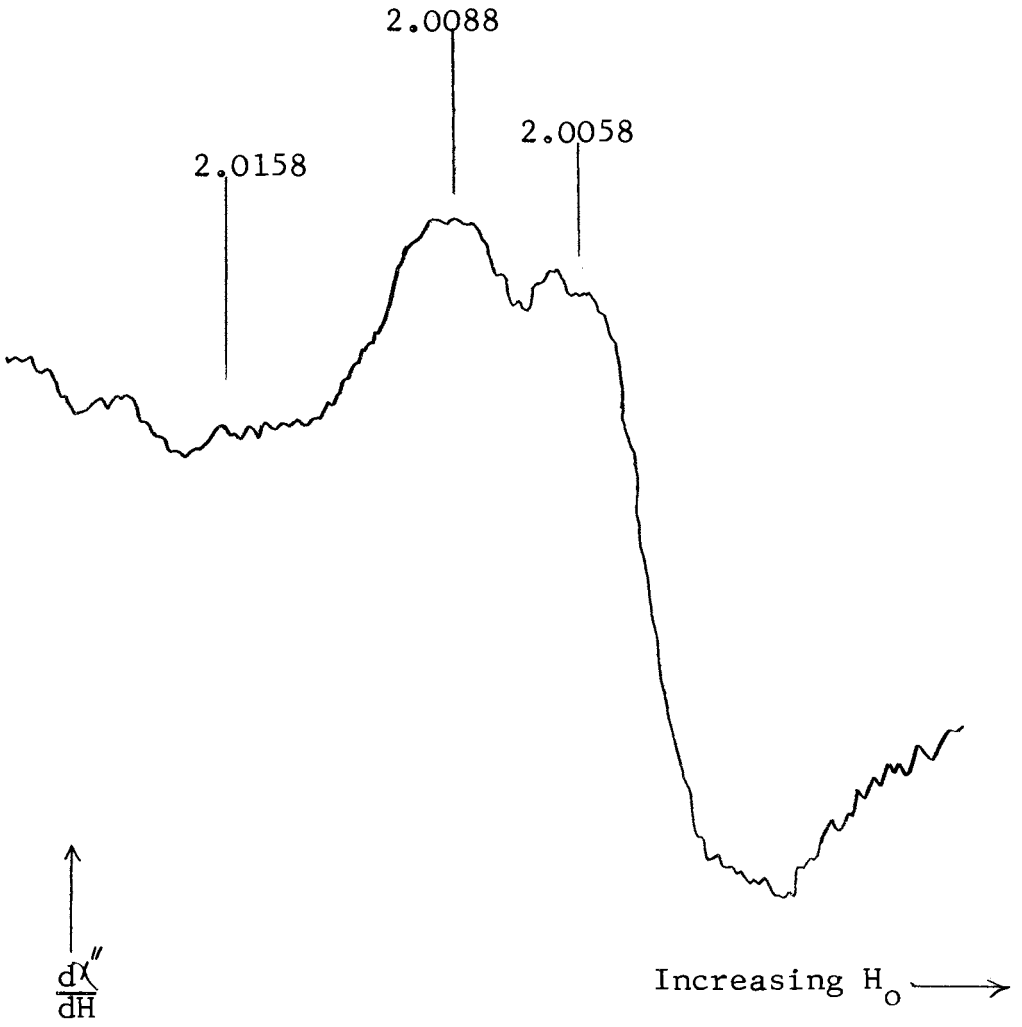

Figure 10. Spectrum of red cells from six week old, weaned calf, gain 8x100, M.A. 4x100, -15db, 25°C.

is present.

Samples of red cell membrane were also investigated, and Figure 11 represents two of the spectra obtained. The comparison of spectra from infected and normal membrane, unlike the red blood cell comparison, showed a marked difference in the two signals. The infected red cell membrane samples displayed a very weak absorption spectrum even at the maximum microwave power normally applied to samples in this study (-10db attenuation). The signal is centered at g=2.0102 and has an overall width of only 24.1 gauss. Figure 11(b) represents the spectrum of normal bovine red blood cell membrane. This sample has a much stronger ESR absorption spectrum than 11(a) even though 11(b) was run at a much lower microwave power (-15db attenuation). The signal is centered at g=2.0036 and has an overall width of 39.6 gauss. The scan rates for Figure 11(a) and 11(b) were 19.3 and 19.8, respectively.

The signal source in the red cell membrane is not yet fully understood and more ESR work on phospholipid bilayers and other liquid crystals must be undertaken to clarify these questions. It is possible that the anaplasma bodies may alter the composition of the membrane enough to allow the reticloendothelial system to detect a change, thus promoting erythrophagocytosis. The ESR spectra seem to indicate that a significant change does take place. There is also some physical evidence of change in the infected red cell membrane. The consistency of the separated infected

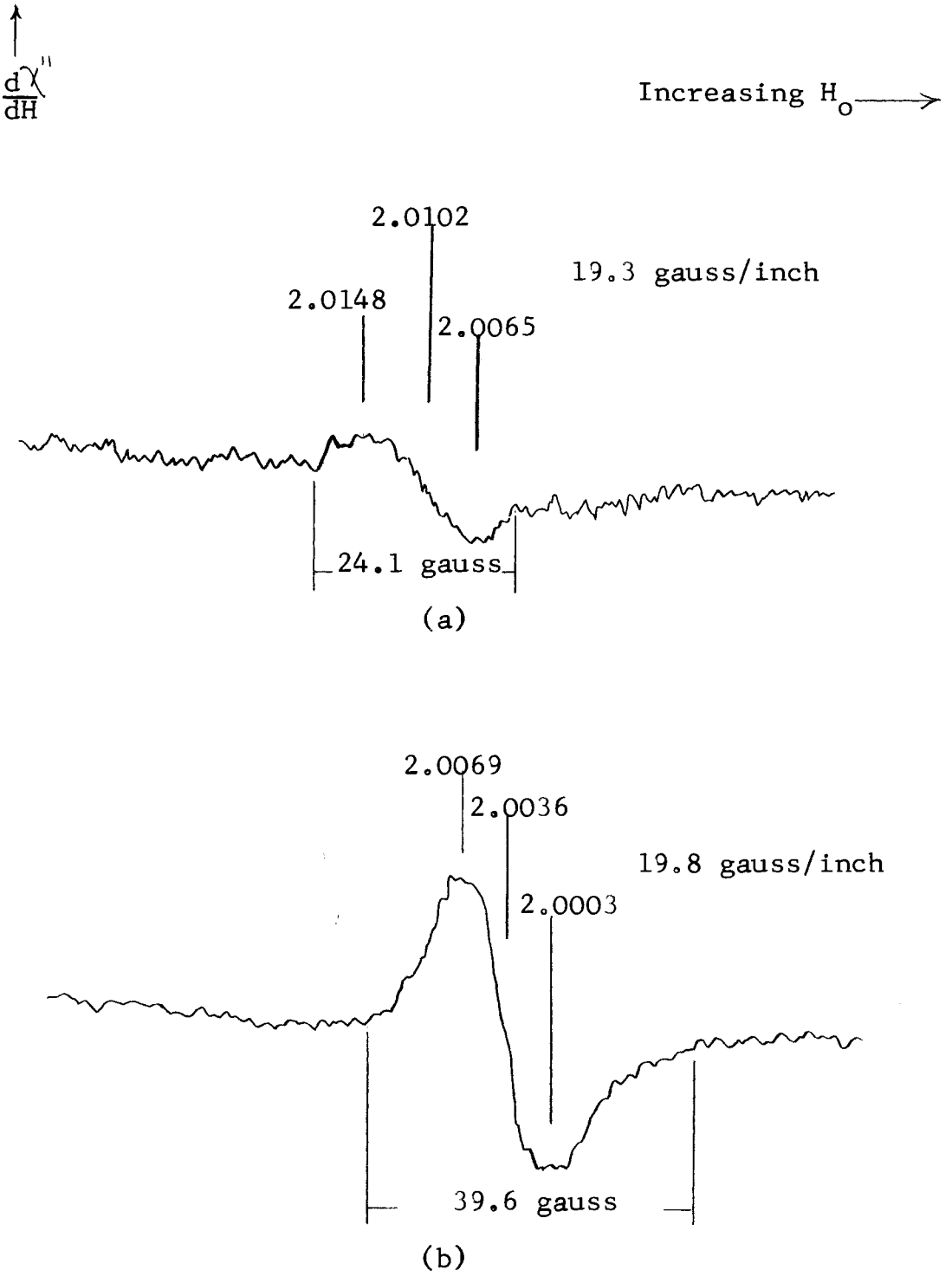

Figure 11. Infected and normal red cell membrane. (a) infected, -10db, (b) normal, -15db, gain 5x100, M.A. 4x100 on both runs.

membrane was observed to be much more liquid in nature. The normal membrane formed a closely packed group which could easily be transferred, as one mass, from centrifuge tube to sample tube. The infected membrane was not easily recovered from the centrifuge tube and was often lost during transfer. A very large sample of infected red blood cells was required to obtain an infected membrane sample volume of .055cc.

After the initial investigative phase of this study had been completed, all samples were exposed to various external treatments, and their ESR spectra were again examined. Samples were separated into several sample tubes which were labeled to indicate the type of external treatment to be applied. Some of the sample portions were treated before lyophilization while other portions of the same sample were lyophilized before treatment.

Irradiation

Several portions of each sample were irradiated with ultraviolet light. Other portions were exposed to x-ray irradiation. The source of UV-irradiation was a Gates Deuterium tube (D100B) with a range down to 1800^{o}A. A General Electric XRD unit was used for x-ray irradiation.

The first few samples investigated during this phase of the study were irradiated through the 3mm ID Varian fused-quartz tubes. Figure 12 represents the absorption signal observed when these samples were inserted into the

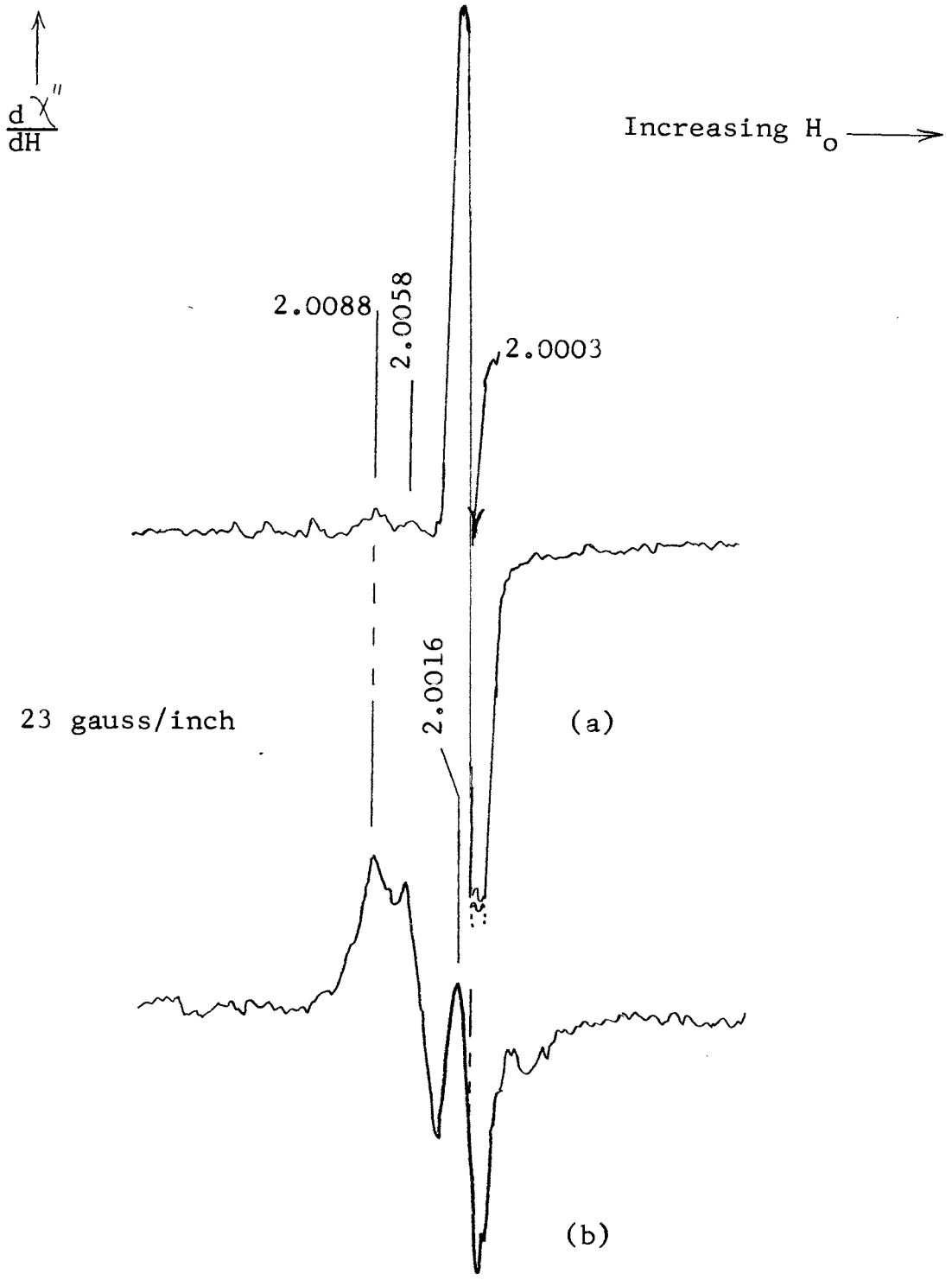

Figure 12. Irradiated ESR samples. (a) by x-rays, gain 4x100, M.A. 4x100, -32db, (b) by UV-light, gain 5x100, M.A. 4x 100, -20db.

ESR cavity. Figure 12(a) shows a sample of normal red blood cells irradiated for 15 minutes with 35 kev x-rays at 10 milliamps. The dose of radiation the sample obtained is related to the energy of the x-rays and the duration of the exposure.

The absorption spectrum shows an additional signal centered at g=2.0003. The signal amplitude is very large, and the spectrometer microwave power had to be reduced to a very low level to keep it on the trace. The run was made with an attenuation setting of -32db, and the normal signals at g=2.0088 and g=2.0058 are barely detectable. Figure 12(b) represents a portion of the same sample after UV-irradiation for 35 minutes. There is an additional signal at g=2.0016 (also centered at 2.0003). The origin of these new signals was questioned because of the extremely large amplitude of the x-ray signal, and the investigation was repeated using empty quartz tubes. The quartz tubes were checked for ESR absorption signals before being irradiated and were found to possess no detectable signal. They were then subjected to irradiation for the same time periods used in Figure 12(a,b). The resulting ESR absorption spectra are shown in Figure 13. The signal in Figure 13(a) was detected in a quartz tube irradiated with 35 kev x-rays for 15 minutes. It is identical to the additional signal observed in Figure 12(a). The spectrum represented by Figure 13(b) was obtained from a quartz tube exposed to UV-irradiation for 35 minutes. This signal and the additional

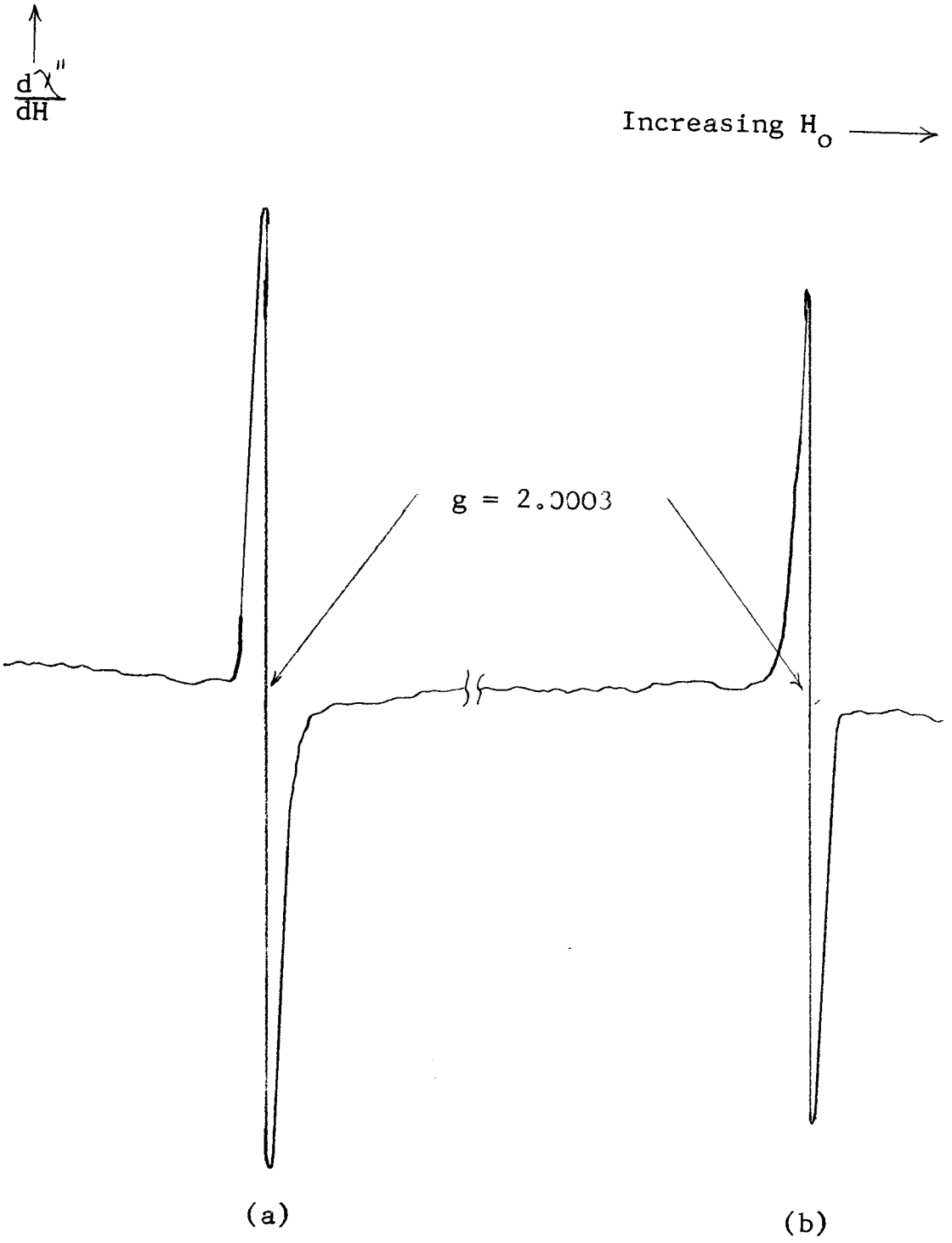

Figure 13. ESR spectra of irradiated quartz tubes. (a) by x-rays, gain 5x10, -20db, (b) by UV-light, gain 1.25x100, -10db, M.A. 4x100 on both runs.

signal in Figure 12(b) are identical. Some variation was observed in the amplitudes of the comparable signals. The signals shown in Figure 13 were greater in amplitude than those in Figure 12. This difference was apparently caused by a variation in the age of the signal when it was observed. The spectra in Figure 13 were obtained immediately after the samples had been exposed, while those in Figure 12 were obtained 6 weeks after irradiation took place. This apparent decay in signal amplitude was investigated further and the results are shown in Figure 14. The spectrum in Figure 14(a) was obtained immediately after exposure to x-ray irradiation for 15 minutes. The gain is down to 5x10 and the microwave power is attenuated by -20db. Figure 14(b) is the same quartz tube 2 weeks later. The gain is up to 8x10 and the microwave attenuation is reduced to -10db.

A search of the literature uncovered a study by J. H. E. Griffiths and others in 1955 (61). They report obtaining a similar signal after irradiating natural quartz with x-rays in the 1.2 to 3.15cm wavelength range. They report g-values of 2.06 $\pm$ .005 which do not agree with those observed in this study. They also remark that their absorption signals are removed by UV-irradiation and report no new signals being formed. Griffiths, et. al. also report that their signals can be completely removed by heating the quartz to 350^{o}C. An investigation of this annealing phenomenon was undertaken as the last stage of this phase

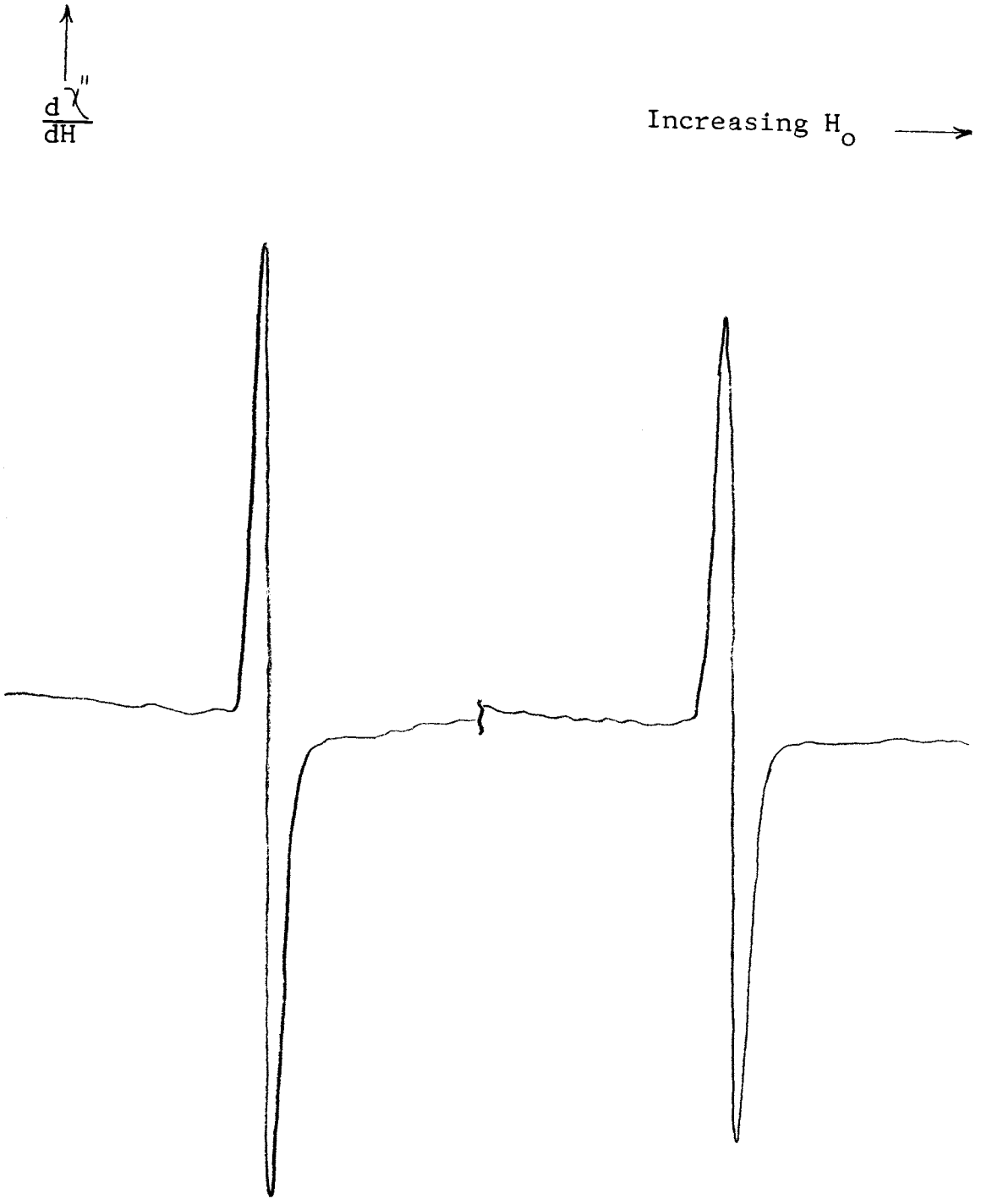

(a) 5 x 10, -20db (b) 8 x 10, -10db

Figure 14. Decay of x-ray irradiation ESR spectra. (a) immediately after exposure, gain 5x10, -20db, (b) two weeks later, gain 8x10, -10db, M.A. 4x10 on both runs.

of the study. The results are represented by Figure 15(a, b,c). The effect of heating was clearly observed although a temperature in excess of 400°C was necessary to completely anneal out the absorption signal. The decrease in the signal size shown in Figure 15(b) represents a stable level reached after 15 minutes at an excess of 400°C. The signal decreased no farther after an additional two hours at this temperature. There was no additional decrease in signal size after exposure to a bunsen flame for 1, 3, and 5 minutes allowing for cooling between each heating. Upon exposure to a bunsen flame for 6 minutes the signal abruptly and completely disappeared. These same observations were carried out for the other quartz tubes containing irradiation damage and similar results were obtained. Once the signal was annealed out, it did not reappear, and the quartz tubes were free of any ESR absorption signals.

Many of the workers doing ESR studies on irradiated biological samples report that they irradiate their samples in quartz tubes similar to the ones used in this study (27-30). None of these studies have reported the phenomenon just discussed, but most report additional signals in their samples due to irradiation. The nature and origin of these reported signals would seem to be suspect as many of them may be due to signals created in the sample tubes. All of the samples used in this study were placed in separate test tubes and irradiated with x-rays and UV-irradiation. They were then transferred to quartz tubes

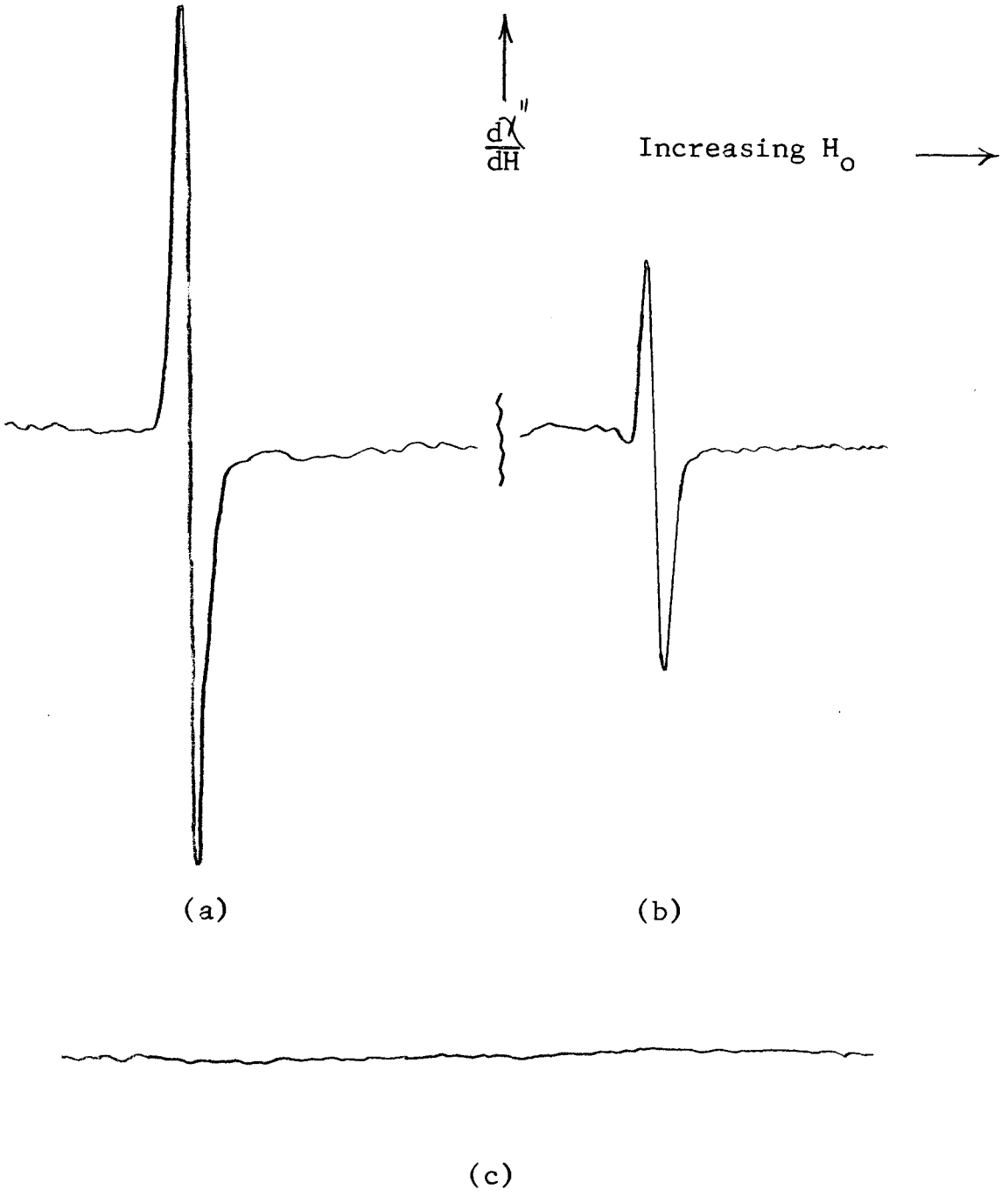

Figure 15. Heat treatment of UV-light irradiation ESR spectra. (a) before heat, (b) stable signal after 15 minutes at excess 400°C, (c) after 6 minutes in bunsen flame. All runs at: gain 1.25x100, M.A. 4x100, -10db.

and their ESR spectra were recorded. None of the samples displayed changes in their normal ESR signal.

Paramagnetic Labeling

Nitric oxide (98.5 percent minimum) gas was obtained from Matheson Company, Inc. (East Rutherford, New Jersey). The gas was filtered through molecular sieve type 5-A and applied to the samples by the methods of Kon and Vanin (43,42). Each of the methods discussed in these reports was utilized several times on all samples investigated in this study. Exposing the dried sample to (NO) for as much as 5 hours created no change in the signal, but exposing the samples in this manner before drying created a very broad signal of low amplitude. Nitric oxide was then bubbled through solutions of red blood cells and red blood cell membranes for all samples used in this study. This treatment resulted in an ESR signal composed of the original spectrum superimposed on a broad envelope of high amplitude. Figure 16 represents the spectra obtained during this phase of the study. All samples displayed the same reaction and their original signal shapes were not altered.

Heat Treatment

Each sample was exposed to heat treatment and each responded in the same manner. The results of these observations are represented by the spectra in Figure 17. The

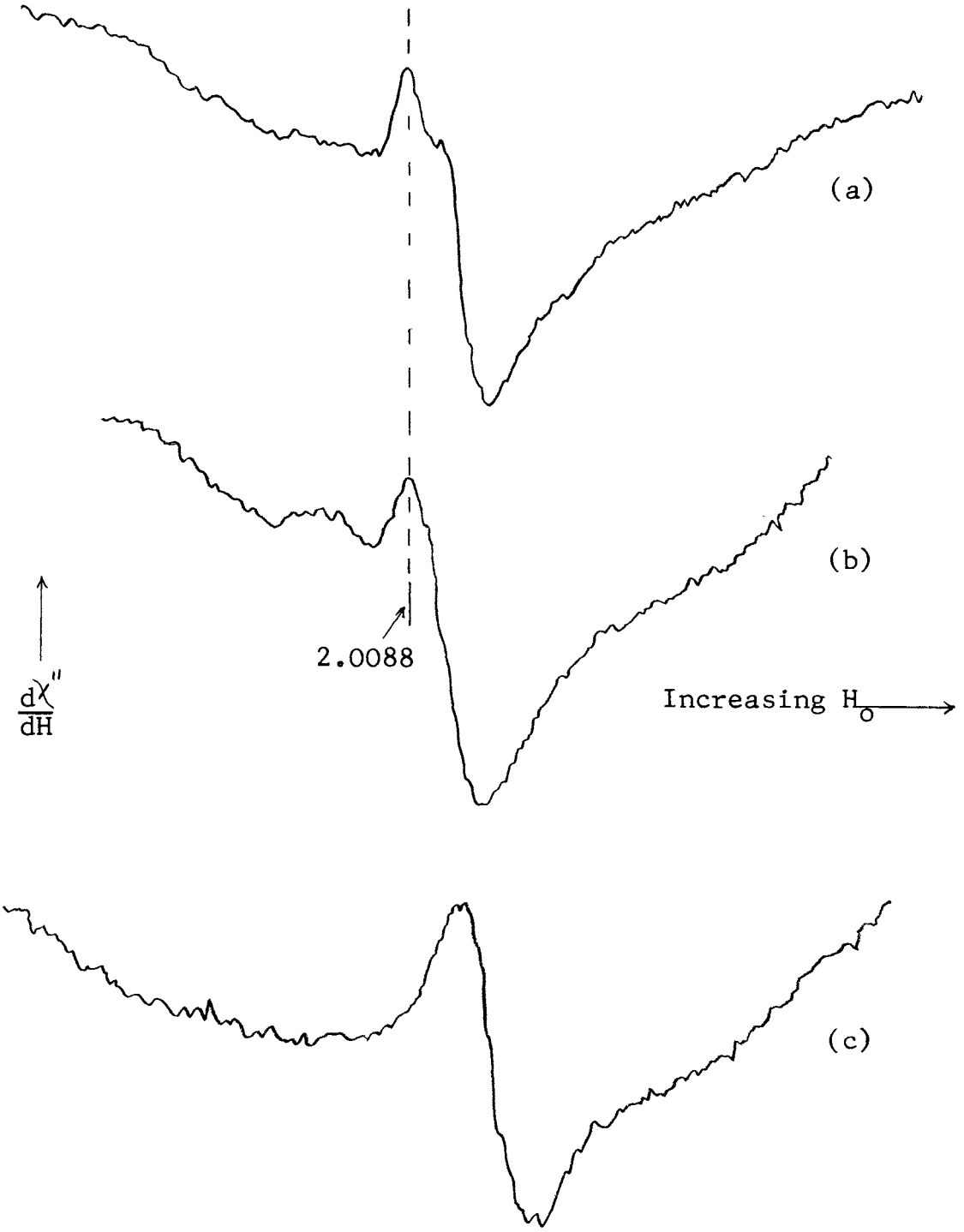

Figure 16. Nitric oxide paramagnetic labeling. (a) adult red blood cell spectrum, -10db, (b) fetal red blood cell, -15db, (c) red cell membrane, -15db. Gain 5x100, M.A. 4x100 on all three runs.

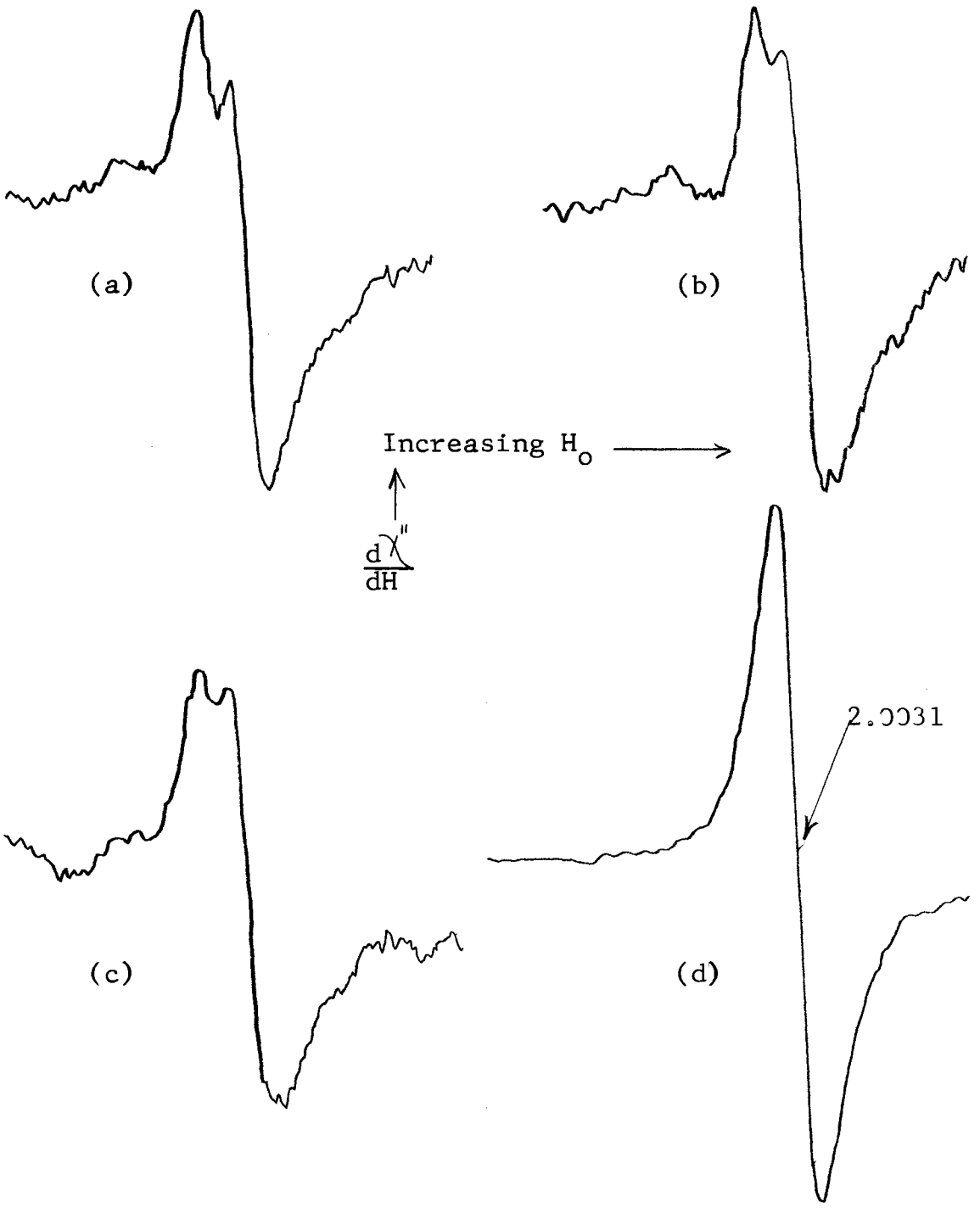

Figure 17. Heat treatment ESR spectra. (a) initial signal, (b) after 10 minutes at 100°C, (c) after 1 hour at 100°C, (d) after spontaneous combustion. Gain on (a,b,c) 5x100, gain on (d) 2x100.

initial signal is shown in Figure 17(a). The sample was exposed to temperatures from 20°C to 100°C for increasing time periods. No change was observed in the sample spectrum until it had been exposed to 100°C for 10 minutes. The resulting absorption spectrum is shown in Figure 17(b). The exposure time was incremented at 10 minute intervals while holding the temperature constant at 100°C. No change was noticed in the spectrum until the sample was exposed to 100°C for 1 hour. The resulting spectrum is shown in Figure 17(c). Exposure time was then incremented at 30 minute intervals until 5 hour exposure times were reached. The temperature was then incremented in 50°C intervals until approximately 250°C was detected at the sample. The spectrum shown in Figure 17(c) did not change. After only 5 seconds at approximately 300°C the samples underwent spontaneous combustion in the sealed quartz tubes. Figure 17(d) represents the absorption spectrum of the burnt samples. The spectra shown in Figure 17(a,b,c) were run at the same amplifier gain settings (5x100), but the spectrum shown in Figure 17(d) was much larger and the gain was reduced to 2x100. The signal is centered about a g-value of 2.0031.

All samples investigated demonstrated a similar reaction to heating and no obvious distinction could be made between the samples on the basis of this phase of the study. The signals did not revert to their initial spectrum after cooling and were permanently altered.

Atmospheric Contamination

Several portions of all samples were exposed to the atmosphere by removing the sealed end of their quartz tubes. The absorption spectrum of each sample was investigated at regular intervals over a period of several weeks. Figures 18, 19, and 20 represent a summary of the spectra observed during this phase of the investigation. The initial ESR spectra of adult and fetal red blood cells are shown in Figure 18(a,b). These signals were obtained immediately before the quartz tube seals were broken, and they display the characteristic signals previously discussed. Figure 19(a,b) represents the spectra of these two signals 5 days later. The ESR spectrometer gain settings are the same, but the microwave power settings have been raised to a higher attenuation than those used in the spectra of Figure 18. The signal size has increased in amplitude. Figure 19(a) is the spectrum of fetal red blood cells. The signal at (g) equal 2.0158 is barely observed as the signal at g= 2.0088 has almost obscured it completely. The 2.0158 signal has neither increased nor decreased in amplitude. The spectrum of the adult red blood cells after 5 days exposure is shown in Figure 19(b). The signal at g=2.0058 is still visible, but the 2.0088 signal shows a large amplitude increase and almost hides it. This phase of the study was terminated after the samples had been exposed to air for 59 days. The spectra observed at that time are shown

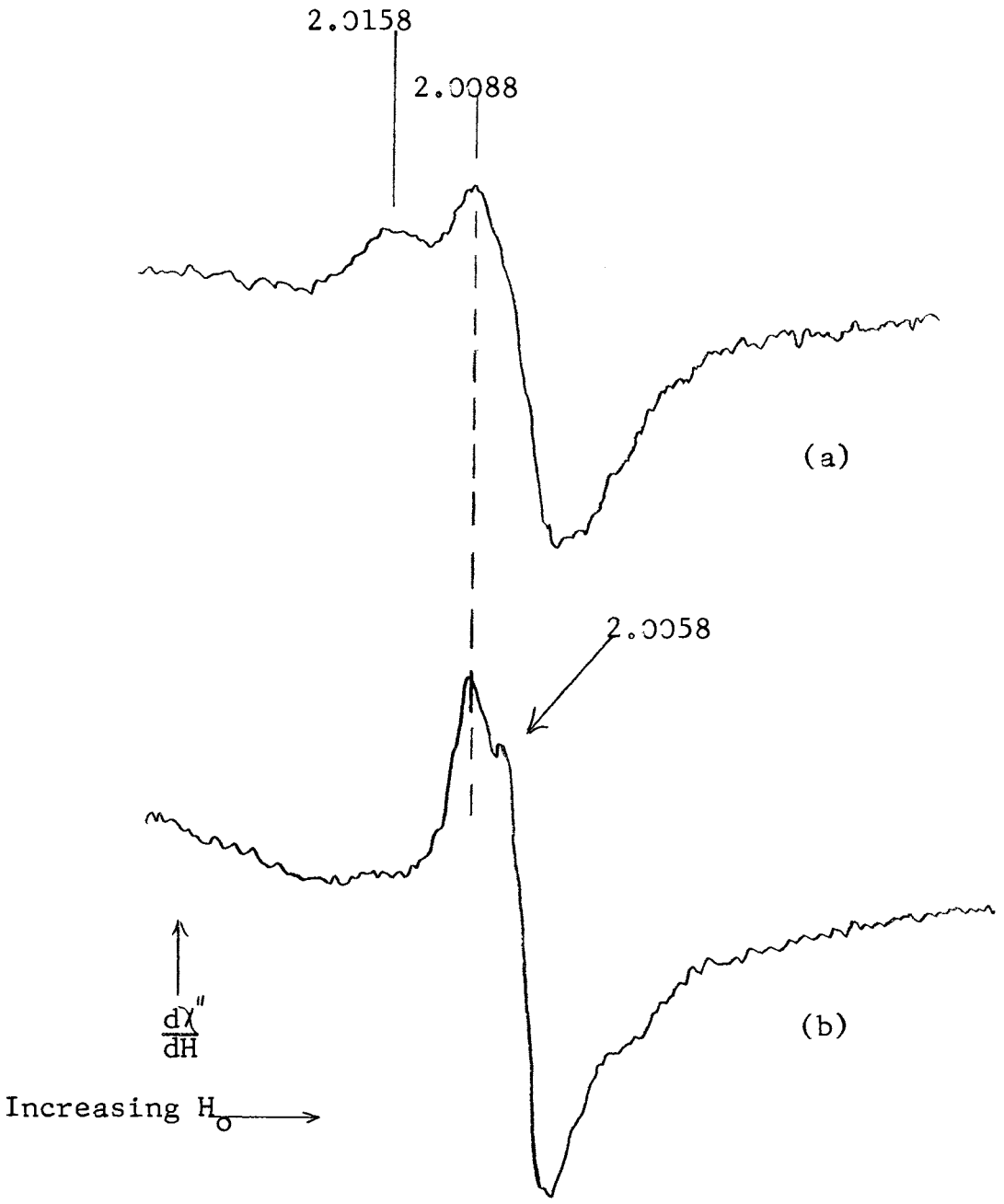

Figure 18. Fetal and adult ESR spectra before exposure to air. (a) fetal, (b) adult. Gain 5x100, M.A. 4x100, -10db on both runs.

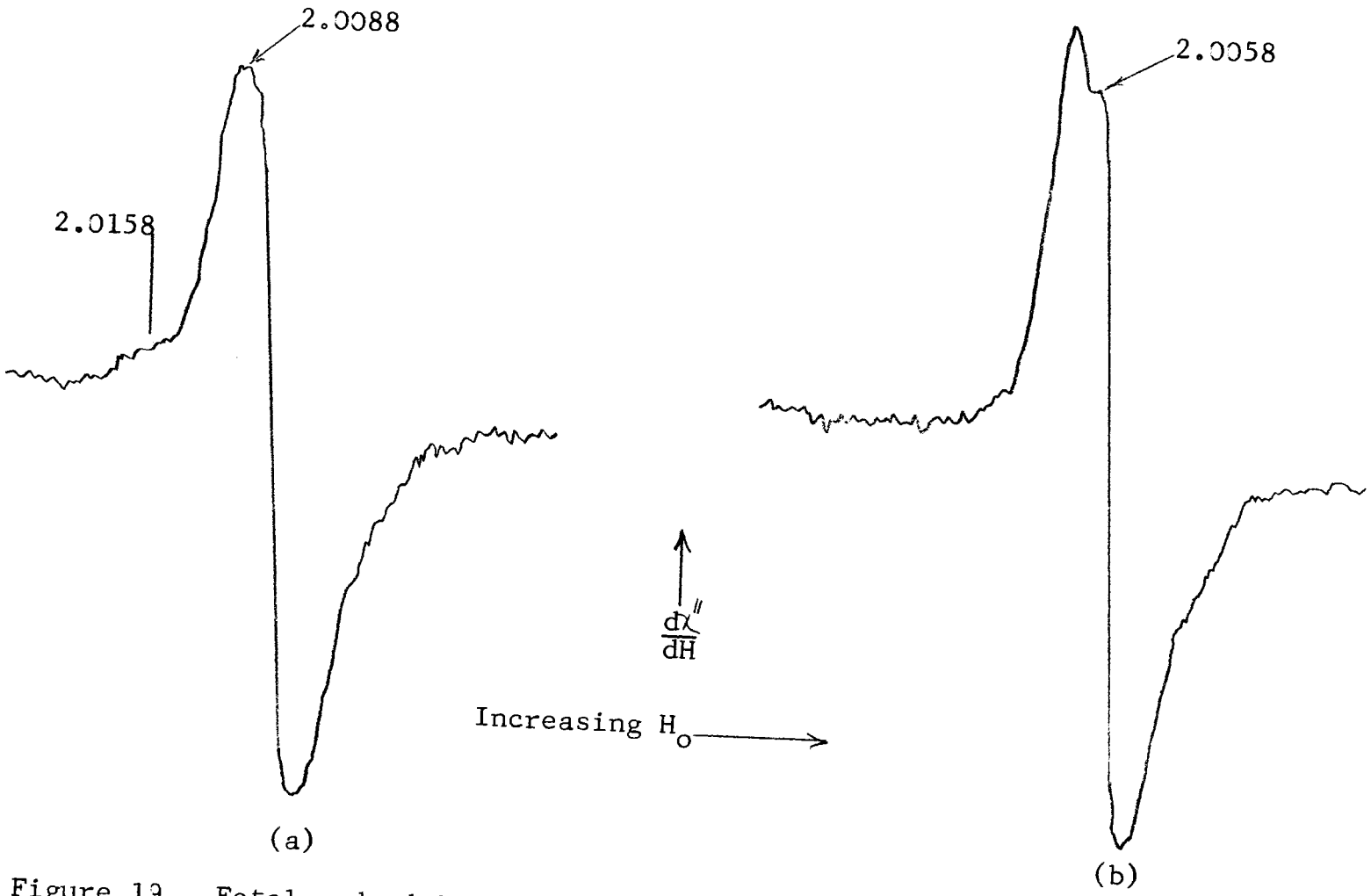

Figure 19. Fetal and adult ESR spectra after 5 days exposure to air. (a) fetal, -10db, (b) adult, -15db. Gain 5x100, M.A. 4x100 on both runs.

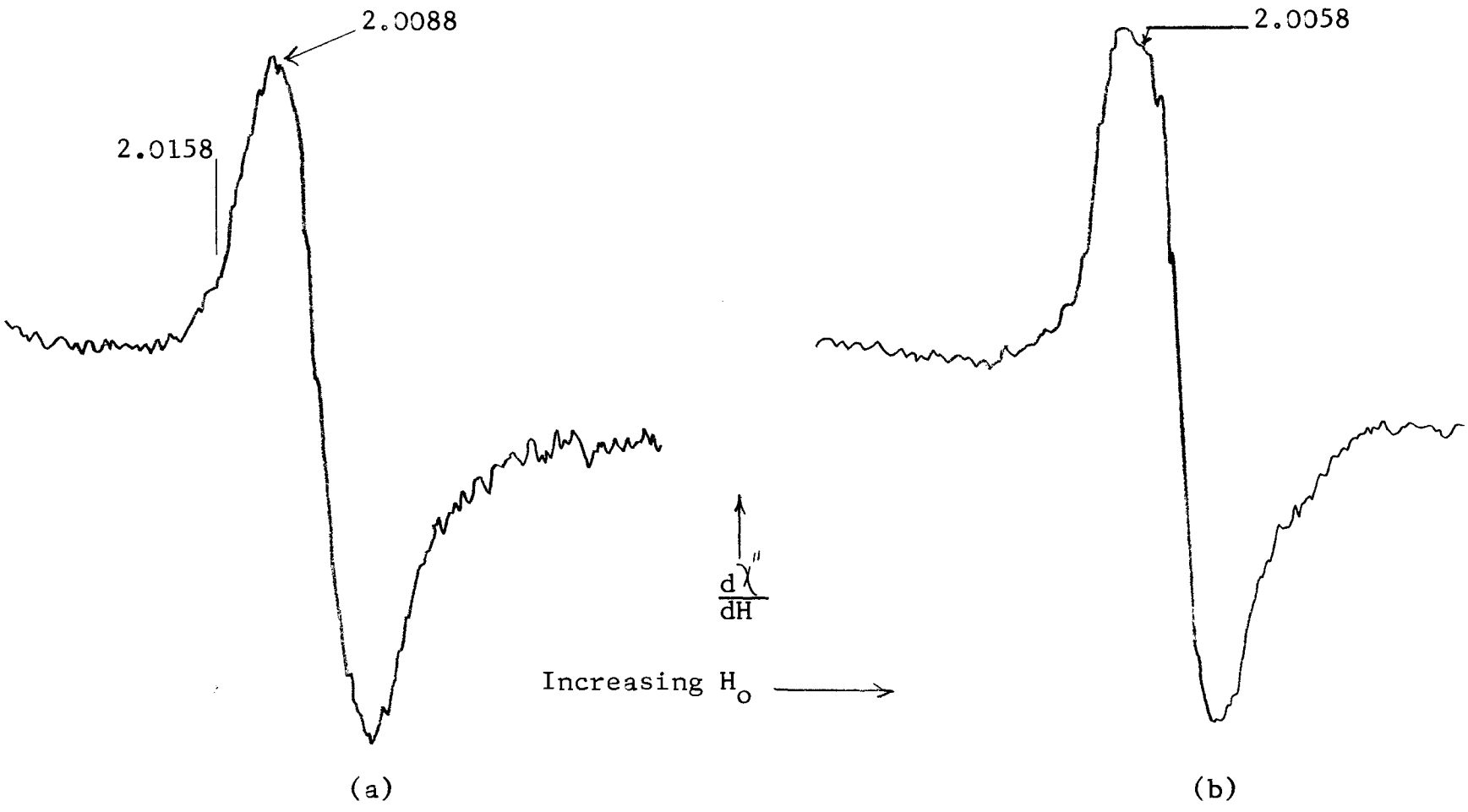

Figure 20. Fetal and adult ESR spectra after 59 days exposure to air. (a) fetal, -10db, (b) adult, -15db. Gain 5x100, M.A. 4x100 on both runs.

in Figure 20(a,b). Figure 20(a) is a representation of the fetal red blood cell absorption spectrum. The power and gain settings are the same as those used in Figure 18(a). The signal amplitude has decreased from that observed in 19(a), but the width of the 2.0088 signal has increased and the 2.0158 signal is no longer clearly visible. The same changes were observed in the adult red blood cell absorption spectrum shown in Figure 20(b).

Portions of each sample were reevacuated at various stages of this phase of the investigation. The changes in the spectra were found to be irreversible and the spectrum displayed by samples after hours of re-lyophilization was identical to that observed immediately before reevacuation.

Discussion and Summary

The ESR spectra of normal adult, infected adult, and normal fetal bovine red blood cells and red blood cell components were obtained, standardized, and compared. The samples were then subjected to various external treatments to determine the effects of each treatment on the ESR absorption of the samples.

The ESR absorption spectra of fetal and adult bovine red blood cells were found to be significantly different. Adult bovine red blood cells display a spectrum with signals at g-values of 2.0088, 2.0058, and 2.0019. Fetal red blood cells display a spectrum with g-values of 2.0158, 2.0088, and 2.0002. These differences are probably caused

by differences in the amino acid chains of the hemoglobin molecules. Hemoglobin-A (adult) is characterized by Alpha and Beta chains while hemoglobin-F (fetal) contains Alpha and Gamma chains.

No difference was observed in the spectra of infected and normal adult red blood cells, but the absorption spectra of their separated red cell membranes was significantly different. Infected red cell membrane displayed a spectrum which was 24.1 gauss wide. This signal was centered about a g-value of 2.0102. The infected red blood cell membrane was difficult to separate from other red cell components and seemed to be thin and watery. The spectrum displayed by normal red blood cell membrane was 39.6 gauss wide. The signal was centered about a g-value of 2.0036. The normal red blood cell membrane was thick and easily separated from the other red cell components.

Samples of fetal and adult red blood cells were exposed to air for several days and the changes in their ESR absorption spectra were observed. After five days the signal at g=2.0088 had increased in amplitude until it partially obscured the signals at 2.0158 and 2.0058 in the spectrum of fetal and adult red blood cells respectively. After ten days the 2.0088 signal was the only one clearly observable in either sample. When the investigation was terminated after 59 days of exposure to air, the signal amplitude had begun to show a slight decrease in both samples. Reevacuation for extended periods did not reverse the process

and the two smaller signals remained obscured.

Samples displayed a slight variation in their ESR signal after being treated with heat for varying time periods at various temperatures. At approximately 300^{o}C the samples underwent spontaneous combustion in the sealed quartz sample tubes,and their ESR absorption spectra were reduced to a single, high amplitude, peak. The slight variations observed before combustion may have been caused by atmospheric contamination. Heating the samples in the quartz tubes probably caused the seal to become defective. The changes observed were similar to those discussed in the atmospheric contamination study.

All samples displayed identical responses to the other external treatments applied. Exposure to nitric oxide gas produced a broad signal of low amplitude which was superimposed upon the original ESR signal but did not alter the original signals shape. Irradiation of the samples with ultraviolet and x-ray irradiation produced large signals in the fused quartz tubes but did not alter the spectra of the samples.

This investigation concentrated mainly on red blood cells and red blood cell components, but many interesting studies could be done on other types of biological materials such as collagen, tissues of many organs, tumors, liquid crystals, RNA, and DNA to name a few. This study used only polycrystalline materials but single, solid crystals of some biological materials are now available. These crystals

could possess orientation dependent ESR spectra which could be quantitatively analyzed at low temperatures near the temperature of liquid helium.

A SELECTED BIBLIOGRAPHY

(1) Michaelis, "Theory of Oxidation-Reactions," The Enzymes ed J. B. Summer and K. Myrback, 1-46 (New York: Academic Press Inc. 1951).

(2) Wyard, S. J., Solid State Biophysics, (McGraw-Hill, New York, 1969).

(3) Heckly, R. J. and Dimmick, R. L., "Electron Paramagnetic Resonance in Frozen and Dried Biological Materials," Nature 242(3), 393-397 (1967).

(4) Shore, B. W. and Menzel, D. H., Principles of Atomic Spectra, (John Wiley and Sons, Inc., New York, 1968).

(5) Bell, M. D., "Electron Spin Resonance in Diamond," (Ph. D. thesis, Oklahoma State University, 1964).

(6) Smith, Ian C. P. and Schneider, Henry, "Epr in The Life Sciences," Varian Instrument Applications 4(2), 4(1970).

(7) Chetverikov, A. G., "Study of the Spectra of Electron Paramagnetic Resonance of Biological Specimens," Biofizika 9(6), 738-741 (1963).

(8) Commoner, B., Townsend, J., and Pake, G. E., Nature 174, 689-691 (1954).

(9) Commoner, B., Heise, J. J. and Townsend, J., "Light Induced Paramagnetism in Choloroplasts," Proceedings of the National Academy of Science 42, 710 (1956).

(10) Vithayathil, A. J., Ternberg, J. L., and Commoner, B., "Changes in Electron Spin Resonance Signals of Rat Liver During Chemical Carcinogenesis," Nature 207, 1246-1249 (1965).

(11) Commoner, B. and Ternberg, J. L., Pro. Nat. Acad. Sci. (USA) 47, 1374 (1961).

(12) Kent, M. and Mallard, J. R., "Advantages Resulting

from the Addition of a Versatile Multichannel analyser to an Electron Spin Resonance Spectrometer, Nature 207, 1195 (1965).

(13) Swartz, H. M. and Molenda, R. P., "Electron Spin Resonance Characteristics of Some Normal Tissues: Effect of Microwave Power," Science 148, 94 (1965).

(14) Holmes, D. E. and Myers, L. S., "Electron Spin Resonance Technique for Investigating Reactions of Free Radicals with Compounds of Biological Interest: Nucleic Acid Constituents," Nature 209, 1017 (1966).

(15) Dettmer, C. M., Driscoll, D. H., and Wallace, J. D., "Pitfalls in Electron Spin Resonance Spectrometry in Biological Tissues," Nature 214, 492 (1967).

(16) Kent, M. and Mallard, J. R., "Electron Spin Resonance in Biological Tissues," Nature 215, 736 (1967).

(17) Vanin, A. F., Chetverikov, A. G., and Blyumenfel'D, L. A., "Effect of Lyophilization on the EPR Spectra of Animal Tissues," Biofizika 13, 66 (1967).

(18) Chetverikov, A. G. and Vanin, A. F., "Change in the EPR Spectra of Animal Tissues on Heat Treatment," Biofizika 13(2), 302 (1968).

(19) Vanin, A. F. and Ruuge, E. K., "Determination of the Relaxation Parameters of Paramagnetic Centries in Biological Specimens by the Method of Continuous Saturation of the EPR Signals and from the Traversal Effects," Biofizika 13(3), 564 (1967).

(20) Pavlova, N. I. and Livenson, A. R., "Spectra of Electron Paramagnetic Resonance (EPR) of Human Blood in Normal Conditions and in Leukaemias," Biofizika 10(1), 186 (1965).

(21) Gordy, W., Radiat. Res. Suppl 1, 491 (1959).

(22) Gordy, W., Ard, W. B., and Shields, H., Proc. Natl. Acad. Sci. U.S.A. 41, 983 (1955).

(23) Gordy, W., Pruden, B., and Snipes, W., Proc. Natl. Acad. Sci. U. S. A. 53, 751 (1965).

(24) Gordy, W., and Shields, H., Proc. Natl. Acad. Sci. U.S.A. 46, 1124 (1960).

(25) Rexroad, H. N., and Gordy, W., Proc. Natl. Acad. Sci. U.S.A. 45, 256 (1959).

(26) Shields, H., and Gordy, W., Proc. Natl. Acad. Sci. U.S.A. 45, 269 (1959).

(27) Drew, R. C. and Gordy, W., "Electron Spin Resonance Studies of Radiation Effects on Amino Acids," Radiation Res. 18, 552 (1963).

(28) Henriksen, Thormod, "Effect of Oxygen on Radiation-Induced Free Radicals in Proteins," Radiation Research 32, 892 (1967).

(29) Patten, R. and Gordy, W., "Further Studies of Radiation Effects on the Proteins and there Constituents," Radiation Res. 22, 29 (1961).

(30) Forbes, W. F. and Sullivan, P. D., "Electron Spin Resonance Spectra of 2537 A-Irradiated Collagen," Biochim & Biophys Acta 120, 222 (1966).

(31) Bemski, G., Arends, T., and Blanc, G., "Electron Spin Resonance of Cu(II) In Copper-Hemoglobin Complexes," Biochemical and Biophysical Res. Communications 35(5), 599 (1969).

(32) Pincres, P., "Magnetic Properties of Liquid Crystals," Journal of Applied Physics 41(3), 974 (1970).

(33) Schara, M. and Sentjurc, M., "Electric Field Ordering of Para-Oyoxyanisole Liquid Crystals Molecules Studied by Electron Spin Resonance," Solid State Communications 8, 593 (1970).

(34) Keith, A. D., et. al., Proceedings of the National Academy of Science U.S.A. 61, 819 (1968).

(35) Waggoner, A. S., et. al., "A Spin-Labeled Lipid for Probing Biological Membranes," Chemistry and Physics of Lipids 3, 245 (1969).

(36) Fergason, J. L., "Liquid Crystals," Scientific American 211, 77 (1964).

(37) Fergason, J. L., "Liquid Crystals in Nondestructive Testing," Applied Optics 7(9), 1721 (1968).

(38) Selawry, Oleg S., et. al., "The Use of Liquid Cholesteric Crystals for Thermographic Measurement

of Skin Temperature in Man," Liquid Crystals, eds. Brown, Glenn, H., et. al., (Gordon and Breach, New York, 1966).

(39) Stewart, G. T., "Liquid Crystals as Ordered Components of Living Substances," Ordered Fluids and Liquid Crystals, (American Chemical Society, Washington, D. C., 1967).

(40) Keilin, D. and Hartree, E. F., "Reaction of Nitric Oxide with Hemoglobin and Methemoglobin," Nature, 548 (1937).

(41) Shiga, Takeshi, Hwang, Kun-Joo, and Tyuma, Itiro, "An Electron Spin Resonance Study of Nitric Oxide Hemoglobin Derivatives," Arch Biochem & Biophys 123(1), 203 (1968).

(42) Vanin, A. F. and Chetverikov, A. G., "Paramagnetic Nitrosyl Complexes of Haem and Non-Haem Iron," Biofizika 13(4), 608 (1968).

(43) Kon, Hideo, "Paramagnetic Resonance Study of Nitric Oxide Hemoglobin," J. Biol. Chem. 243(16), 4350 (1968).

(44) Jones, E. W. and Brock, W. E., "Bovine Anaplasmosis: Its Diagnosis, Treatment, and Control," Journal of the American Veterinary Medical Association 149, 1624 (1966).

(45) Jones, E. W. and Norman, B. B., "Anaplasmosis, the Disease. Its Clinical Diagnosis and Prognosis," Proc. 4th Nat. Anaplasmosis Conf., 3 (1962).

(46) Howell, D. E., "Transmission of Anaplasmosis by Arthropods," Proc. 3rd Nat. Res. Comf.: Anaplasmosis in Cattle, 14 (1957).

(47) Norman, B. B., Jones, E. W., and Brok, W. E., "A System for Assembling Hematologic Data for Computer Analysis," Am. J. Vet. Res 27, 829 (1966).

(48) Brock, W. E., "A Study of the Pathogenesis of the Anemia in Acute Anaplasmosis," Ph.D. Thesis, University of Oklahoma, (1958).

(49) Asimov, I., The Living River, (abelard-Schumann, London, 1960).

(50) Swanson, C. P., The Cell, (Prentice-Hall, New Jersey, 1960).

(51) Ingram, V. M., Hemoglobin and Its Abnormalities, (Charles C. Thomas, Illinois, 1961).

(52) Perutz, M. F., Muirhead, H., Cox, J. M., and Goaman, L. C. G., "Three-Dimensional Fourier Synthesis of Horse Oxyhaemoglobin at 2 8 A Resolution: The Atomic Model," Nature 219, 131 (1968).

(53) Tasaki, Akira, "Electronic State of Iron Ion in Hemoproteins," Journal of Applied Physic 41, 1000 (1970).

(54) Kugelmass, N., Biochemistry of Blood, 386 (Thomas: Springfield 1959).

(55) Haemoglobin, eds. Roughton, F. and Kendrew, 261 (London, 1949).

(56) Hayashi, A., Shimizu, A., Yamamura, Y., and Watari, H., "Electron Spin Resonance of Haemoglobin M Iwate and M Osaka," Bio chem Biophys Acta 102, 626 (1965).

(57) Hayashi, A., Suzuki, T., Shimizu, A., Morimoto, H., and Watari, H., "Changes in EPR Spectra of M-type Abnormal Haemoglobins Induced by Deoxygenation and Their Implication for Haem-Haem Interaction," Biochim Biophys Acta 147, 407 (1967).

(58) Chernoff, A. I., and Singer, K., "Studies on Abnormal Hemoglobins. IV. Persistance of Fetal Hemoglobin in the ERythrocytes of Normal Children," Pediatrics 9, 409 (1952).

(59) Allison, A. C., "Malaria in Carriers of the Sicle-Cell Trait and in Newborn Children," Exp. Parasitol 6, 418 (1957).

(60) DuMond, J. W. M. and Cohen, E. R., Handbook of Physics, (McGraw-Hill Co., New York, 1962).

(61) Griffiths, J. H. E., Owen, J., and Ward, I. M., "Magnetic Resonance in Irradiated Diamond and Quartz," Conf. on Defects in Crystalline Solids, (Physical Society, 1955).

(62) Squires, T. L., An Introduction to Electron Spin Resonance, (Academic Press, New York, 1964).

(63) Rabi, J. I., Ramsey, N. F., and Schwinger, J., "Use of Rotating Coordinates in Magnetic Resonance Problems," Rev. Mod. Phys. 26, 167 (1954).

(64) Bloch, F., "Nuclear Induction," Phys. Rev. 70, 460 (1946).

(65) Abragam, A., Principles of Nuclear Magnetism, (Oxford University Press, London, 1961).

(66) King, J. P., "Effects of Light on the Electron Spin Resonance of Diamond," (Ph. D. thesis, Oklahoma State University, 1966).

(67) Ingram, D. J. E., Free Radicals as Studied by Electron Spin Resonance, (Butterworths Scientific Publications, London, 1958).

(68) Gorden, J. P., "Variable Coupling Reflection Cavity for Microwave Spectroscopy," Rev. Sci. Instr. 32, 658 (1961).

(69) Ager, R., Cole, T., and Lambe, J., "Coupling Scheme for Microwave Cavities," Rev. Sci. Instr. 32, 658 (1961).

(70) Faulkner, F. A., "Improved Circuit for an Electron Spin Resonance Spectrometer," J. Sci. Instr. 39, 135 (1962).

(71) Lax, B., and Button, K. J., Microwave Ferrites and Ferrimagnetics, (McGraw-Hill Co., New York, 1962).

(72) Portis, A. M., "Electronic Structure of F centers: Saturation of the Electron Spin Resonance," Phys. Rev. 91, 1071 (1953).

(73) Pound, R. V., "Frequency Stablization of Microwave Oscillators," Proc. of IRE 34, 1405 (1947).

(74) Zaffarano, F. P, and Galloway, W. C., "Notes on the Pound Microwave Frequency Stabilizer," Technical Report #31, Research Laboratory of Electronics, MIT (1947).

(75) Montgomery, C. G., Techniques of Microwave Measurements, MIT Radiation Lab. Series, Vol. 11, (McGraw-Hill, New York, 1947).

(76) Low, W., "Paramagnetic Resonance in Solids," Solid State Phys. Supplement 2, 1 (1960).

APPENDIX A

ELECTRON SPIN RESONANCE

Simple Theory

Solids with covalent or ionic bonds contain no unpaired spins and are diamagnetic but natural crystals contain defects caused by impurities and crystal lattice defects. These defects may have an unpaired spin associated with them which would make the solid paramagnetic.

In considering electron spin resonance the interaction of an electron spin system with an externally applied alternating magnetic system must be considered in more detail. The simple system previously considered will be referred to again here for clarity. Figure 21 shows the separation of the energy levels of an unpaired electron by a static magnetic field H_o as previously discussed in Chapter I.

The spin system is in thermal equilibrium before the microwave power is applied. The expression for the distribution of spins between the two levels is given by the Boltzmann expression

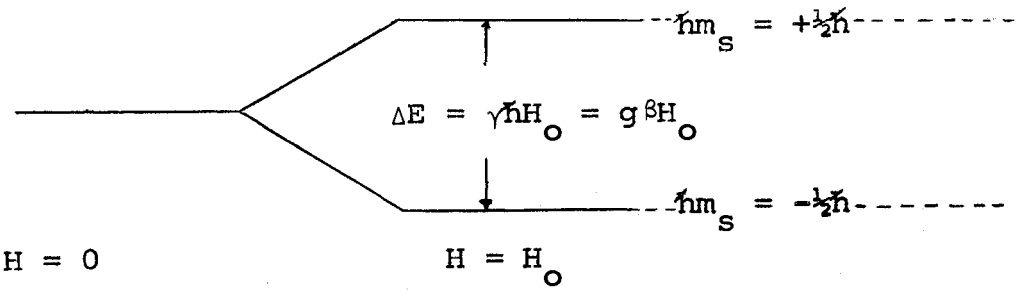

Figure 21. Separation of the energy levels of an unpaired electron by a static magnetic field H_o.

$$\frac{n+}{n-} = \exp - \frac{\Delta E}{kT} \qquad (A.1)$$

where n_+ is the number of spins in the upper level, n_- is the number in the lower level, T is the absolute temperature, and k is Boltzmann's constant. Equally populated levels result in just as many spins taking part in stimulated emission as there are in absorption and no net energy absorption occurs. A net absorption energy can occur under equilibrium conditions until the two levels become equally populated. Spin-lattice relaxation is one mechanism by which thermal equilibrium can be re-established. Coupling between the spin system and the lattice results in the spins losing energy to the lattice and thermal equilibrium is restored. Under these conditions a net absorption of energy from the microwave field can continue. The length of time required for

thermal equilibrium to be restored is known as "spin-lattice relaxation time". Weak coupling between the spin system and the lattice will result in a long relaxation time, whereas strong coupling produces short times. The phenomenon known as "saturation" occurs when weak coupling produces long relaxation times and a sufficiently high microwave power is introduced. Under these conditions thermal equilibrium cannot be completely restored by the coupling and the net absorption signal decreases or saturates.

When a nucleus possessing a magnetic moment is associated with the unpaired electron, the electron will see an internal field due to the magnetic moment of the nucleus. There will be an interaction between the unpaired electron and the nucleus, and the energy levels will split into several components depending upon the spin of the nucleus. For a nucleus of spin I there will be (2I+1) component levels and the ESR signal will have (2I+1) peaks. Figure 22 shows splitting of the levels for I=3/2. This hyperfine interaction makes it possible to identify the nucleus around which the electron is moving.

Rotating Coordinates and Resonance

The electron is considered to be a small magnet with

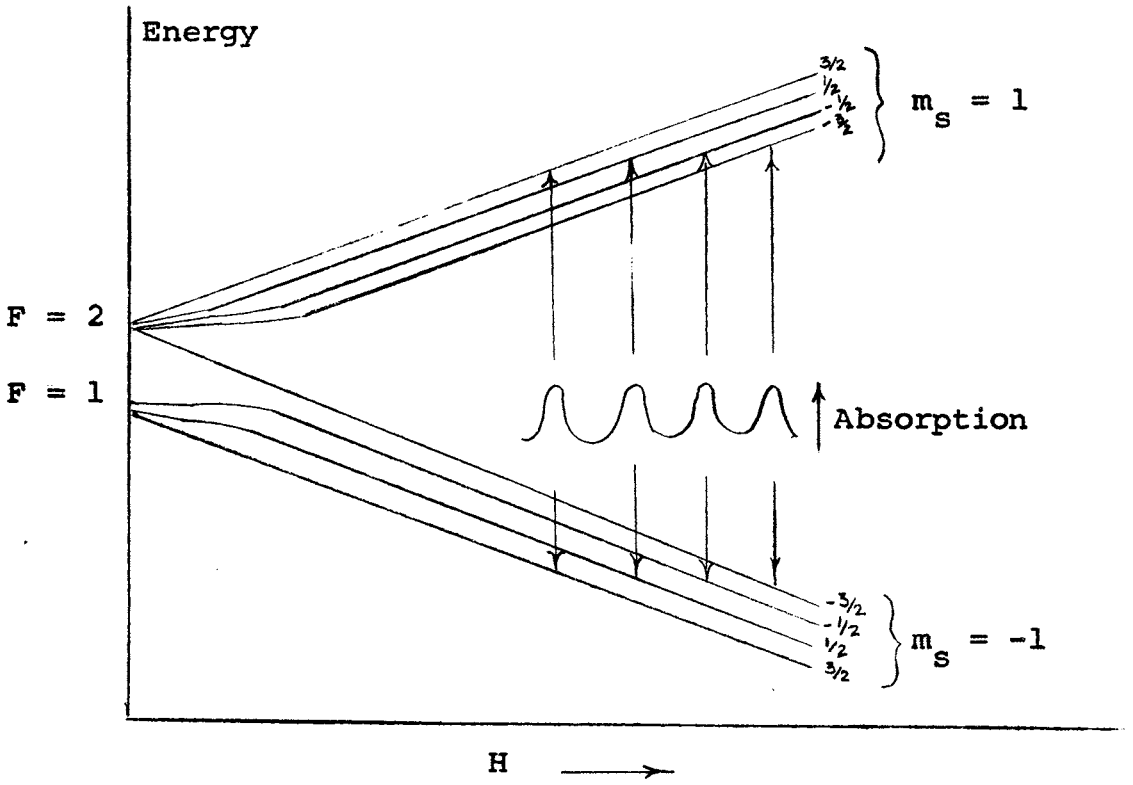

Figure 22. Electron spin resonance from an electron associated with a nucleus of spin I = 3/2.

magnetic moment $\vec{\mu}$ (62). In the presence of an external static magnetic field $\vec{H}$ the electron will experience a torque $\vec{T}$ given by

$$\vec{T} = \vec{\mu} \times \vec{H}. \qquad (A.2)$$

In the fixed laboratory system the z-axis of a rectangular coordinate system x, y, z is taken so that the static magnetic field is in the z-direction and is given by $\vec{H} = H_o \hat{k}$. The magnetic moment of the electron is related to the spin angular momentum by $\vec{\mu} = -\gamma \vec{S}$ where

$\vec{S} = \frac{3}{2}\hbar$. The equation of motion can then be obtained by noting that the time rate of change of angular momentum is just the torque $\vec{T}$ and is given by

$$\frac{d\vec{S}}{dt}. \tag{A.3}$$

This results in the following classical equation of motion in a fixed coordinate system:

$$\frac{d\vec{S}}{dt} = \gamma \vec{S} \times \vec{H}$$

and

$$\frac{d\vec{\mu}}{dt} = \vec{\mu} \times \gamma \vec{H}. \tag{A.4}$$

Since $\vec{\mu}$ cannot line up directly with $\vec{H}$, it will precess about $\vec{H}$ with a frequency $\vec{\omega} = \gamma H_o \hat{k}$, known as the Larmor frequency.

A solution to equation (A.4) can be obtained conveniently by transforming to a rotating coordinate system about the z-axis (63). The axes x' and y' rotate about the common z-axis with a constant angular frequency $\vec{\omega}$. An observer rotating with x' would see the time rate of change of $\vec{\mu}$ given by

$$\left(\frac{d\vec{\mu}}{dt}\right)_{rot}$$

and the rate of change due to the rotation of the axes would be given by

$$\vec{\omega} \times \vec{\mu}.$$

The equation of motion given in terms of the rotating system becomes

$$\frac{d\vec{\mu}}{dt} = \left(\frac{d\vec{\mu}}{dt}\right)_{rot} + (\vec{\omega} \times \vec{\mu}) \qquad (A.5)$$

and solving for $\left(\frac{d\vec{\mu}}{dt}\right)_{rot}$ (A.5) becomes

$$\left(\frac{d\vec{\mu}}{dt}\right)_{rot} = \frac{d\vec{\mu}}{dt} - (\vec{\omega} \times \vec{\mu}).$$

Using equation (A.4) and rearranging gives

$$\left(\frac{d\vec{\mu}}{dt}\right)_{rot} = \gamma \left(\vec{H} - \frac{\vec{\omega}}{\gamma}\right) \times \vec{\mu}. \qquad (A.6)$$

This is the equation for $\vec{\mu}$ in the rotating system. It has the same form as (A.4) except that $\vec{H}$ has been replaced by the effective field $\vec{H}_{eff}$, where $\vec{H}_{eff}$ is given by

$$\vec{H}_{eff} = \vec{H} - \frac{\vec{\omega}}{\gamma}. \qquad (A.7)$$

If $\vec{\omega}$ is chosen such that $\vec{\omega} = \gamma H_o \hat{k}$ where $H_o \hat{k} = \vec{H}$ then $\left(\frac{d\vec{\mu}}{dt}\right)_{rot}$ will vanish. Therefore, when

$$\omega_o = \gamma H_o \qquad (A.8)$$

where $\vec{\omega} = \omega_o \hat{k}$, the magnetic moment $\vec{\mu}$ is a constant vector and the magnetic moment precesses about $\vec{H}$ with a frequency $\omega_o = \gamma H_o$, the Larmor frequency. By comparing equation (A.8) with equation (1.2) it is seen that the Larmor precessional frequency is identical to the ESR absorption frequency.

The transformation just completed does not allow the

precession of the individual electron spins to be observed. Since the electron spin precesses about $\vec{H}$ at a constant frequency ω_o, an additional alternating magnetic field $\vec{H}_1$ must be introduced in the plane perpendicular to the static field $\vec{H}$ in order to cause spin-flip and allow resonance to be observed. The relative position of the field and the spin are shown in Figure 23c. The change of $\vec{S}$ is perpendicular to both $\vec{S}$ and H_o with angle θ being constant.

The alternating magnetic field $\vec{H}_1$ must be circularly polarized in the x and y plane and must have components

$$H_x = H_1 \cos \omega_1 t; \; H_y = H_1 \sin \omega_1 t \qquad (A.9)$$

where ω_1, is the microwave angular frequency. The component of $\vec{H}_1$ which is rotating in the same sense as $\vec{\mu}$ as the frequency approches the resonance condition is given by

$$H_{rot} = H_1 [\hat{i} \cos \omega_1 t + \hat{j} \sin \omega_1 t] \qquad (A.10)$$

where $\hat{i}$, $\hat{j}$, $\hat{k}$ are the unit vectors along x, y, z respectively. An additional torque is applied by $\vec{H}_{rot}$ in the z-direction, and the equation of motion (A.4) can be written

$$\frac{d\vec{\mu}}{dt} = \vec{\mu} \times \gamma [\vec{H} + \vec{H}_r]. \qquad (A.11)$$

A transformation to the rotating coordinate system

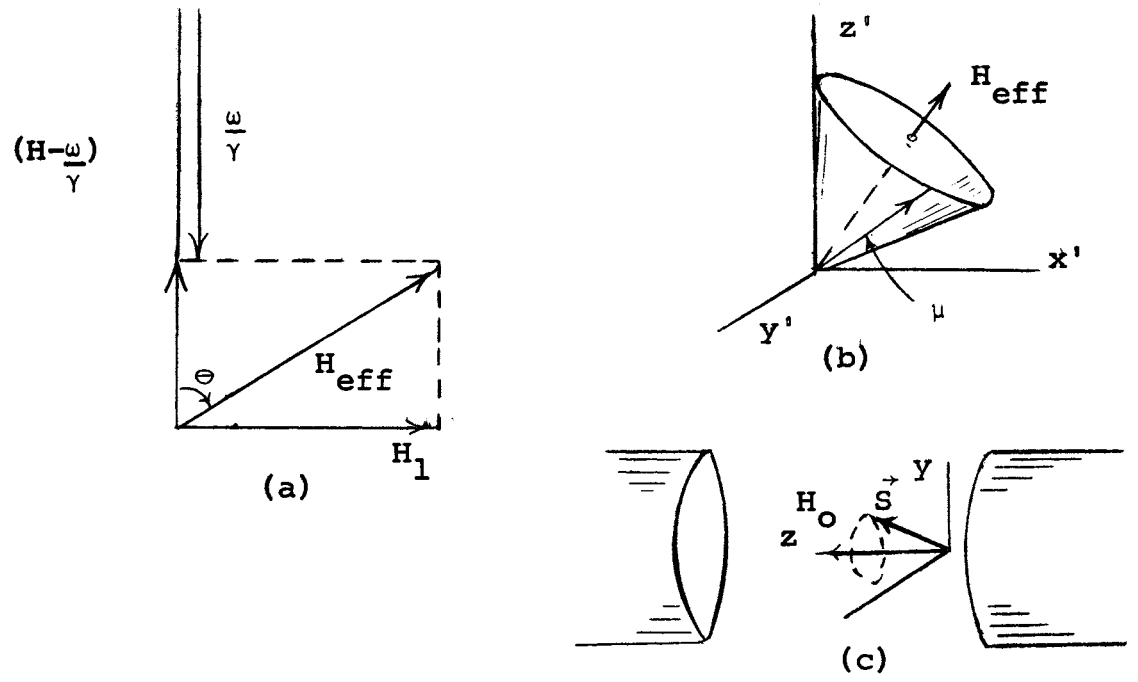

Figure 23. The Motion of the Magnetic Moment $\vec{\mu}$ in the effective magnetic field $\vec{H}_{eff}$ and the precession of $\vec{S}$ in the magnetic field H_o.

may also be used to treat the combined fields and equation (A.11) can be transformed to rotate with angular frequency $\vec{\omega} = \omega_1 \hat{k}$. Equation (A.11) in the rotating system is given by

$$\left(\frac{d\vec{\mu}}{dt}\right)_{rot} = \vec{\mu} \times \gamma \left[\left(H_o - \frac{\omega}{\gamma}\right) \hat{k} + H_1 \hat{i}' \right] \qquad (A.12)$$

where $\vec{H}_r$ is a constant in the xy-plane directed along the x-axis as shown in Figure 23a and $\vec{H}_r$ is given by $\vec{H}_r = H_1 \hat{i}'$. The effective field, as seen from the rotating system, acts as a constant field. The magnetic moment precesses, as shown in Figure 23b, about $\vec{H}_{eff}$ in a cone at frequency

$\vec{\omega}_{eff} = \gamma \vec{H}_{eff}$ where $\vec{H}_{eff}$ is given by

$$\vec{H}_{eff} = H_1 \hat{i}' + (H_o - \frac{\omega_1}{\gamma})\hat{k}'. \qquad (A.13)$$

When the microwave frequency ω_1 is at the resonance condition the effective field is $H_1 \hat{i}'$ and $\vec{\mu}$ precesses about $\vec{H}_1$ with a frequency $\vec{\omega}_p = \gamma \vec{H}_1$. The magnetic moment of the electron in the rotating system is

$$\vec{\mu} = [\mu_x' \hat{k}' \cos \omega_p t - \mu_y' \hat{j}' \sin \omega_p t] \qquad (A.14)$$

where $\vec{\mu}$ precesses in a plane perpendicular to $\vec{H}_{eff}$ and changes its orientation periodically. The orientation of $\vec{\mu}$ changes from parallel to antiparallel with respect to the static field $\vec{H}$ with a frequency $\omega_p << \omega_o$ which causes a slow tipping of $\vec{\mu}$ as it rapidly precesses around $H_o >> H_1$.

Bloch Equations

The previous discussion did not include equilibrium conditions caused by relaxation effects. After application of the static magnetic field in the z-direction, before any energy is introduced into the system the electrons will align themselves parallel or antiparallel to the field as previously stated. At thermal equilibrium the spins populate the two levels approximately with a Boltzmann distribution and there is a resulting magnetization $M_o \hat{k}$, which is given by

$$M_o \hat{k} = \chi_o H_o \hat{k} \qquad (A.15)$$

where χ_o is the static magnetic susceptibility. The rate of change of the x, y and z components of the magnetization as the system approches equilibrium are given by Bloch (64) to be

$$\frac{dM_x}{dt} = \dot{M}_x = -\frac{M_x}{T_2} \qquad \text{(a)}$$

$$\dot{M}_y = -\frac{M_y}{T_2}, \qquad \text{(b)} \qquad \text{(A.16)}$$

$$\dot{M}_z = -\frac{(M_z - M_o)}{T_1} \qquad \text{(c)}$$

where T_2 is the "spin-spin relaxation time" in the transverse x and y directions, and T_1 is the "spin-lattice relaxation time" in the longitudinal z direction. Equations (A.16 a, b, c) are known as the Bloch equations.

The equation of motion without the relaxation effects was previously given as

$$\frac{d\vec{M}}{dt} = \gamma \vec{H} \times \vec{M}. \qquad \text{(A.4)}$$

When relaxation effects are included, and assuming $H_1 << H_o$, equation (A.4) becomes

$$\frac{d\vec{M}}{dt} = \gamma \vec{H} \times \vec{M} - \frac{M_x \hat{i} + M_y \hat{j}}{T_2} - \frac{M_z - M_o}{T_1} \hat{k} \qquad \text{(A.17)}$$

which transforms into the rotating system as

$$\left(\frac{d\vec{m}}{dt}\right)_{rot} = \gamma(\vec{H}_e \times \vec{M}) + \frac{M_o - M_{z'}}{T_1}\hat{k}' - \frac{M_{x'}}{T_2}\hat{i}' - \frac{M_{y'}}{T_2}\hat{j}' \quad \text{(A.18)}$$

When the substitutions $\vec{H}_e = (H_o + \frac{\omega}{\gamma})\hat{k}' + H_1\hat{i}'$, $\omega_o = -\gamma H_o$, and $\omega_1 = -\gamma H_1$ are made into equation (A.18) it may be solved and simplified to give

$$\dot{M}_{x'} = -M_{y'}(\omega_o - \omega) - \frac{M_{x'}}{T_2}, \qquad \text{(a)}$$

$$\dot{M}_{y'} = -M_{z'}\omega_1 + M_{x'}(\omega_o - \omega) - \frac{M_{y'}}{T_2}, \qquad \text{(b)} \quad \text{(A.19)}$$

$$\dot{M}_{z'} = M_{y'}\omega_1 + \frac{M_o - M_{z'}}{T_1}. \qquad \text{(c)}$$

If the rate at which H_o is swept through resonance is long compared to the relaxation time, the magnetization can be assumed to maintain its equilibrium value, and to a first approximation

$$\dot{M}_{x'} = \dot{M}_{y'} = \dot{M}_{z'} = 0.$$

Assuming a weak alternating field $\vec{H}_1$ so that $T_1T_2\omega_1^2 \ll 1$, the equations (A.19 a, b, c) may be solved and simplified to give equations (A.20 a, b, c) as shown on the following page. The solutions to these equations are obtained using an approximation utilizing slow passage because this condition relates the scanning rate to the relaxation times. When this is done equation (A.19) becomes

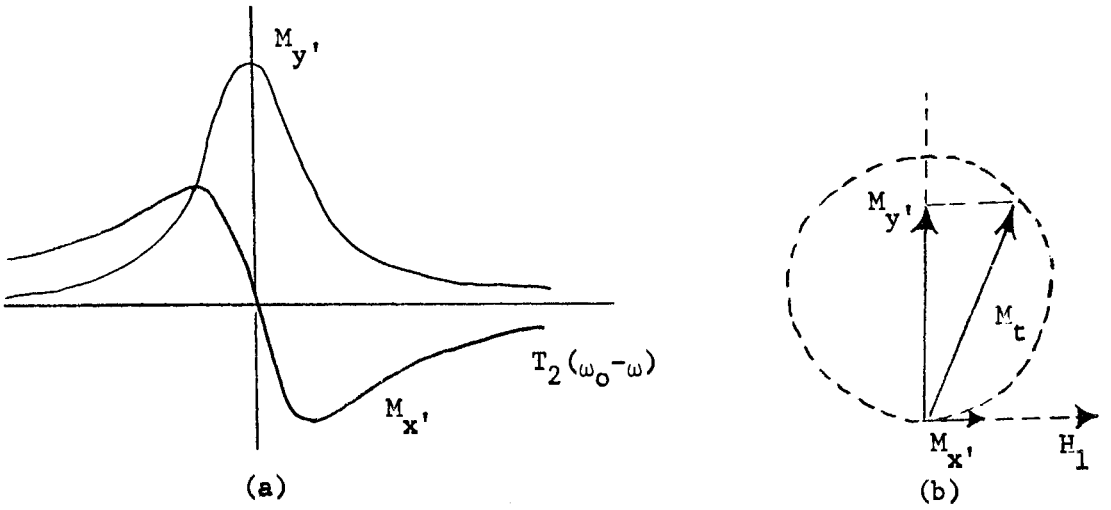

Figure 24. Transverse magnetization; (a) dispersive and absorptive modes, (b) vector relationship in a rotating frame.

$$M_{x'} = \frac{M_o T_2^2 \omega_1 (\omega_o - \omega)}{1 + T_2^2 (\omega_o - \omega)^2}, \qquad \text{(a)}$$

$$M_{y'} = -\frac{M_o T_2 \omega_1}{1 + T_2^2 (\omega_o - \omega)^2} \qquad \text{(b)} \quad \text{(A.20)}$$

$$M_{z'} = M_o. \qquad \text{(c)}$$

The equations (A.20 a, b) can be graphed, yielding $M_{x'}$ and $M_{y'}$ as functions of $T_2(\omega_o-\omega)$ as in Figure 24a. Such a plot shows the curves as representations of the dispersive and absorptive modes of a harmonic oscillator. The transverse magnetization vector $\vec{M}_t$ is found to move in a circle as shown in Figure 24b. At resonance $\vec{M}_t$ is shifted from $\vec{H}_1$ by 90^o and is equal to $\vec{M}_{y'}$ maximum.

If the high frequency susceptibility χ is now introduced where χ is given by

$$\chi = \chi' - i\chi'', \tag{A.21}$$

and M_x is taken as the real part of $\chi\,[2H_1 \exp(i\omega t)]$ then M_x is given by

$$M_x = \chi' \, 2H_1 \cos\omega t + \chi'' \, 2H_1 \sin\omega t. \tag{A.22}$$

Consideration of the components of $M_{x'}$ and $M_{y'}$ in the x-direction allow M_x to be written in the form

$$M_x = M_{x'} \cos\omega t - M_{y'} \sin\omega t. \tag{A.21}$$

Comparing equations (A.22) and (A.21) shows that

$$\chi' = \frac{M_{x'}}{2H_1}, \qquad \chi'' = -\frac{M_{y'}}{2H_1} \tag{A.22}$$

where χ' gives the dispersion curve and χ'' gives the absorptive curve.

It should be noted that the power absorbed from the alternating field depends on χ'' and is given by

$$P = 2\omega H_1^2 \chi''$$

so that

$$P = \chi \cdot \omega \frac{T_2 \omega_o H_1^2}{[1 + T_2^2(\omega_o - \omega)^2]}$$

$$= \pi \chi_o \omega \omega_o H_1^2 L(\omega) \tag{A.23}$$

where

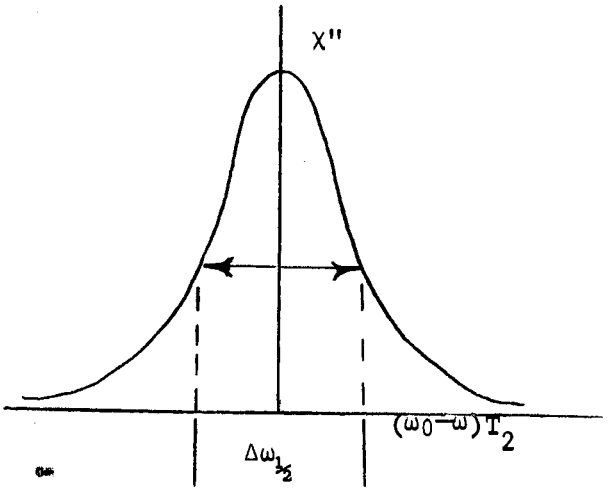

Figure 25. The Lorentzian line shape for χ''.

$$L(\omega) = \frac{T_2}{\pi}\left[\frac{1}{1 + T_2^{\,2}(\omega_o - \omega)^2}\right]$$

is the Lorentzian line shape as shown in Figure 25. Note that the width of the resonance line at half intensity is given by

$$\Delta\omega_{\frac{1}{2}} = 2(\omega_o - \omega) = \frac{2}{T_2} \quad . \tag{A.24}$$

In terms of units of magnetic field (2.24) can be written as

$$\Delta H = \frac{2}{\gamma T_2} \quad . \tag{A.25}$$

To obtain a more detailed discussion of the Bloch method refer to the book by Abragam (65).

APPENDIX B

A DESCRIPTION OF THE SPECTROMETER USED IN THE STUDY

The spectrometer used in this study was constructed mainly by Bell of this laboratory using fundamental ESR design techniques. It has characteristics which closely parallel those discussed in Chapter I and consist of many of the components previously mentioned. It also contains many additional features and modifications which serve to increase its stability and sensitivity. It is a microwave bridge spectrometer which utilizes a sample reflection cavity and a reference reflection cavity. It operates at a klystron frequency of approximately 9.5 ghz in the x-band region of the microwave spectrum. It displays resonance signals, for g-values near 2, in the range of 3,300 gauss to about 3,500 gauss. The complete spectrometer used in this research is shown in Figure 26. The spectrometer is discussed in detail in the pages that follow and a brief description of the functions of the various components is given.

The Electromagnet

The magnet system is the most expensive single system

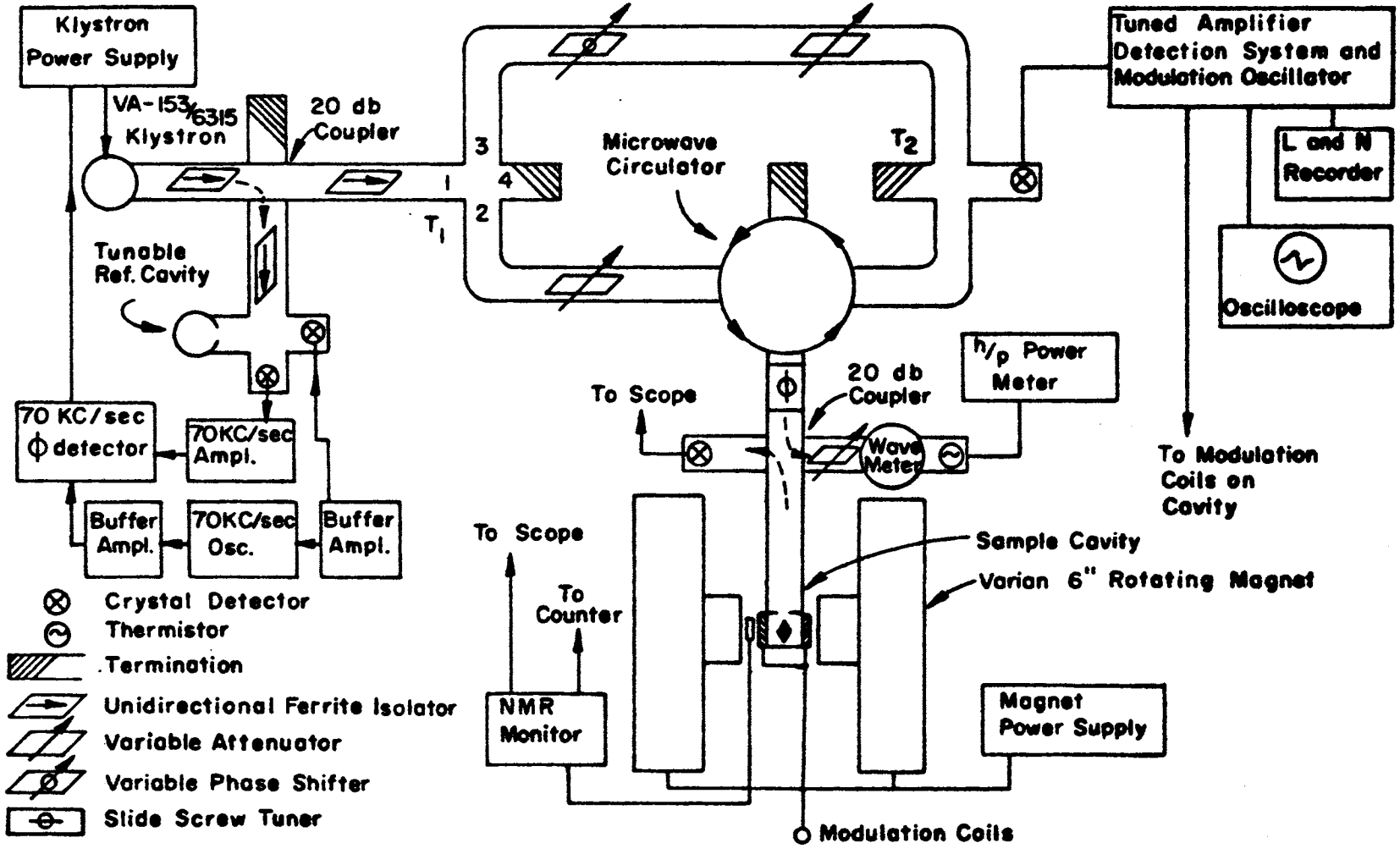

Figure 26. Electron spin resonance spectrometer used in the study. (After King (66).)

in the spectrometer and usually must be chosen from an economic viewpoint; however, an x-band ESR spectrometer must have a homogeneity of better than 0.1 gauss in $1cm^3$ and these minimum requirements must be met (67). The pole gap must be large enough to accomodate the cavity and all necessary accessories. Although it would be advantageous to have a very large gap and high homogeneity, the cost of these features must be considered. A practical median between cost and quality should determine the type of magnet to be used.

The magnet used in the study is a Varian 6" electromagnet, Model 4007-1. It can be turned through 200^{o} about the vertical axis and has 6" ring shim pole pieces with a 2.875" gap. A Model V-2200 Varian regulated power supply is used with the magnet. The magnetic field contours produced by the 6" pole pieces with a 2.875" gap are shown in Figure 27.

The scan rate of the field and the contours of the field are measured using a nuclear magnetic resonance detector. The detector probe is supported by a clamp around one of the magnetic pole pieces and the frequency of the nuclear magnetic resonance oscillator is measured with a h/p 524 D electronic counter. The frequency of the oscillator is related to the proton resonance and the

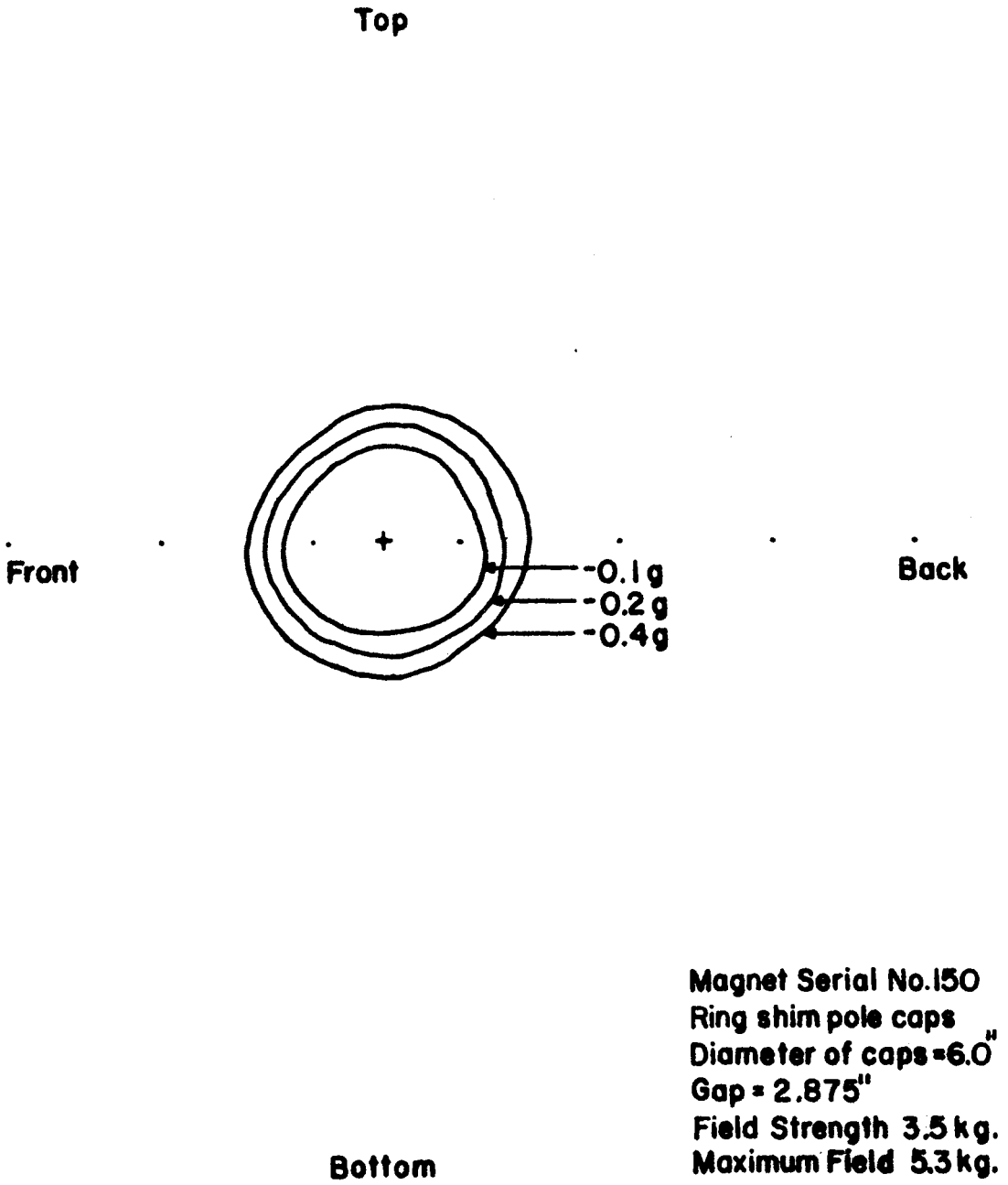

Figure 27. Magnetic field plot of Varian Model V4007-1 electromagnet. (After King (66).)

relationship between this frequency and the magnetic field is given by

$$H = \frac{2\pi}{\gamma_p} \nu_p = 2.34868 \times 10^4 \nu_p \qquad (B.1)$$

where $\gamma_p = 2.67530 \times 10^4$ radian sec.$^{-1}$ gauss^{-1} is the gyromagnetic ratio of the proton (60).

Modulation System

In order to avoid the instability of the dc amplifiers the field is usually modulated so that ac amplifiers may be used. The modulation coils may be placed on the pole pieces, on the sides of the cavity, or inside the cavity. The modulation amplitude should be variable so that very small as well as very large modulating fields are available allowing maximum sensitivity for the line width and shape of the ESR lines to be studied. The maximum sensitivity is obtained when the peak to peak modulation amplitude is on the order of the line width of the ESR signal, but distortion occurs if the modulation amplitude exceeds 1/10 of the line width (67).

Although a low frequency modulation system with bolometers used as detectors is available for use with the spectrometer, a 100kc modulation system was used exclusively (5). The system consist of a pair of modulation

coils mounted on the cavity walls, so that the modulation field is parallel to the large dc magnetic field, and a Varian 100kc modulation control unit containing a tuned amplifier, a phase detector, a crystal oscillator, and a modulation amplifier.

Several effects must be considered when choosing the frequency of modulation to be used. When a crystal detector is used to detect the ESR signal the crystal noise voltage is proportional to $(f)^{-\frac{1}{2}}$ and the crystal noise power varies as $\Delta f/f$, where Δf is the band width of the modulation frequency f. This means that at some low frequency, 100cps for instance, the noise voltage is $(f/100)^{\frac{1}{2}}$ times that at f. Therefore, at 100kc the noise voltage is approximately 1/30 that at 100cps for the same band width. Bolometers do not have the f^{-1} dependence and can be used as detectors at very low frequencies without serious noise problems. It would seem that, if crystal detectors are to be used, a very high modulation frequency would be most desireable. However, for frequencies much higher than 100kc other problems begin to appear. At extremely high modulation frequencies the walls of the cavity begin to attenuate the signal and the large modulation amplitudes needed at the sample are hard to obtain. Even at 100kc the walls of the cavity must be metallic

plated glass or ceramic. If higher frequencies are to be used the modulation must be introduced directly into the cavity by the use of a high frequency loop rigidly connected and inserted properly into the cavity.

Sample Cavity

The sample cavity is one of the most important components of a microwave spectrometer and special cavity designs are necessary for measurements under particular conditions. The choice between several cavity structures is determined by the space available in the magnet gap, the size and shape of the sample, the necessary Q for the cavity, the desired microwave magnetic field configuration at the sample, and the special effects which are to be observed. Two of these several cavity structures are shown in Figure 28. The sample is placed in the position of maximum microwave magnetic field and minimum microwave electric field.

The Varian V-4531 rectangular ESR cavity (Figure 28), operating in the TE_{102} mode, is the only cavity used in the present study. It is equipped with varible temperature capabilities from -185°C to 300°C, but all data taken in this study was at room temperature and these capabilities were not used. The rectangular cavity has the

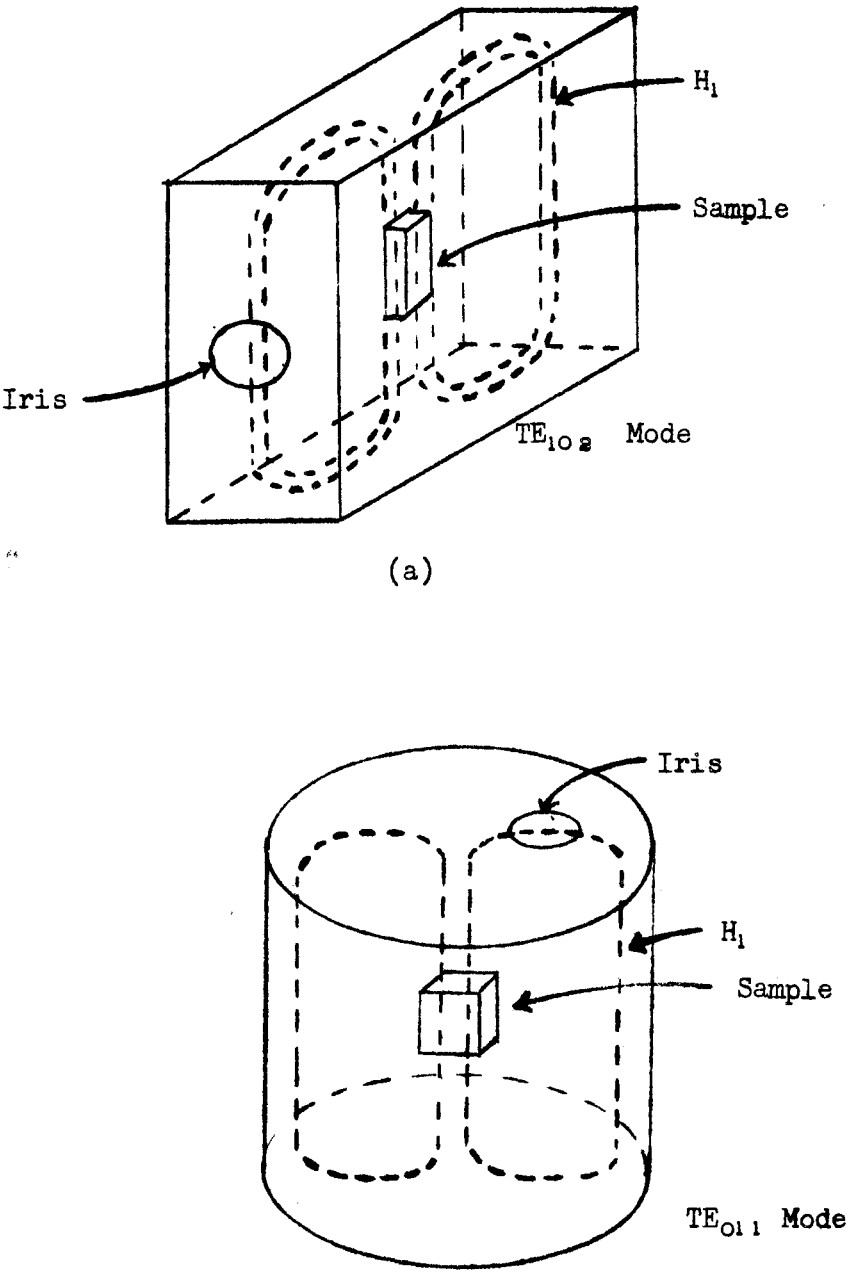

Figure 28. Sample cavities showing microwave magnetic field and location of sample. (After King (66).)

disadvantage that the microwave magnetic field is introduced in the horizontal plane when placed in the magnet gap and the rotatable magnet cannot be moved. If rotation is necessary the sample must be rotated by turning the quartz rod that suspends the sample in the middle of the cavity.

The cavity is coupled to the waveguide by means of a variable dielectric coupling scheme (68,69). The cavity is not adjusted for critical coupling but is adjusted so that the cavity is slightly undercoupled. If critical coupling were used the possibility of mixing the absorptive and dispersive modes would be present; this is an undesirable situation.

The Microwave Circuit

The microwave bridge and circuit is shown in Figure 26. Its basic function is to introduce the microwave energy into the cavity and permit monitoring of the reflected energy (70). The power from the klystron is divided by a magic Tee (T_1) and travels into the upper and lower branches of the circuit. The power down arm 2 is introduced into the circulator after passing through a Varian adjustable precision attenuator. The attenuator controls the amount of energy incident on the sample in

the cavity. The power entering arm 1 of the circulator must exit by arm 2 and is coupled to the cavity (71). The power reflected from the cavity enters the circulator at arm 2 and must exit from arm 3 into magic Tee (T_2). Half the power is detected by the crystal detector in arm 2 of T_2 and the other half is dissipated in arm 3 of T_2. A small amount of power is coupled from the cavity arm into a 20 db coupler and is detected by a crystal detector. The detected signal feeds a wavemeter, a power meter, and an oscilloscope.

The power that travels up through arm 3 of T_1 is used to bias the crystal detector. This arm contains a ferrite isolator, an adjustable phase shifter, and an adjustable attenuator. The phase shifter and the attenuator control the bias on the crystal detector. The energy in this arm enters the magic Tee (T_2) by the upper arm and travels into arm 2 and 3 of T_2. The bias attenuator maintains the desired bias voltage on the detector and the bias phase shifter controls the phase of the bias voltage. These controls determine whether the bridge is sensitive to dispersive (χ'), or the absorptive (χ'') component of the magnetic susceptibility.

The slide screw tuner in the cavity arm is adjusted so that the reflected power from the cavity is independent

of the incident power to the cavity and the bridge is balanced so that no reflected power reaches the detector arm until the sample resonance is reached. A suitable adjustment of the phase shifter will enable the desired mode of operation to be selected. By proper adjustment of the reference voltage to be sensitive to either amplitude or phase unbalance, the desired component can be obtained (68,72).

Stablized Klystron

The microwave energy is supplied by a Varian reflex klystron, VA 201B, which produces approximately 100 milliwatts of power. A commercial klystron power supply is used as the source of power to the klystron and the klystron is mounted on vibration free supports. The entire klystron is thermally isolated in a water cooled silicone oil bath.

It is necessary to keep the klystron frequency stable over at least the entire period of time required to record the passage through resonance. Stablization increases the signal-to-noise ratio and helps prevent the admixture of the real (χ') and imaginary (χ'') parts of the magnetic susceptibility with a great simplification of the recorded data. The stabilization system used in the present study

is the modified Pound circuit shown in Figure 29 (73, 74, 75.

A small part of the microwave power from the klystron is coupled through a 20 db coupler into arm 1 of the magic Tee shown in Figure 29 and Figure 26. The power divides into arm 2 and 3 which are adjustable to be of equal effective lengths. Arm 3 is a matched load, and there is no reflected power if the 70kc modulation is not present. When modulation voltage is present the signal that enters arm 3 is mixed with 70kc signal at the crystal. The crystal superimposes the 70kc frequency and the microwave frequency to produce side bands 70kc above and 70kc below the klystron frequency. When the reference cavity is critically coupled, there is no reflected energy from arm 2 if the klystron frequency coincides with the reference cavity resonance frequency. If the frequencies do not coincide, the reflected wave from the cavity has a magnitude dependent upon the frequency difference.

At the crystal detector in arm 4 the three signals come together and are mixed at the detector giving a 70kc signal proportional to the reactive part of the wave reflected from the cavity. There is a 180° phase difference on either side of the cavity resonance, and

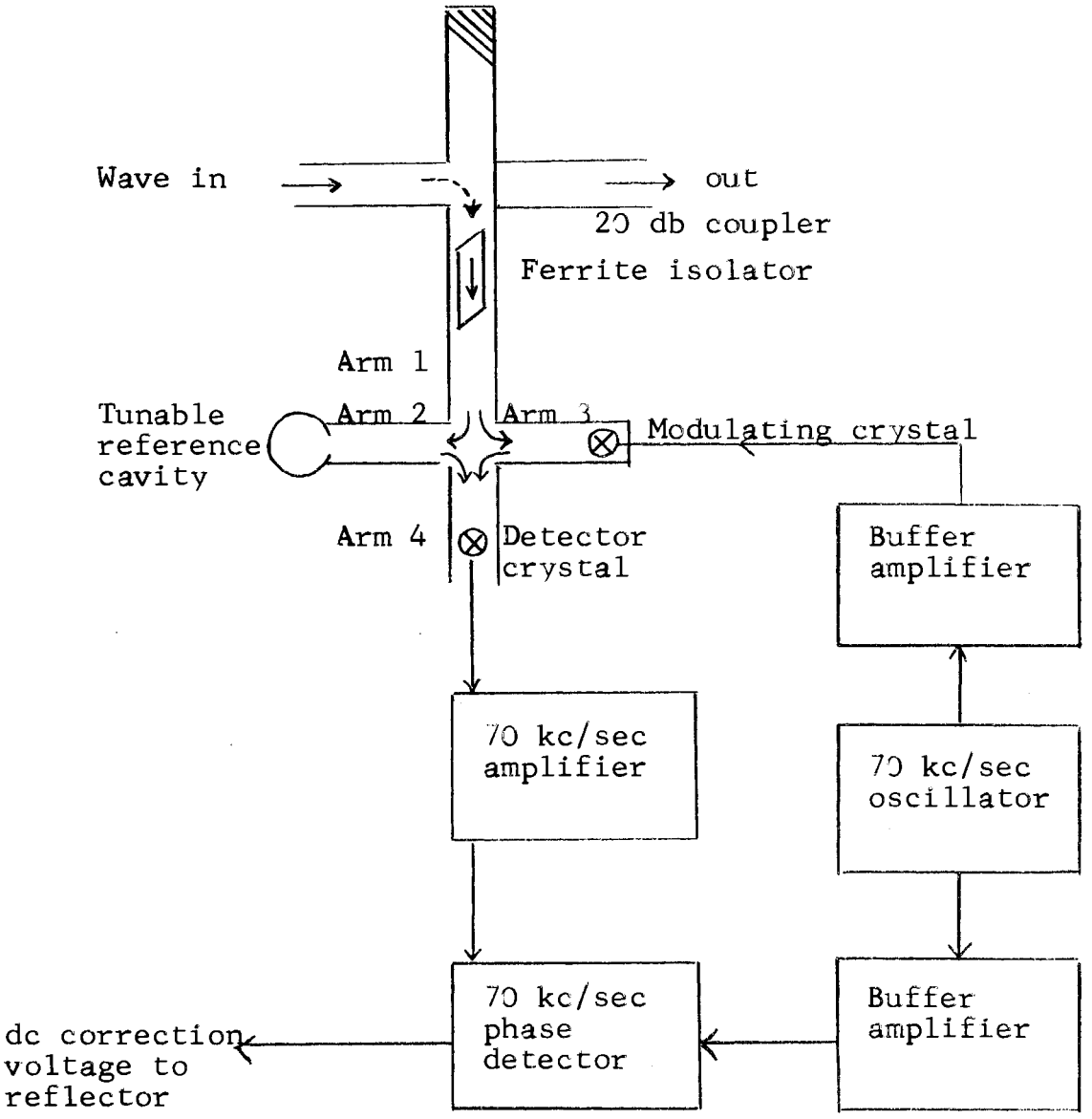

Figure 29. Modified Pound frequency stabilizer. (After King (66).)

the deviation of the klystron on either side of resonance will affect the phase of the crystal output (70). The 70kc error signal is amplified, demodulated, and compared with the reference phase signal in the phase detector. The output of the phase detector is a ±dc signal with an amplitude determined by the error signal strength and a sign determined by the error signal phase. The error signal is amplified and applied to the klystron reflector to adjust the klystron frequency. Since the reflector of the klystron operates at high negative potentials, the phase detector cannot be grounded and must be carefully isolated from ground. The frequency of the klystron is now regulated, or locked, to the resonant frequency of the reference cavity which can be manually set to a desired frequency by moving the cavity bottom plate as shown in Figure 30.

Signal Detection and Display

When the bridge is adjusted for the absorptive mode the incident waves on the crystal detector in arm 2 of Tee (T_2) are the bias signal and the amplitude modulated reflected signal from the sample cavity. These signals are mixed at the detector and sent to the Varian modulation and control unit as shown in Figure 26.

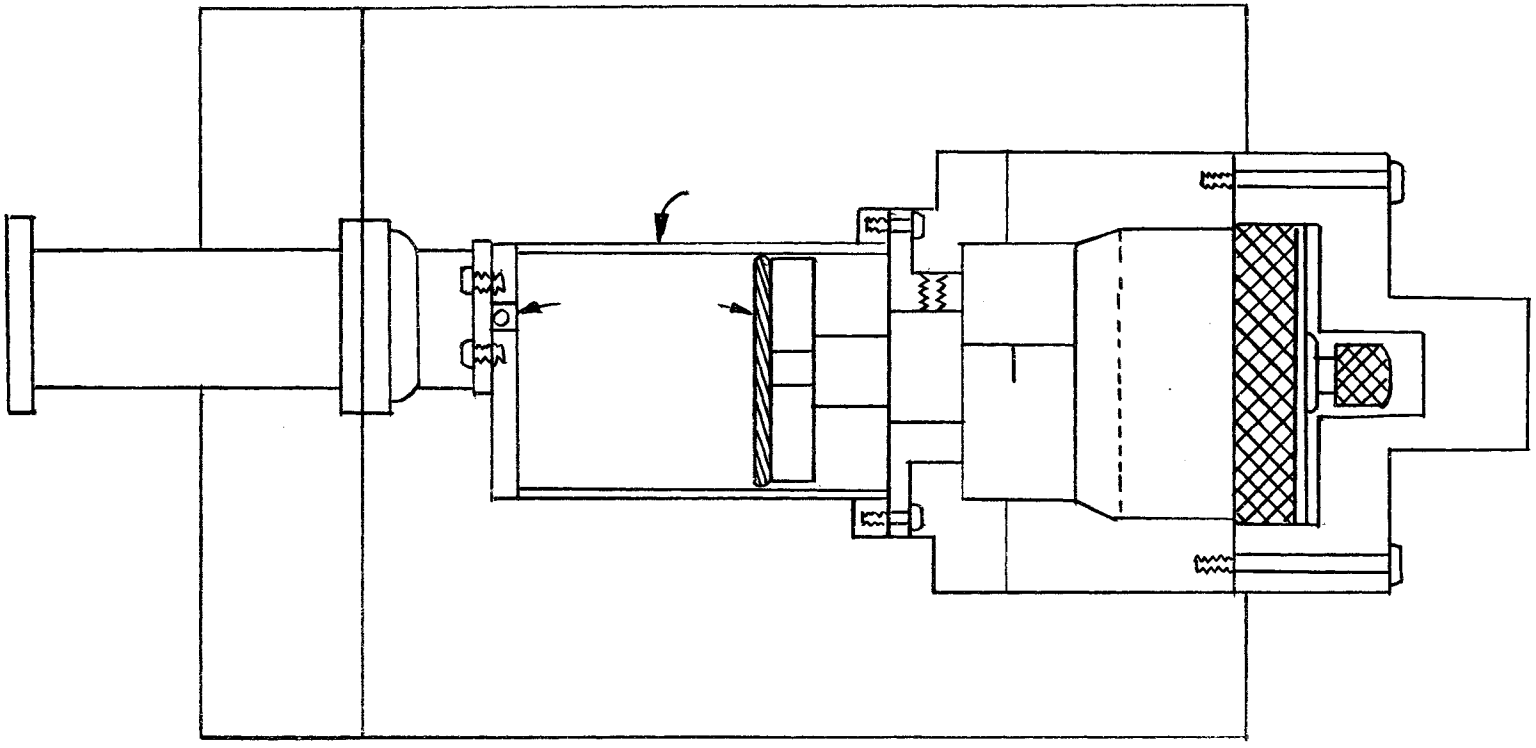

A - Styrofoam Insulation
B - Moveable Cavity Bottom Plate
C - Resonance Cavity
D - Iris and Coupling Screw
E - Eccosorb Epoxy
G - Plexiglas
H - Waveguide
I - Micrometer

F - Silver Plated Quartz Cylinder

Figure 30. Cylindrical reference cavity. (After King (66).)

The components of the Varian control unit have been described previously but will be mentioned again for the sake of clarity. The unit consist of a 100kc crystal oscillator which acts as a reference for the phase detector and provides 100kc modulation to the modulation coils, a 100kc amplifier and demodulator, and a rectification integration circuit from which the signal is sent to the graphic recorder for display.

The phase detector locks onto the input signal which is a continuous vector sum of the amplitude modulated signal voltage and the bias voltage. The detector output can be operated with respect to the phase of the reference signal either in phase or in varying degrees of phase displacement from the reference voltage. In the present study only in-phase and 90^{o} displacement was utilized. The signal output of the detector system is the first derivative of the actual absorption line. It is sent to the integrator circuit and then to the graphic recorder.

If low frequency modulation is desired, the twin bolometers (barretters) available with the spectrometer can be used as detectors. Bolometers respond only to changes on the order of one millisecond (76). They are used with modulation frequencies of 28,400 and 1,000cps

and a phase detector with a range from zero to 1,800cps produced by using a Bristol synchroverter (5). The bolometers contain a wire filament which changes resistance as the microwave energy incident upon it changes and a low-noise amplifier is used in connection with the bolometer bridge.

APPENDIX C

THE G-VALUE AND SCAN-RATE PROGRAM

A standard FORTRAN IV program was written and employed to calculate the scan-rate and g-values of the signals observed in the study. The program was written in three parts. The first part is the main program. It contains all reading and writing and invokes the two subroutine subprograms. The second part is the subroutine used to calculate the scan-rate of the magnetic field for each run. A NMR probe was used to establish nuclear resonance at various points in the range of the magnetic field swept out during each run. These points were marked on the recorder trace and their displacements from the starting mark were recorded in 64th inch. The scan-rate subroutine finds the slope of the NMR frequency vs displacement graph and converts this slope to gauss/inch. The g-value subroutine is the third part of the program. It uses a DPPH reference signal to calculate a magnetic field correction value for each run. The values of the magnetic field at the signals is then calculated and corrected. These field values are used to calculate the g-values of the signals. A sample of output data is also shown. The sample-plus-DPPH reference runs were coded with positive run numbers, while the sample

runs without the DPPH follow their respective reference run and are coded with a negative run number. The type of sample used in each run has been typed in to the right of the run.

```
      $JOB    *****,***-**-****, SAM E. GIUOCO
      C    N  IS THE NUMBER OF DIFFERENT EQUATIONS BEING SOLVED.................
      C  THE MAXIMUM WORD SIZE ALLOWED FOR IN THE WRITE FORMATS IS 9 BITS WITH  5 TO
      C  THE RIGHT OF THE DECIMAL  AND 3 TO THE LEFT.....................................
      C::::::::::::::::::THIS IS A CRUDE BUT OPERABLE FORTRAN IV PROGRAM:::::::::::::::
      C-------------------------------------------------------------------------------
      C::::::::IT CALCULATES SCAN RATES ,FIELD VALUES AND G-VALUES, ASSOCIATED WITH
      C::::::::WORK IN ELECTRON SPIN RESONANCE:::::::::::::::::::::::::::::::::::::::::
      C-------------------------------------------------------------------------------
      C::::::::::::TO THE BEST KNOWLEDGE OF THE AUTHOR ..IT IS STANDARD..EXCEPT FOR
      C::::::::::::LITERAL HOLERITH USED IN SOME FORMAT STATEMENTS:::::::::::::::::::::
      C*******************************************************************************
      C*******************************************************************************
      C                ***************************************
      C                        ********************
      C                                *****
      C  ..........THIS IS THE MAIN PROGRAM.....................................
      C  I USE IT TO READ IN MY DATA AND CALL THE TWO SUBROUTINES :FIT AND FIELD CORR-
      C ECTION.  FIT DOES A LEAST SQUARES FIT AND CALCULATES SCAN RATES...FIELD CORR-
      C ECTION IS USED TO CALCULATE THE FIELD,THE CORRECTION TO THE FIELD DUE TO
      C MAGNETIC FIELD BEING MEASURED OUTSIDE THE SAMPLE CAVITY IS ALSO CALCULATED.
      C IT TAKES THE CORRECTED FIELD VALUES AND CALCULATES G-VALUES FOR THE SIGNALS...
      C.......OUTPUT IS : SCAN-RATE,FIELD VALUES(CORRECTED AND UNCORRECTED), AND G-
      C  VALUES.............
      C  MOST OF THE CALCULATIONS ARE DONE IN DOUBLE PRECISION. SOME OF THE VARIBLES
      C  ARE: D...THE DISTANCE BETWEEN FIELD MEASUREMENTS IN 1/64 INCH...;FRQ... THE
      C  NUCLEAR MAGNETIC RESONANCE FREQUENCY AT EACH POINT D (NMR WAS USED TO MEASURE
      C  MAGNETIC FIELD); SLOPE...THE SCAN RATE IN GAUSS/INCH;GRR..THE POSITION OF THE
      C  SECONDARY REFERENCE SIGNAL(NOT DPPH); GR..THE POSITION OF THE DPPH SIGNAL;
      C  X...THE POSITION OF THE REMAINING SIGNALS;FQ.. THE KLYSTRON FREQUENCY  EACH
      C  RUN;INTG...THE NUMBER OF DATA RUNS BEING PROCESSED; INT...THE NUMBER OF NMR
      C  POINTS USED TO FIND MAGNETIC FIELD..............
 1          DIMENSION FRQ(20),D(20),X(20)
 2          DOUBLE PRECISION D,FRQ,SLOPE,RAM,RB,GRR,GR,X,FIELD1,FIELD2,GRFLD,
           1GRFLD,FQ,GSAMP,HX1,HX2,GX1,GX2,HCOR,HGRR
 3          WRITE(6,22)
      C...READ IN THE NUMBER OF DATA RUNS BEING PROCESSED..........
 4          READ (5,10)INTG
      C....READ IN THE DATA FOR EACH RUN ON EACH LOOP.........
 5        1 READ(5,10)J
 6          READ(5,11)INT,(FRQ(I),I=1,INT)
 7          READ(5,12)(D(I),I=1,INT)
      C...SINCE DISTANCE DATA WAS READ IN AS  SO MANY  64 THS INCH ..CHANGE TO  INCHES
 8          DO 2 I=1,INT,1
 9        2 D(I)=D(I)/64.
10          SLOPE=0.
      C......INITIALIZE VARIBLES NOT PREVIOUSLY DEFINED......
11          RAM=0.
12          RB=0.
      C......INVOKE THE SCAN RATE SUBROUTINE..............
13          CALL FIT(D,INT,FRQ,SLOPE,RAM,RB)
      C  READ IN ADDITIONAL DATA NECESSARY FOR FIELD AND G-VALUE CALCULATIONS.....
14          READ(5,15)FQ
15          READ(5,13)GRR
16          IF(J.GE.0)GO TO 3
17          READ(5,14)(X(I),I=1,2)
      C.......CONVERT TO INCHES..............
18          X(1)=X(1)/64.
19          X(2)=X(2)/64.
20          GO TO 4
```

```
      3 READ(5,13)GR
        GR=GR/64.
      4 GRR=GRR/64.
C      INITIALIZE AGAIN.....
        FIELD1=0.
        FIELD2=0.
        GRFLD=0.
        GRRFLD=0.
        GSAMP=0.
C.................CALL THE SUBROUTINE TO CALCULATE FIELDS AND CORRECT THEM AND TO
C..CALCULATE G-VALUES.....**********************
        CALL FLDCOR(GR,GRR,X,6.6254D-27,.927320-20,FIELD1,FIELD2,GRFLD,
       1GRRFLD,2.0036D0,RAM,RB,FQ,J,GSAMP,HX1,HX2,GX1,GX2,HCOR,HGRR)
C..IF THE RUN IS WAS A DPPH REFERENCE RUN SKIP TO 5 BELOW AND WRITE OUT THE APP-
C ROPRIATE ANSWERS FOR REFFRENCE SAKE.....IF THE RUN WAS  A SAMPLE RUN ALONE
C...THEN  GO ON AND WRITE OUT THE DESIRED ANSWERS ************************
        IF(J.GE.0)GO TO 5
        WRITE(6,20)J,SLOPE,FIELD1,FIELD2,HCOR,HX1,HX2,GX1,GX2
        GO TO 6
      5 WRITE(6,21)J,SLOPE,GRFLD,GRRFLD,HCOR,HGRR,GSAMP
      6 INTG=INTG-1
        IF(INTG.GT.0)GO TO 1
     10 FORMAT(I4)
     11 FORMAT(I4,9F8.4)
     12 FORMAT(9F4.1)
     13 FORMAT(F4.1)
     14 FORMAT(2F4.1)
     15 FORMAT(D12.6)
     20 FORMAT(/,' RUN NUMBER...',I4,'  SCAN RATE=',F8.4,' GAUSS/INCH',/,
       1' UNCORRECTED FIELDS:',/,'  FIELD1=',F9.4,' GAUSS',/,'  FIELD2=',
       2F9.4,'  "  ',/,' FIELD CORRECTION=',F9.4,' GAUSS',/,' CORRECTED
       3 FIELDS ARE:',/,'  H1=',F9.4,' GAUSS',/,'  H2=',F9.4,'  "  ',/,'
       4*G-VALUES ARE:',/,'  G1=',F9.7,/,'  G2=',F9.7)
     21 FORMAT(/,'**DPPH REFERENCE RUN NUMBER...',I4,'  SCAN RATE=',F8.4,
       1' GAUSS/INCH',/,'  UNCORRECTED FIELDS ARE:',/,'  DPPH=',F9.4,' GAU
       2SS',/,'  GRR=',F9.4,'  "  ',/,' FIELD CORRECTION=',F9.4,' GAUSS',/
       3 ,' CORRECTED GRR=',F9.4,' GAUSS',/,' G-VALUE OF GRR=',F9.7)
     22 FORMAT(1H1'                THE DATA FOR THESE RUNS  PROCESSED AS SEEN
       1 BELOW:    ****************************************'////)
        STOP
        END
```

```
47          SUBROUTINE FIT(FD,NINT,FFRQ,SLP,AM,B)
    C             THIS IS THE LEAST SQUARES FIT PROGRAM.....................................
48          DIMENSION DIST(20),FD(20),FFRQ(20),FREQ(20)
49          DOUBLE PRECISION DIST,FD,SUMFD,SUMFSQ,SUMD,SUMFQ,FFRQ,A,DELT,ANUMM
           1,ANUMB,AM,B,SLP,FREQ
50          DIST (1) = 0.00
51          DO 1 I=2,NINT,1
52          II=I-1
53          DIST(I)=FD(I)+DIST(II)
54        1 CONTINUE
    C...INITIALIZE THE PARAMETERS FOR LEAST SQUARES......
55          SUMFD = 0.0
56          SUMFSQ = 0.0
57          SUMD = 0.0
58          SUMFQ = 0.0
    C.....ENTER THE LEAST SQUARES FIT ROUTINE DO -LOOP*********************************
59          DO 2 I=1,NINT,1
60          FREQ(I)=FFRQ(I)
61          SUMFQ=SUMFQ + 23.4868*FREQ(I)
62          SUMD = SUMD + DIST(I)
63          SUMFSQ=SUMFSQ+23.4868*23.4868*FREQ(I)*FREQ(I)
64        2 SUMFD=SUMFD+23.4868*FREQ(I)*DIST(I)
65          A=NINT
66          DELT = A*SUMFSQ -SUMFQ*SUMFQ
67          ANUMM = A*SUMFD - SUMFQ*SUMD
68          ANUMB = SUMD *SUMFSQ - SUMFD*SUMFQ
69          AM = ANUMM / DELT
70          B = ANUMB /DELT
    C...SINCE WE PLOTTED INCH / GAUSS MATHMATICALLY TO ALLOW FOR LEAST SQUARES SHIFT
    C..ING IN THE D-VALUES AND NOT THE MORE ACCURATE FREQUENCY VALUES WE MUST NOW
    C..INVERT TO GET GAUSS/INCH AS DESIRED ****************************************
71            SLP = 1.0000 / AM
72          RETURN
73          END
```

```
74          SUBROUTINE FLDCOR(FGR,FGRR,FX,H,BETA,FLD1,FLD2,FLDGR,FLDGRR,GDPPH,
           1AM,B,F,JJ,GGRR,CFLD1,CFLD2,GFLD1,GFLD2,FLDCR,CFLGRR)
      C... THIS ROUTINE CALCULATES FIELD VALUES FOR THE REFERENCE DPPH AND THE SIGNALS
      C..AND CORRECTS THEM FOR ERRORS INTRODUCED BY MEASUREING THE FIELD OUTSIDE THE
      C...SAMPLE CAVITY. IT ALSO USES THESE FIELD VALUES TO CALCULATE THE DESIRED G-VA
      C LUES AND PASSES ALL INFORMATION BACK TO THE MAIN PROGRAM WHERE IT IS WRITTEN.
      C.... THE G-VALUE VALUE CALCULATIONS ARE DONE USING THE STANDARD G=HF/H*BETA
      C..WHERE H IS PLANCKS CONST. F IS THE KLYSTRON FREQ. FOR THAT RUN ;H* IS THE
      C..CORRECTED FIELD AT WHICH THE THE SIGNAL OCCURS; AND BETA IS A CONSTANT*******
      C....THE BOHR MAGNETON.....................
75          DIMENSION FX(20)
76          DOUBLE PRECISION BETA,H,FLD1,FLD2,FLDGRR,FLDGR,B,AM,F,FGR,FGRR,FX,
           1GDPPH,GGRR,GPEAK,CFLDGR,CFLGRR,FLDCR,CFLD1,CFLD2,GFLD1,GFLD2
77          FLDCR=0.
78          FLDGRR=(FGRR-B)/AM
      C...CHECK TO SEE THAT A DPPH REFERENCE IS BEING  PROCESSED OR IF NOT , THAT THE
      C..PREVIOUS RUN WAS A DPPH REF. RUN...THIS IS NECESSARY AS DATA FOR SAMPLE RUNS
      C..IS FIRST CALCULATED IN THE DPPH RUN FOR THAT SAMPLE.....*****
79          IF(JJ.GE.0)GO TO 1
80          IF(ICK.NE.1)GO TO 3
81          ICK=0
82          FLD1=(FX(1)-B)/AM
83          FLD2=(FX(2)-B)/AM
84          GO TO 2
      C IF WE ARE ON A DPPH REFERENCE RUN WE USE THE KNOWN VALUE OF G-DPPH TO FIND
      C..OUR  NECESSARY FIELD CORRECTION.( A DPPH REF. RUN IS CODED AS A POSITIVE RUN.
85        1 FLDGR=(FGR-B)/AM
86          ICK=1
87          CFLDGR=(H*F)/(GDPPH*BETA)
88          FLDCR=CFLDGR-FLDGR
89          CFLGRR=FLDGRR+FLDCR
90          GPEAK=(H*F)/(CFLGRR*BETA)
91          GGRR=GPEAK
92          GO TO 4
      C..IF WE ARE ON A SAMPLE ONLY RUN WE USE A G-VALUE CALCULATED ON THE PREVIOUS
      C..DPPH RUN TO CALCULATE THE FIELD CORRECTION FOR  THE SAMPLE RUN**************
93        2 CFLGRR=(H*F)/(GPEAK*BETA)
94          FLDCR=CFLGRR-FLDGRR
95          CFLD1=FLD1+FLDCR
96          CFLD2=FLD2+FLDCR
97          GFLD1=(H*F)/(CFLD1*BETA)
98          GFLD2=(H*F)/(CFLD2*BETA)
99          GO TO 4
100       3 WRITE(6,5)
101       5 FORMAT(/,'  THE SUBROUTINE FAILED AS WE DID NOT SOLVE FOR GRR 1ST'
           1 )
102       4 RETURN
103         END

      $ENTRY
```

A SAMPLE OF THE DATA FOR THESE RUNS PROCESSED AS SEEN BELOW: **********

```
*DPPH REFERENCE RUN NUMBER... 131  SCAN RATE= 19.3711 GAUSS/INCH
 UNCORRECTED FIELDS ARE:
 DPPH=3254.2271 GAUSS
 GRR=3246.4787  "
FIELD CORRECTION=    0.7300 GAUSS                          NORMAL RBC
CORRECTED GRR=3247.2087 GAUSS
G-VALUE OF GRR=2.0083810

RUN NUMBER...-129  SCAN RATE= 19.2505 GAUSS/INCH
UNCORRECTED FIELDS:
 FIELD1=3249.5866 GAUSS
 FIELD2=3255.6927  "
FIELD CORRECTION=    1.5513 GAUSS
CORRECTED    FIELDS ARE:
 H1=3251.1379 GAUSS
 H2=3257.2439  "
 *G-VALUES ARE:
 G1=2.0057239
 G2=2.0019639

*DPPH REFERENCE RUN NUMBER... 121  SCAN RATE= 19.2352 GAUSS/INCH
 UNCORRECTED FIELDS ARE:
 DPPH=3253.1971 GAUSS
 GRR=3245.4429  "
FIELD CORRECTION=    2.2155 GAUSS                          INFECT. RBC
CORRECTED GRR=3247.6583 GAUSS
G-VALUE OF GRR=2.0093838

RUN NUMBER...-124  SCAN RATE= 19.5978 GAUSS/INCH
UNCORRECTED FIELDS:
 FIELD1=3250.5292 GAUSS
 FIELD2=3256.2861  "
FIELD CORRECTION=    1.5704 GAUSS
CORRECTED    FIELDS ARE:
 H1=3252.0996 GAUSS
 H2=3257.8564  "
 *G-VALUES ARE:
 G1=2.0053770
 G2=2.0018334

*DPPH REFERENCE RUN NUMBER... 169  SCAN RATE= 23.3360 GAUSS/INCH
 UNCORRECTED FIELDS ARE:
 DPPH=3253.7667 GAUSS
 GRR=3244.7240  "
FIELD CORRECTION=    2.6613 GAUSS                          FETAL RBC
CORRECTED GRR=3245.3853 GAUSS
G-VALUE OF GRR=2.0091827

RUN NUMBER...-157  SCAN RATE= 23.2480 GAUSS/INCH
UNCORRECTED FIELDS:
 FIELD1=3233.4625 GAUSS
 FIELD2=3239.6065  "
FIELD CORRECTION=    1.8221 GAUSS
CORRECTED    FIELDS ARE:
```

```
 H1=3235.2746 GAUSS
 H2=3261.4286  "
 *G-VALUES ARE:
 G1=2.0159954
 G2=1.9998287

*DPPH REFERENCE RUN NUMBER... 135  SCAN RATE= 19.1985 GAUSS/INCH
 UNCORRECTED FIELDS ARE:
 DPPH=3254.1281 GAUSS
 GRR=3248.7585  "                                          NORMAL RBC MEMBRANE
FIELD CORRECTION=   5.6372 GAUSS
CORRECTED GRR=3249.3957 GAUSS
G-VALUE OF GRR=2.0069109

RUN NUMBER...-133  SCAN RATE= 19.7960 GAUSS/INCH
UNCORRECTED FIELDS:
 FIELD1=3253.3235 GAUSS
 FIELD2=3258.6746  "
FIELD CORRECTION=   1.5839 GAUSS
CORRECTED    FIELDS ARE:
 H1=3254.9074 GAUSS
 H2=3260.2585  "
 *G-VALUES ARE:
 G1=2.0036115
 G2=2.0003230

*DPPH REFERENCE RUN NUMBER... 136  SCAN RATE= 19.4409 GAUSS/INCH
 UNCORRECTED FIELDS ARE:
 DPPH=3253.7776 GAUSS
 GRR=3249.0693  "                                          NORMAL RBC MEMBRANE
FIELD CORRECTION=   4.9784 GAUSS
CORRECTED GRR=3250.0477 GAUSS
G-VALUE OF GRR=2.0065026

RUN NUMBER...-134  SCAN RATE= 19.3939 GAUSS/INCH
UNCORRECTED FIELDS:
 FIELD1=3252.5176 GAUSS
 FIELD2=3257.3661  "
FIELD CORRECTION=   2.0675 GAUSS
CORRECTED    FIELDS ARE:
 H1=3254.5851 GAUSS
 H2=3259.4336  "
 *G-VALUES ARE:
 G1=2.0037937
 G2=2.0008130

*DPPH REFERENCE RUN NUMBER... 137  SCAN RATE= 19.5280 GAUSS/INCH
 UNCORRECTED FIELDS ARE:
 DPPH=3254.0074 GAUSS
 GRR=3235.9135  "                                          INFECT. RBC MEMBRANE
FIELD CORRECTION=   0.2455 GAUSS
CORRECTED GRR=3236.1590 GAUSS
G-VALUE OF GRR=2.0148025

RUN NUMBER...-140  SCAN RATE= 19.3208 GAUSS/INCH
UNCORRECTED FIELDS:
 FIELD1=3252.7243 GAUSS
 FIELD2=3258.6111  "
FIELD CORRECTION=  -9.1726 GAUSS
CORRECTED    FIELDS ARE:
```

```
 H1=3243.5517 GAUSS
 H2=3249.4385  "
 *G-VALUES ARE:
 G1=2.0101894
 G2=2.0065476

*DPPH REFERENCE RUN NUMBER... 138  SCAN RATE= 19.9112 GAUSS/INCH
 UNCORRECTED FIELDS ARE:
 DPPH=3253.7142 GAUSS
 GRR=3237.9408  "
FIELD CORRECTION=   0.5419 GAUSS
CORRECTED GRR=3238.4827 GAUSS
G-VALUE OF GRR=2.0133588

RUN NUMBER...-139  SCAN RATE= 19.4771 GAUSS/INCH
UNCORRECTED FIELDS:
 FIELD1=3252.7237 GAUSS
 FIELD2=3259.1146  "
FIELD CORRECTION=  -6.9138 GAUSS
CORRECTED    FIELDS ARE:
 H1=3245.8099 GAUSS
 H2=3252.2008  "
 *G-VALUES ARE:
 G1=2.0087904
 G2=2.0048429
```

INFECT. RBC MEMBRANE

APPENDIX D

SELECTED SAMPLES OF ACTUAL RECORDER GRAPHS USED IN THE STUDY

The actual recorder graphs could not be photographed directly because of the color of ink used in the recorder pen. It was necessary to trace the actual graphic representations as accurately as possible and use these tracings to represent the data runs for this study in the body of the text. Since it was desirable to include actual copies of selected recorder graphs showing all noise and exact signal ratios, these were Xeroxed individually. They appear on the following pages.

Mod.Amp..4 x 100
Gain.....5 x 100
Power....-15 db
Phase....0 deg
Temp.....25 deg C

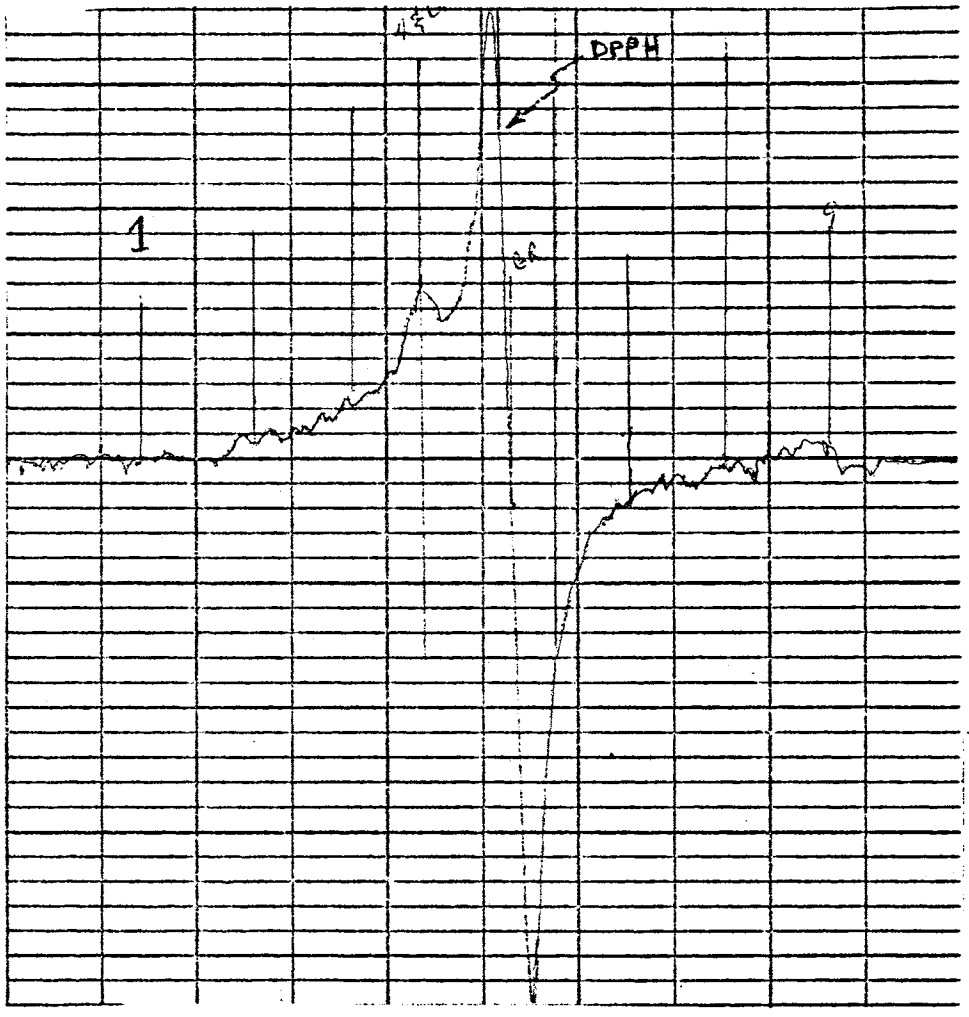

Figure 31. DPPH Reference Run

Mod.Amp..4 x 100
Gain.....5 x 100
Power....-15 db
Phase....0 deg
Temp.....25 degC

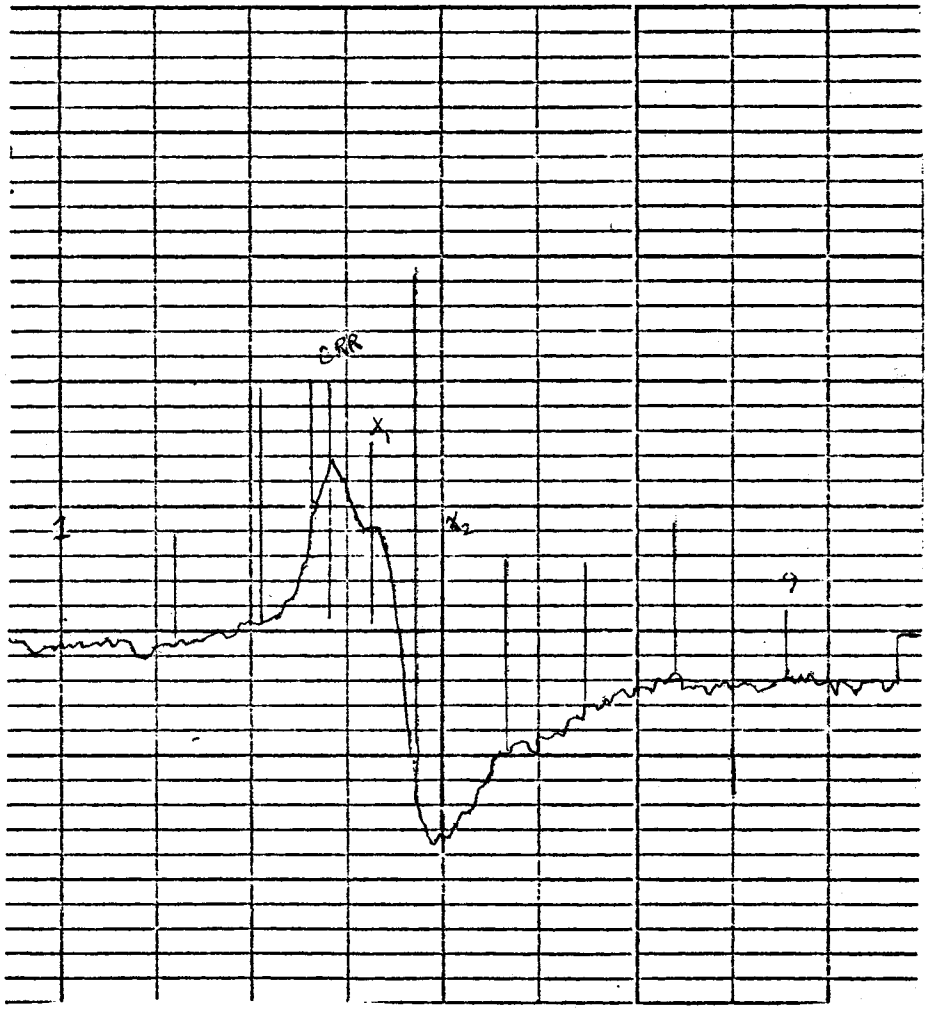

Figure 32. Sample Run

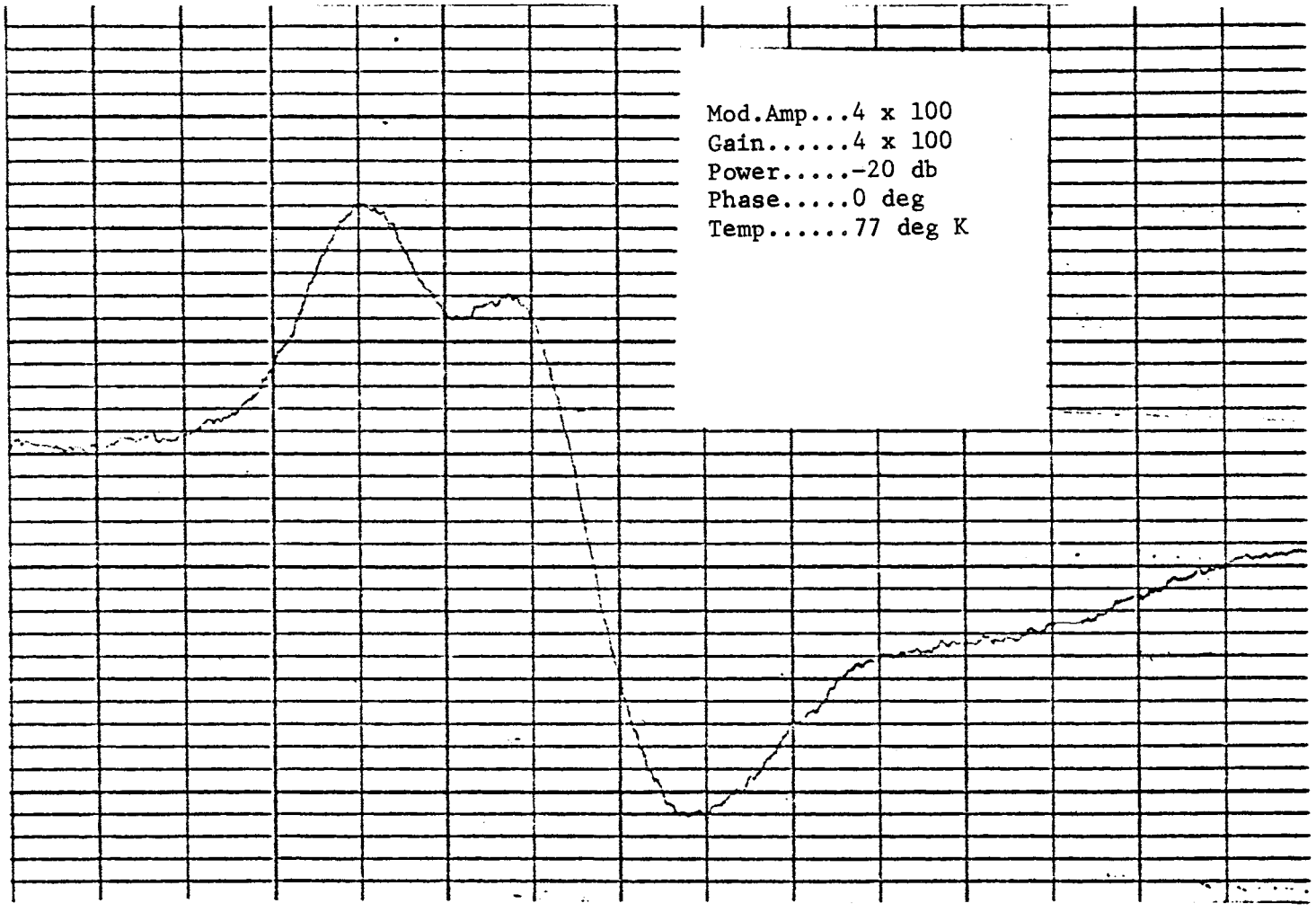

Figure 33. Adult Infected Red Cell ESR Spectrum

Mod.Amp..4 x 100
Gain.....4 x 100
Power....-20 db
Phase....0 deg
Temp.....77 deg K

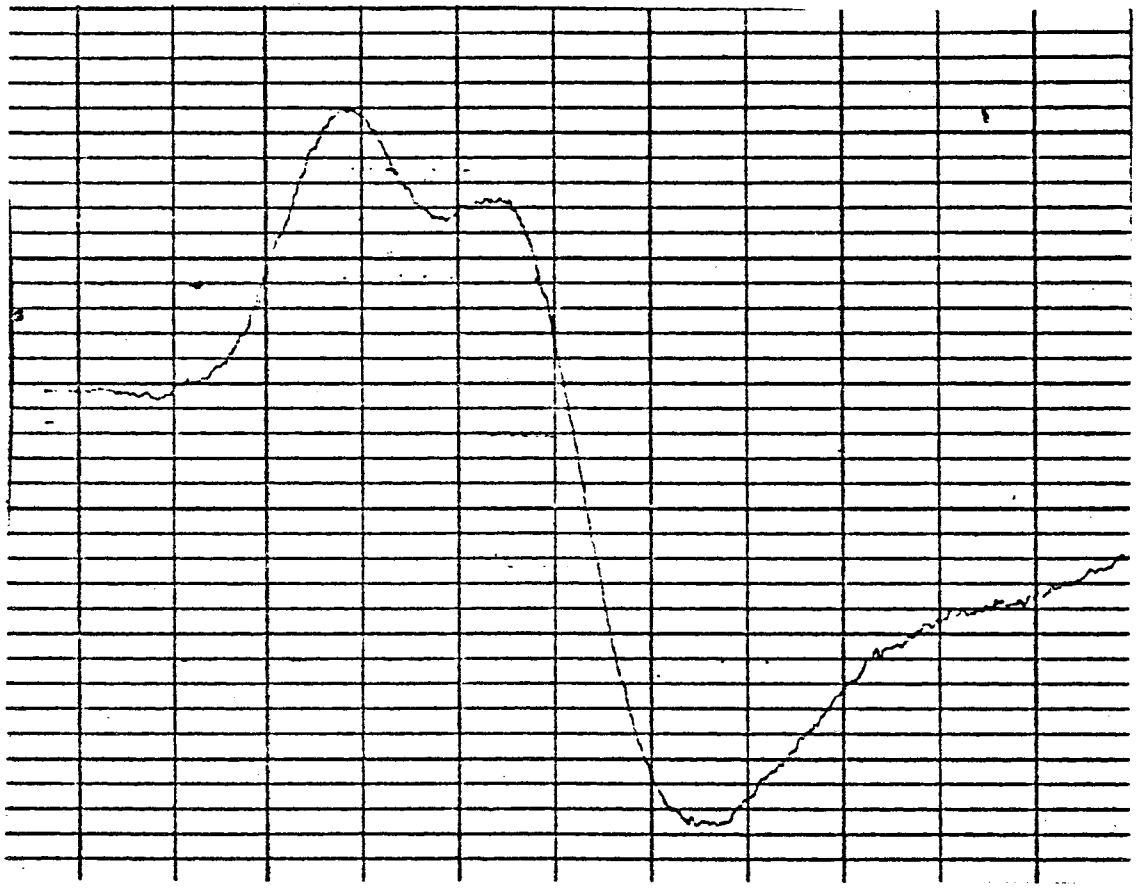

Figure 34. Adult Normal Red Cell ESR Spectrum

Mod.Amp..4 x 100
Gain.....5 x 100
Power....-10 db
Phase....0 deg
Temp.....25 deg C

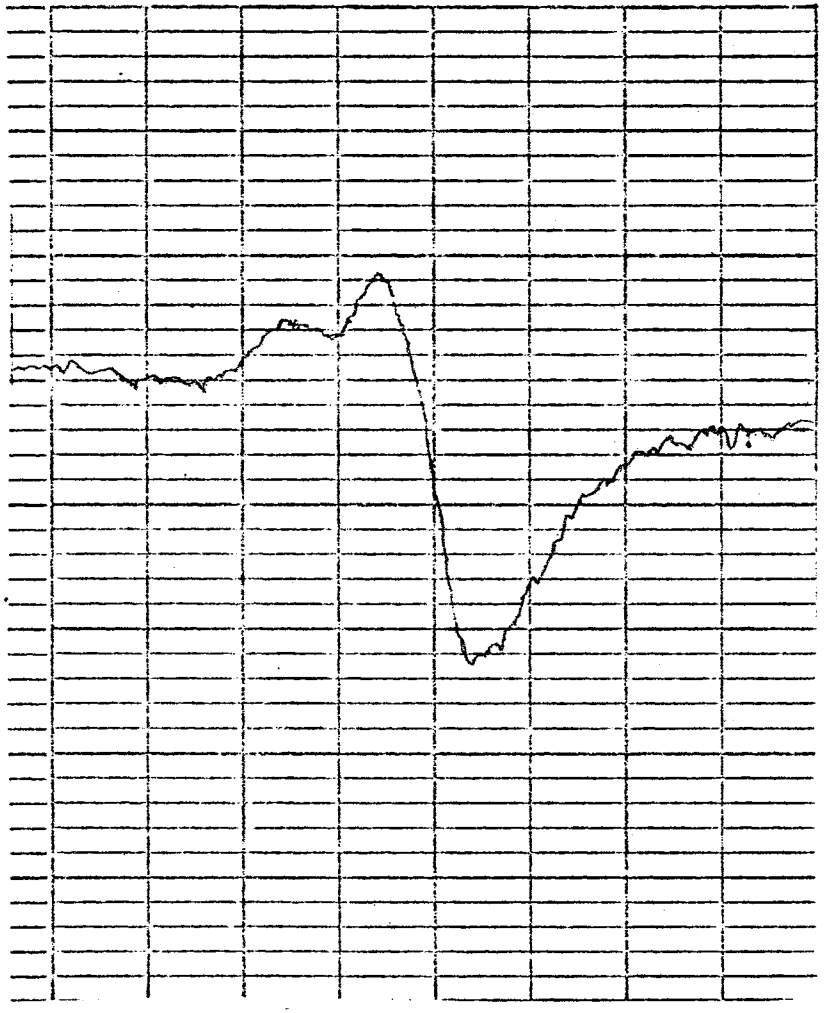

Figure 35. Fetal Red Cell ESR Spectrum

Mod.Amp..4 x 100
Gain.....5 x 100
Power....-15 db
Phase....0 deg
Temp.....25 deg C

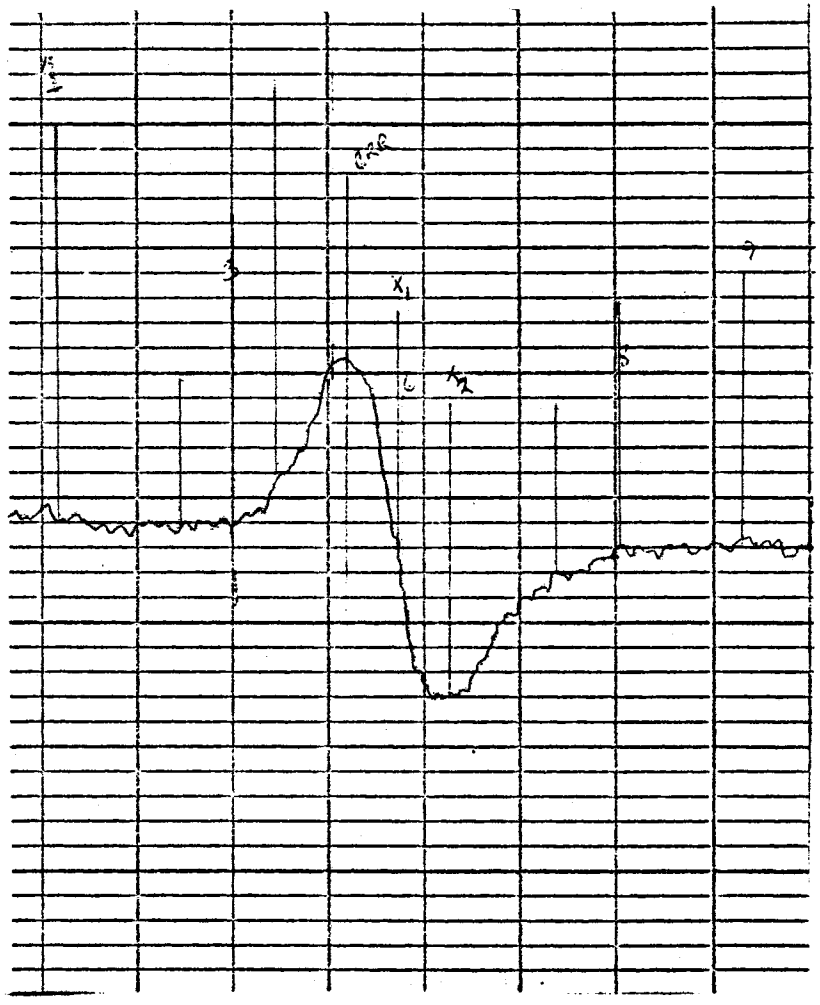

Figure 36. Normal Red Cell Membrane ESR Spectrum

Mod.Amp..4 x 100
Gain.....5 x 100
Power....-20 db
Phase....0 deg
Temp.....25 deg C

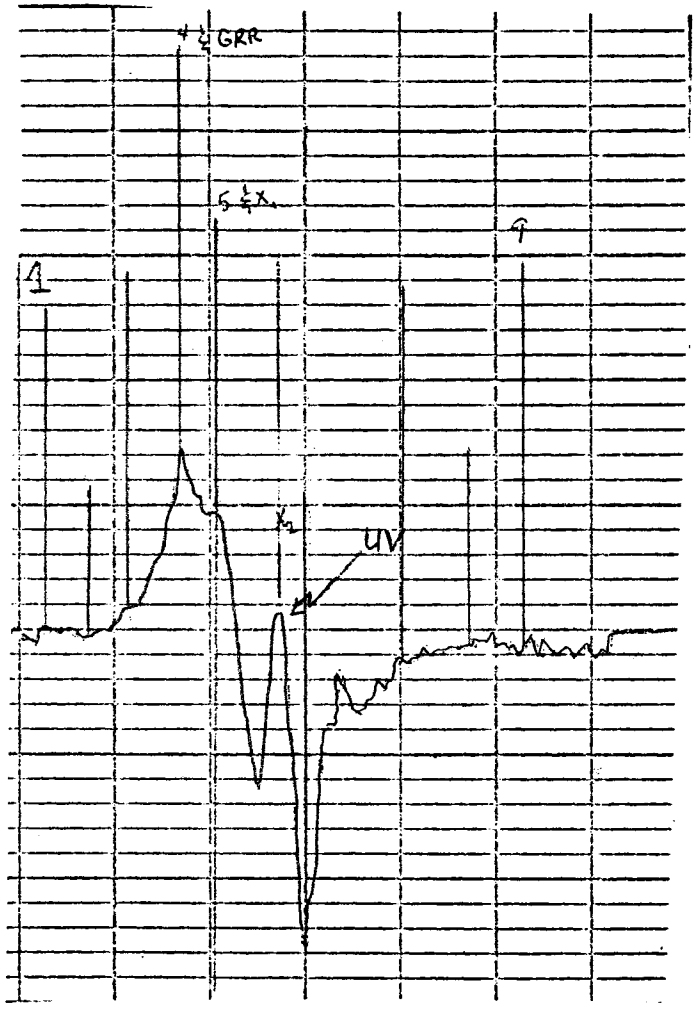

Figure 37. UV-Irradiation ESR Spectrum

Mod.Amp..4 x 100
Gain.....5 x 100
Power....-15 db
Phase....0 deg
Temp.....25 deg C

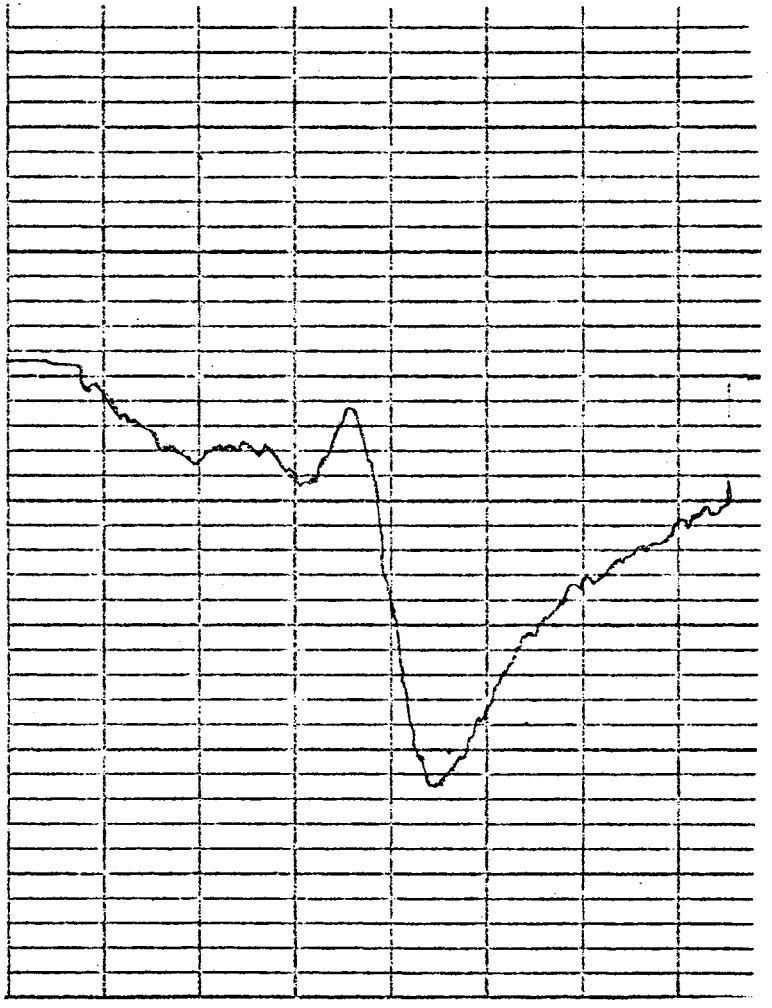

Figure 38. Nitric-Oxide Labeled ESR Spectrum

VITA

Sam E. Giuoco

Candidate for the Degree of

Doctor of Education

Thesis: ELECTRON SPIN RESONANCE OF ADULT, FETAL, AND ANAPLASMA MARGINALE INFECTED BOVINE RED BLOOD CELLS

Major Field: Higher Education

Biographical:

Personal Data: Born in Pharr, Texas, September 26, 1940, the son of Frank and Odell Giuoco.

Education: Attended grade school in Pharr, Texas; graduated from Pharr-San Juan-Alamo High School in 1959; attended San Antonio College in San Antonio, Texas, 1964; received the Bachelor of Science degree from Pan American College, with majors in Physics and Mathmatics, in January, 1968; attended Oklahoma State University, Stillwater, Oklahoma, from January 1968 until May, 1971; received a Master of Science degree in May, 1969; completed requirements for the Doctor of Education degree in May, 1971.

Experience: Employed as a laboratory assistant in the physics department of Pan American College, Edinburg, Texas (1964-1968); graduate teaching assistant in the physics department of Oklahoma State University (1968-1971).

Organizations: Member of Sigma Pi Sigma, Society of Physics Students, and Mathematical Association of America.